NAVAL POSTGRADUATE SCHOOL
Monterey, California

THESIS

PITCHFORK BIFURCATIONS AND DIVE PLANE REVERSAL
OF
SUBMARINES AT LOW SPEEDS

by

Jeffery Scott Riedel

June 1993

Thesis Advisor: Fotis A. Papoulias

Unclassified
SECURITY CLASSIFICATION OF THIS PAGE

REPORT DOCUMENTATION PAGE

Form Approved
OMB No 0704-0188

1a REPORT SECURITY CLASSIFICATION UNCLASSIFIED	1b RESTRICTIVE MARKINGS
2a SECURITY CLASSIFICATION AUTHORITY	3. DISTRIBUTION AVAILABILITY OF REPORT Approved for public release; distribution is unlimited
2b DECLASSIFICATION DOWNGRADING SCHEDULE	
4 PERFORMING ORGANIZATION REPORT NUMBER(S)	5 MONITORING ORGANIZATION REPORT NUMBER(S)
6a NAME OF PERFORMING ORGANIZATION Naval Postgraduate School — 6b OFFICE SYMBOL (If applicable) 34	7a NAME OF MONITORING ORGANIZATION Naval Postgraduate School
6c ADDRESS (City, State, and ZIP Code) Monterey, CA 93943-5000	7b ADDRESS (City, State, and ZIP Code) Monterey, CA 93943-5000
8a NAME OF FUNDING SPONSORING ORGANIZATION — 8b OFFICE SYMBOL (If applicable)	9 PROCUREMENT INSTRUMENT IDENTIFICATION NUMBER
8c ADDRESS (City, State, and ZIP Code)	10 SOURCE OF FUNDING NUMBERS PROGRAM ELEMENT NO / PROJECT NO / TASK NO / WORK UNIT ACCESSION NO

11 TITLE (Include Security Classification)
PITCHFORK BIFURCATIONS AND DIVE PLANE REVERSAL OF SUBMARINES AT LOW SPEEDS

12 PERSONAL AUTHOR(S)
Jeffery Scott Riedel

13a TYPE OF REPORT	13b TIME COVERED	14 DATE OF REPORT (Year, Month, Day)	15 PAGE COUNT
Engineers Thesis	FROM ____ TO ____	1993 June	137

16 SUPPLEMENTARY NOTATION
The views expressed in this thesis are those of the author and do not reflect the official policy or position of the Department of Defense or the U S. Government.

17 COSATI CODES			18 SUBJECT TERMS (Continue on reverse if necessary and identify by block number)
FIELD	GROUP	SUB-GROUP	Bifurcations, Submarine Motions, Dive Planes

19 ABSTRACT (Continue on reverse if necessary and identify by block number)

The ability of a submarine to maintain ordered depth, especially during periscope depth operations at low speeds, is vital for the vessel to perform its mission and avoid detection. Modern submarines exhibit an inherent phenomenon that produces an undesirable ship response at low speeds, commonly referred to as dive plane reversal. The physical parameters that govern this occurrence are related in this thesis to the problem of multiple steady state solutions in the vertical plane.

Generic solution branching, in the form of pitchfork bifurcations, can occur when the nominal level flight path loses its stability. A systematic study reveals the existence of a critical Froude number, based on the vessel's speed and metacentric height, where this branching occurs. Bifurcation theory techniques and numerical computations are utilized to classify the effect that geometric parameters, trim and ballast conditions, and hydrodynamic properties have on the existence of these multiple solutions.

20 DISTRIBUTION AVAILABILITY OF ABSTRACT [X] UNCLASSIFIED UNLIMITED [ ] SAME AS RPT [ ] DTIC USERS	21 ABSTRACT SECURITY CLASSIFICATION Unclassified
22a NAME OF RESPONSIBLE INDIVIDUAL Fotis A. Papoulias	22b TELEPHONE (Include Area Code) 408-656-3381 — 22c OFFICE SYMBOL ME/Pa

DD Form 1473, JUN 86 — Previous editions are obsolete — SECURITY CLASSIFICATION OF THIS PAGE
S/N 0102-LF-014-6603 — Unclassified

Approved for public release; distribution is unlimited

PITCHFORK BIFURCATIONS AND DIVE PLANE REVERSAL OF SUBMARINES AT LOW SPEEDS

by

Jeffery Scott Riedel
Lieutenant, United States Navy
B.S., Maine Maritime Academy, 1986

Submitted in partial fulfillment of the
requirements for the degrees of

MASTER OF SCIENCE IN MECHANICAL ENGINEERING
and
MECHANICAL ENGINEER

from the

NAVAL POSTGRADUATE SCHOOL

June, 1993

Author: _____
Jeffery Scott Riedel

Approved by: _____
Fotis A. Papoulias, Thesis Advisor

_____
Matthew D. Kelleher, Chairman,
Department of Mechanical Engineering

_____
Richard S. Elster
Dean of Instruction

ABSTRACT

The ability of a submarine to maintain ordered depth, especially during periscope depth operations at low speeds, is vital for the vessel to perform its mission and avoid detection. Modern submarines exhibit an inherent phenomenon that produces an undesirable ship response at low speeds, commonly referred to as dive plane reversal. The physical parameters that govern this occurrence are related in this thesis to the problem of multiple steady state solutions in the vertical plane.

Generic solution branching, in the form of pitchfork bifurcations, can occur when the nominal level flight path loses its stability. A systematic study reveals the existence of a critical Froude number, based on the vessel's speed and metacentric height, where this branching occurs. Bifurcation theory techniques and numerical computations are utilized to classify the effect that geometric parameters, trim and ballast conditions, and hydrodynamic properties have on the existence of these multiple solutions.

TABLE OF CONTENTS

LIST OF FIGURES

ACKNOWLEDGMENT

I would like to express my most sincere appreciation to my wife, Ellen, son, Taylor, and daughter, Chelsea, for their constant support in pursuit of my Master's and Engineer's Degrees and in the development of this thesis. The sacrifices they have endured were great and will never be forgotten.

My heartfelt thanks go to Professor Fotis A. Papoulias, my thesis advisor, for the dedication he displayed toward this thesis and my education, and to Professor Charles N. Calvano, the Total Ship Systems Engineering faculty advisor, for the professional guidance and counseling he provided during my tour at the Naval Postgraduate School. They have both made this graduate education experience everything it was meant to be.

Finally, I must thank the United States Navy, specifically the Engineering Duty Officer community, for providing me this educational opportunity.

I. INTRODUCTION

One of the most critical functions of a submersible is accurate depth keeping at the commanded depth. Such a function can be carried out either manually or automatically, especially in cases where human intervention is not possible or desirable. Due to the technological significance and numerous scientific applications of submersible vehicle systems, design issues of appropriate depth keeping control laws have received wide attention in the past. Such control system designs include linear and nonlinear controllers [Refs. 1&2], model based compensators [Ref. 3], adaptive control [Ref. 4], and sliding mode control laws [Refs. 5&6].

Response accuracy and stability are primary considerations in designing depth keeping control law. Of paramount importance, in this area, are the robustness properties of the particular design; i.e., its ability to maintain accuracy and stability in the presence of incomplete sensor and environmental information, as well as actual/mathematical model mismatch. The scope of the work in this thesis is to demonstrate a potential loss of stability that may occur when a submarine is operating at low speeds. This loss of stability can occur regardless of the particular means used for depth control. The study is accomplished through the use of an eigenvalue analysis, a steady state analysis and a controllability analysis [Ref. 7]. It is shown that such a loss of stability is accompanied by a slow divergence of trajectories away from the commanded path. Solution branching occurs in the form of generic pitchfork bifurcations [Refs. 8, 9]. A complete characterization of the problem is given utilizing singularity techniques, which have been proven to be very useful in the analysis of similar problems [Refs. 10, 11, 12]. The use of

bifurcation theory allows the crucial vehicle parameters that govern the problem of solution branching to be determined, and the develop guidelines to prevent its occurrence

Finally, a new look at the problem of dive plane reversal [Ref. 13], based on solution branching results is presented. The term dive plane reversal refers to a well-known phenomenon in submarine operations where, during low speed depth keeping, there is a need to reverse the direction of dive plane deflection in order to execute a given change in depth. Physically, this can be explained by considering the relative magnitude of the hydrodynamic forces. At moderate and high speeds, the normal force on the submarine's hull due to the angle of attack exceeds the normal dive plane force and the boat responds to ordered dive plane angles as expected. The phenomenon of dive plane reversal occurs at speeds below a certain critical speed in which the normal hull force is less than the normal dive plane force and the response of the boat is reversed. [Ref. 14] Vehicle modeling in this work follows standard notation [Ref. 15] and numerical results are presented for the DARPA SUBOFF model [Ref. 16] for which a set of hydrodynamic coefficients and geometric properties is available. Special emphasis is given to identifying the proper non-dimensional parameters in the problem, so that extension of these results to full scale models and other designs is possible using minimal experimental and/or analytical results.

II. VEHICLE MODELING

A. EQUATIONS OF MOTION

1. Introduction

For the purpose of this problem, and the subject of the maneuvering and motion control of the vehicle, the following assumptions are made:

1) The vehicle behaves as a rigid body;
2) The earth's rotation is negligible as far as acceleration components of the center of mass are concerned;
3) The primary forces that act on the vehicle have inertial, gravitational, hydrostatic and hydrodynamic origins.

2. Coordinate Systems And Positional Definitions

A global navigation frame, $OXYZ$, as shown in Figure 2.1, is defined with origin, O, and a set of axes aligned with directions North, East and Down. This produces a right-hand reference frame with unit vectors $\bar{I}$, $\bar{J}$, and $\bar{K}$. Ignoring the earth's rotation rate in comparison to the angular rates produced by the vessel's motion, it can be said that the $\bar{I}$, $\bar{J}$, and $\bar{K}$ coordinate frame is an inertial reference frame in which Newton's Laws of Motion will be valid. As seen in Figure 2.1, a vehicle's position $\bar{R}_o$, in this frame will have the vector components, $\bar{R}_o = [X_0\bar{I} + Y_o\bar{J} + Z_o\bar{K}]$. A standard convention that is used in both aircraft and marine vehicle dynamics places the Y axis to the right while looking along the X axis, and the Z axis is positive downwards. Figure 2.1 also shows a vehicle with some general attitude in the original coordinate system.

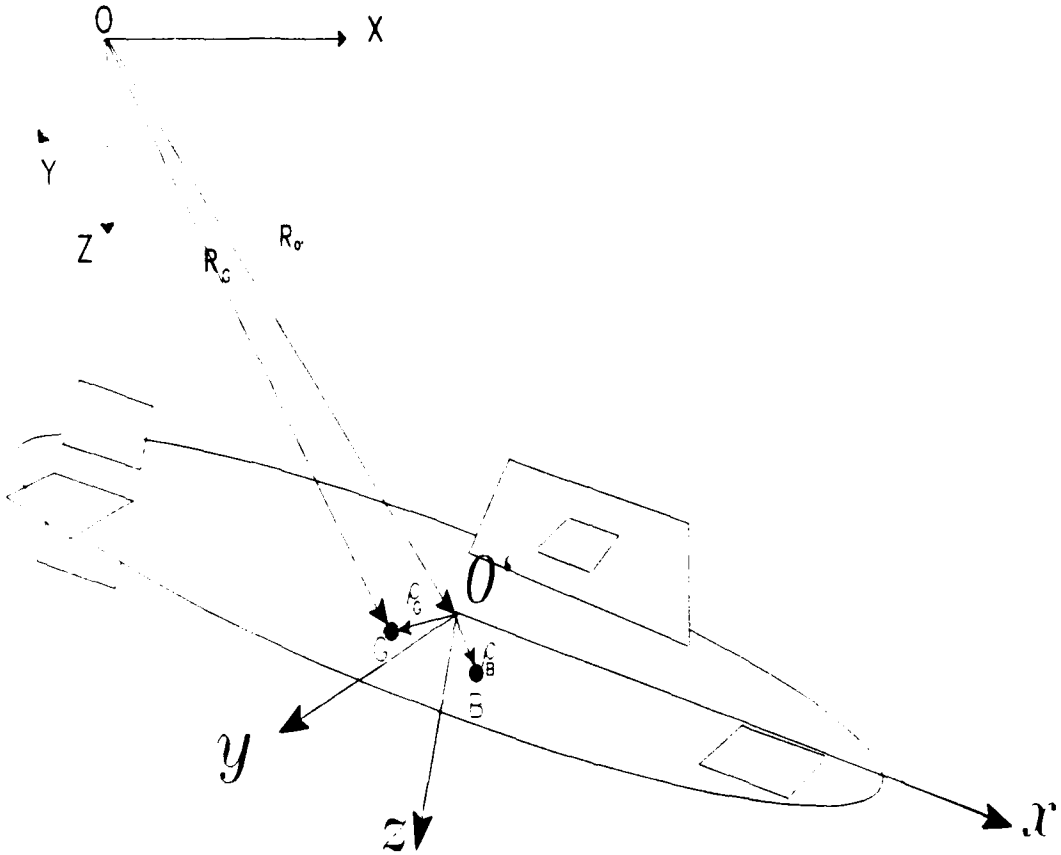

Figure 2-1. Coordinate Axes Convention.

Now define a body fixed frame of reference O'_{xyz}, with the origin O', located on the vehicle centerline, moving and rotating with the vehicle, in which the vehicle's center of mass, G, has some position other than the origin of the vehicle fixed frame (refer to Figure 2-1). This origin will be the point about which all vehicle body force will be computed in later sections of this chapter. The convention used for the vehicle fixed frame, with unit vectors $\vec{i}$, $\vec{j}$, $\vec{k}$, is that its origin lies at the ship's center (origin at the half length), the x axis at main deck level, parallel to the longitudinal centerline, with the z axis vertically down. The vessel's center of gravity and center of buoyancy do not generally lie at the origin of the body fixed frame, nor are they collocated. These points are denoted by G and B respectively. The vector components of $\vec{\rho}_G$ and $\vec{\rho}_B$ are thus $[x_G\vec{i} + y_G\vec{j} + z_G\vec{k}]$, and $[x_B\vec{i} + y_B\vec{j} + z_B\vec{k}]$. The location of the center of mass is important because Newton's Laws of Motion equate forces on a body to the rate of change of linear momentum of the center of mass and moments about the body center of mass to the rate of change of angular momentum. This is a particularly important point to bear in mind for ship and submarine motion dynamics as the center of buoyancy is determined by the shape of the submerged portion of the ship body while the center of gravity is determined by the distribution of the weight over the entire ship body. Having defined a coordinate system that will be used to describe a ship's position, there is a need to define angular orientation of the ship's body, leading to the definition of translational and rotational velocities and accelerations.

3. Angular Position In The Global Reference Frame

There are several different ways that the attitude of a vehicle can be described in reference to the global frame. The most usual and common method is to define three angles, called Euler angles that uniquely define the angular orientation of the vehicle reference frame, relative to the global reference frame. One problem with the Euler angle

approach is that a singularity exists when one of the angles reaches 90 degrees (an aircraft in pure vertical flight cannot distinguish its azimuth angle from its roll angle). This limitation which can sometimes, although rarely, cause trouble in flight simulations and control computations can be overcome by the use of quaternions which introduce four rather than three variables to describe angular position. In this presentation, however, we will use Euler angles as it is the most widely used method, although the use of quaternions has found favor in robotics applications and computer graphics.

While any consistent definition of three base angles would be sufficient, the most convenient formulation of these angles is in the widely used military terms of an azimuth, elevation, and spin notation. The rates of change of these angles do not generally correspond to the other commonly used angular rates describing angular velocity of a vehicle, that is yaw rate, pitch rate and roll rate except, as will be seen, where motion is limited to small angle rotations.

4. Rotational Transformations

Vehicle attitude is important in defining position. Under dynamic conditions, the pitch or roll can cause problems for manned vessels and the heading is critical in navigation. For the purpose of considering angular rotations, consider a forward transformation from a coordinate triad aligned with the global reference frame and perform a sequence of three rotations to finally align the result with a frame that is assumed to be parallel to the vehicle body coordinate axes, and moving with the vehicle at all times. Begin by defining an azimuth rotation, ψ, as a positive rotation about the global Z axis. Next define a subsequent rotation θ, (positive up) about the new Y axis, followed by a positive rotation ϕ, about the new X axis. The triple rotational transformation in terms of these three angles, is then sufficient to describe the angular orientation of the vehicle at any time. It follows that any position vector, $\bar{R}_o$, in an original reference frame given by

$\bar{R}_o = [x_o, y_o, z_o]'$, will have different coordinates in a rotated frame when an azimuth rotation by angle ψ, is made about the global Z axis.

If the new position is defined by, $\bar{R}_1 = [x_1, y_1, z_1]'$, it can be seen that there is a relation between the vector's coordinates in the new reference frame with those that it had in the old reference frame. Using trigonometrical relationships and Figure 2.2 as a guide, it follows that,

$$X_1 = X_o \cos\psi + Y_o \sin\psi \tag{2.1}$$

$$Y_1 = -X_o \sin\psi + Y_o \cos\psi . \tag{2.2}$$

This relation can be expressed in matrix form by the rotation matrix operation,

$$\bar{R}_1 = \left[T_{\psi,Z}\right]\bar{R}_o; \tag{2.3}$$

where the rotation matrix $\left[T_{\psi,Z}\right]$, represents an orthogonal transformation. Premultiplication of this rotation matrix with any vector, $\bar{R}_o$, will produce the components of the same vector in the rotated coordinate frame. Continuing with the series of rotations results in a combined total rotation transformation,

$$T(\phi,\theta,\psi) = T(\phi)T(\theta)T(\psi). \tag{2.4}$$

In expanded notation equation 2.4 takes the form;

$$\begin{bmatrix} \cos\psi\cos\theta & \sin\psi\cos\theta & -\sin\theta \\ \cos\psi\sin\theta\sin\phi - \sin\psi\cos\phi & \sin\psi\sin\theta\sin\phi + \cos\psi\cos\phi & \cos\theta\sin\phi \\ \cos\psi\sin\theta\cos\phi + \sin\psi\sin\phi & \sin\psi\sin\theta\cos\phi - \cos\psi\sin\phi & \cos\theta\cos\phi \end{bmatrix},$$

and it can be said that any position vector in an original reference frame may be expressed in a rotated frame with coordinates given by the operation,

$$\bar{R}_{new} = \left[T(\phi,\theta,\psi)\right]\bar{R}_{old}. \tag{2.5}$$

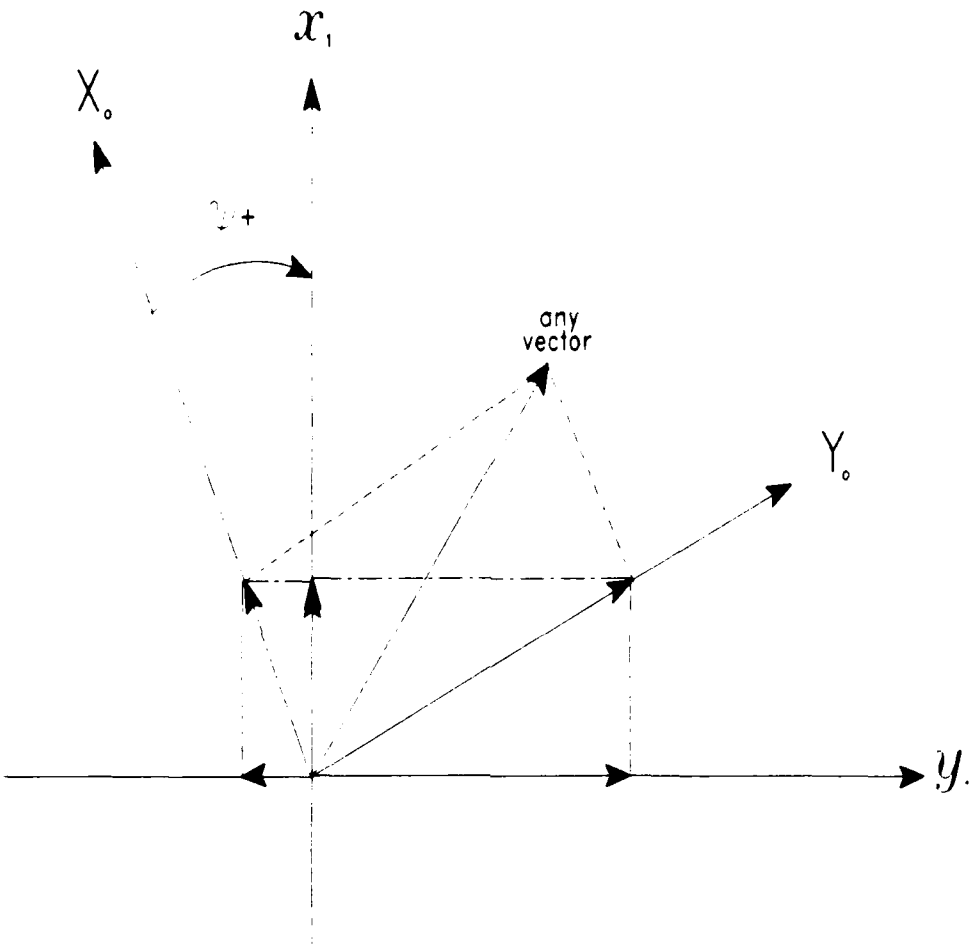

Figure 2-2. Azimuth Rotation.

5. Kinematics

Kinematics deals with the relationships of motion quantities regardless of the forces induced by their prescribed motions. Descriptions of a ship's position both translational and rotational, will need to be related to velocities, both translational and rotational, prior to extending the situation to accelerations. The connection between translational velocity and the rate of change of translational position is straight forward. Define the global velocity as,

$$\dot{\bar{R}} = \begin{bmatrix} \dot{X} \\ \dot{Y} \\ \dot{Z} \end{bmatrix} \tag{2.6}$$

This vector will have components that are different when seen in a body fixed frame. Define the body fixed components of the global velocity vector as [u, v, w]'. These components, in terms of the above global quantities are given by the forward transformation defined earlier to be,

$$\begin{bmatrix} u \\ v \\ w \end{bmatrix} = T(\phi,\theta,\psi) \begin{bmatrix} \dot{X} \\ \dot{Y} \\ \dot{Z} \end{bmatrix} \tag{2.7}$$

It is a simple reverse coordinate transformation from body fixed to global coordinates to see that,

$$\begin{bmatrix} \dot{X} \\ \dot{Y} \\ \dot{Z} \end{bmatrix} = T^{-1}(\phi,\theta,\psi) \begin{bmatrix} u \\ v \\ w \end{bmatrix} \tag{2.8}$$

This shows that the progression of a vehicle in a global frame clearly depends on its local velocity components and its attitude. Put simply, u corresponding to a vehicle's forward

speed (surge), v corresponding to a side slip velocity (sway), and w corresponding to any velocity component in the local Z direction (heave) and the vehicle's global velocity components depend on heading, pitch, and roll attitude.

The connection between angular attitude and angular velocity is not quite so apparent. At first sight, it is tempting to define the instantaneous angular velocity of the vehicle simply as the rate of change of its angular position defined by the Euler angles. This is erroneous however, because the rotation θ, was defined as a rotation about the intermediate frame after a rotation ψ had been made. Vehicle inertial angular rates are defined in terms of components that have angular velocities about the global axes. It is necessary to relate both Euler angles and their rates of change to angular velocity components about the global axes to their components lying along the body fixed axes in any attitude. The prime reason for this is that it is difficult to construct physical sensors to measure rates of change of Euler angles. However, rate gyros in common use today are easily constructed to measure the components of the inertial angular velocity of a vehicle that lie along the vehicle's body axes. It follows that the instantaneous angular velocity of the vehicle can be related to the instantaneous rate of change of angular orientation only after considerations of the intermediate transformations used. In other words, if α is defined as the angular attitude vector, $\alpha = [\psi, \theta, \phi]$, and the inertial components of the vehicle angular rate lying along the body axes as $\omega = [p, q, r]$; then, $\dot{\alpha} = f(\omega)$. The details of the nonlinear functional relations involved are provided by viewing the rate of change of the rotation ψ as a vector quantity lying along the original Z axis. The rate of change of the angle θ is viewed as a vector quantity lying along the Y axis of the first intermediate frame, and the rate of change of the angle ϕ is viewed as a vector lying along the X axis of the final (body fixed) frame. Each of these component rates of change of angular position has component parts that project onto the final frame and it is the sum total of all the

components that give the total angular velocity as seen in the final frame of reference. Using the required transformations for the rate components from each Euler angle, we get,

$$\begin{bmatrix} p \\ q \\ r \end{bmatrix} = \sum T(\phi)T(\theta)T(\psi)\begin{bmatrix} 0 \\ 0 \\ \dot{\psi} \end{bmatrix} + T(\phi)T(\theta)\begin{bmatrix} 0 \\ \dot{\theta} \\ 0 \end{bmatrix} + T(\phi)\begin{bmatrix} \dot{\phi} \\ 0 \\ 0 \end{bmatrix}, \tag{2.9}$$

with the result,

$$\begin{bmatrix} p \\ q \\ r \end{bmatrix} = \begin{bmatrix} -\dot{\psi}\,sin\theta + \dot{\phi} \\ \dot{\psi}\,sin\theta + \dot{\theta}\,cos\phi \\ \dot{\psi}\,cos\theta\,cos\phi - \dot{\theta}\,sin\phi \end{bmatrix}. \tag{2.10}$$

Inverting equation 2.10 yields a solution for the rates of change of the Euler angles in terms of the body fixed components of the angular velocity vector,

$$\begin{bmatrix} \dot{\phi} \\ \dot{\theta} \\ \dot{\psi} \end{bmatrix} = \begin{bmatrix} p + q\,sin\phi\,tan\theta + r\,cos\phi\,tan\theta \\ q\,cos\phi - r\,sin\phi \\ (q\,sin\phi + r\,cos\phi)\ \ cos\theta \end{bmatrix}. \tag{2.11}$$

Notice that for small angular rotations, as expected,

$$\dot{\phi} = p;$$
$$\dot{\theta} = q;$$
$$\dot{\psi} = r.$$

At this point the kinematic relationships between velocities, as seen in the body fixed frame, and the rates of change of global positions and Euler angles have been defined. The resulting set of differential equations forms a consistent set in that given a set of vehicle velocity data versus time, its position and attitude may be computed.

6. Translational Equations Of Motion

The global acceleration of the center of mass is derived by differentiating the velocity vector, $\dot{\vec{R}}_G$, taking into account that the center of mass lies in a rotating reference frame Considering the total differentiation, the global acceleration of the center of mass becomes,

$$\ddot{\vec{R}}_G = \dot{\vec{v}} + \dot{\vec{\omega}} \times \vec{\rho}_G + \vec{\omega} \times \vec{\omega} \times \vec{\rho}_G + \vec{\omega} \times \vec{v}, \tag{2.12}$$

where $\vec{v} = \dot{\vec{R}}_o$ The translational equation of motion is found by equating this acceleration to the net sum of all forces acting on the vehicle in three degrees of freedom (X,Y,Z). One important factor to recognize is that the equation of motion derived in this manner is a vector equation with the components expressed in the body fixed frame and unit vectors $\vec{i}$, $\vec{j}$ and $\vec{k}$ This has been deliberately done because the dominant forces acting on a submerged body in motion are developed in relation to the shape of the vehicle and are more conveniently expressed in relation to the body axes. Equating the applied force vector to the acceleration results in,

$$\vec{F} = m\{\dot{\vec{v}} + \dot{\vec{\omega}} \times \vec{\rho}_G + \vec{\omega} \times \vec{\omega} \times \vec{\rho}_G + \vec{\omega} \times \vec{\rho}_G\}. \tag{2.13}$$

The applied force vector is composed of gravitational (weight) and hydrostatic (buoyancy) forces together with any hydrodynamic forces arising from relative motion between the vehicle and the ocean water particles These will be discussed in further detail in following sections

7. Rotational Equations Of Motion

To develop the rotational equations of motion, the sum of applied moments about the vehicle's center of mass is equated to the rate of change of angular momentum of the vehicle about its center of mass. This equating will provide the necessary equations of motion for the remaining three degrees of freedom. In the practical case of marine vehicles, however, the statement just made is modified slightly because it is much more

difficult to assess the vehicle's mass moments of inertia about its center of gravity (CG) As the CG changes with loading; it becomes simpler to evaluate the mass moments of inertia about the body fixed frame which lies along the axes of symmetry of the vehicle in most cases. The mass moments of inertia for the vehicle to be computed are,

$$I_o = \begin{bmatrix} I_{xx} & I_{xy} & I_{xz} \\ I_{yx} & I_{yy} & I_{yz} \\ I_{zx} & I_{zy} & I_{zz} \end{bmatrix}. \tag{2.14}$$

The angular momentum of the body is thus;

$$\vec{H}_o = I_o \vec{\omega}, \tag{2.15}$$

resulting in the total applied moments about the origin given by,

$$\vec{M}_o = \dot{\vec{H}}_o + \vec{\rho}_G \times (m\ddot{\vec{R}}_G). \tag{2.16}$$

Since the rate of change of angular momentum is given by,

$$\dot{\vec{H}}_o = I_o \dot{\vec{\omega}} + \vec{\omega} \times \vec{H}_o, \tag{2.17}$$

and the acceleration of the global position vector is given by,

$$\ddot{\vec{R}}_o = \dot{\vec{v}} + \vec{\omega} \times \vec{v}, \tag{2.18}$$

then the rotational equation of motion in vector terms is given by,

$$\vec{M}_o = I_o \dot{\vec{\omega}} + \vec{\omega} \times (I_o \vec{\omega}) + m\{\vec{\rho}_G \times \dot{\vec{v}} + \vec{\rho}_G \times \vec{\omega} \times \vec{v}\}. \tag{2.19}$$

The applied moments about the body fixed frame arise from a static balance of weight and buoyancy effects to achieve the proper trim and heel, and hydrodynamic moments from the forces applied through appendages such as control fins, hydrodynamic effects from waves, and hydrodynamic effects from relative motion between the vehicle and the water.

At this point, there are three translational equations obtained from equation 2.13, three rotational equations obtained from equation 2.19, and six unknown velocities ($\vec{\omega}$ and $\vec{v}$). In itself this is a consistent set of dynamic equations if the weight and buoyancy

terms are always self canceling. However, with weight and buoyancy being applied in a global vertical direction, and also being applied at different locations, they represent forces that are dependent on the attitude of the vehicle. Notice that without weight and buoyancy forces, the six consistent equations expressed in the body fixed frame of the vehicle could be solved for the vehicle's velocity (given applied force descriptions). With weight and buoyancy acting, we need additional equations (constraints) that will link vehicle attitude to motion so that the combined set of equations can be solvable. The constraints to be used are developed using the Euler angles which are a general set of angles used to define the attitude of the rigid body. From these angles a relationship between rate of change of attitude and the body rotational rates given earlier as the angular velocity vector $\bar{\omega} = [p, q, r]$, can be developed.

8. Incorporation Of Vertical Forces Into The Equation Of Motion

The weight and buoyant forces that act at the centers of gravity and buoyancy must be defined from static analyses. For submerged bodies the weight and buoyancy force vectors do not change with vehicle attitude. For a surface ship, B will change with attitude, and the righting moments must be computed from Naval Architectural considerations. Assuming that weight and buoyancy are fixed in relation to the body fixed frame, $\bar{W} = 0\bar{I} + 0\bar{J} + (mg)\bar{K}$, and $\bar{B} = 0\bar{I} + 0\bar{J} - (\rho\nabla)\bar{K}$. Since the weight and buoyancy terms in the applied forces act in the global vertical direction, they must be transformed into components in the vehicle fixed frame before they can be added into the equations of motion. Returning to equation 2.4, we therefore find the components along the vehicle fixed frame to be the third column of that transformation matrix. The net vertical force components become,

$$\bar{f}_g = (W - B)\begin{bmatrix} -sin\theta \\ cos\theta sin\phi \\ cos\theta cos\phi \end{bmatrix}. \tag{2.20}$$

The weight portion of the vertical force acts at the center of gravity of the vehicle. The buoyancy portion of the vertical force acts at the center of buoyancy. Because these forces act at positions away from the body center they exhibit a moment about the body center given by,

$$\bar{m}_g = W\bar{\rho}_G \times \begin{bmatrix} -sin\theta \\ cos\theta sin\phi \\ cos\theta cos\phi \end{bmatrix} - B\bar{\rho}_B \times \begin{bmatrix} -sin\theta \\ cos\theta sin\phi \\ cos\theta cos\phi \end{bmatrix}. \tag{2.21}$$

This moment will not be zero even if W and B are identical because it is not usually the case that $\bar{\rho}_G$ and $\bar{\rho}_B$ are collocated. For static stability it is advisable to locate the center of gravity below the center of buoyancy The total vertical force vector can be written as,

$$\bar{F}_G = \begin{bmatrix} f_G \\ m_G \end{bmatrix}, \tag{2.22}$$

and is added negatively to the left hand side of the equations of motion

9. Development Of The Full Six Degrees Of Freedom Non-Linear Equations Of Motion For A Marine Vehicle

Define a vector $\bar{x}$ of vehicle body frame velocities to be, $\bar{x} = [u, v, w, p, q, r]$, and a vector $\bar{z}$ of global positions to be $\bar{z} = [X, Y, Z, \phi, \theta, \psi]$, then considering **M** as a 6×6 mass matrix including translational and rotational inertial elements, the equations of motion can be written in the following vector form,

$$M\dot{\bar{x}} + f(x) + \bar{F}_g(z) = \bar{F}_h \tag{2.23}$$

and,

$$\dot{\bar{z}} + g(x, z) = 0 \tag{2.24}$$

Therefore with suitable knowledge of the excitation force and moment loads, $\bar{F}_h$, as a function of time and/or vessel motion, a solution for the vehicle's dynamics can be obtained. A more detailed insight into the development of the twelve differential equations, in first order form given by the foregoing analysis shows,

$$m\{\dot{\bar{v}} + \dot{\bar{\omega}} \times \bar{\rho}_G\} + m(\bar{\omega} \times \bar{\omega} \times \bar{\rho}_G + \bar{\omega} \times \bar{v}) + \bar{f}_G(z) = \begin{bmatrix} X_f \\ Y_f \\ Z_f \end{bmatrix}, \tag{2.25}$$

and,

$$I_o\dot{\bar{\omega}} + m\{\bar{\rho}_G \times \dot{\bar{v}}\} + \bar{\omega} \times (I_o\bar{\omega}) + m\{\bar{\rho}_G \times \bar{\omega} \times \bar{v}\} + \bar{m}_g(z) = \begin{bmatrix} K_f \\ M_f \\ N_f \end{bmatrix} \tag{2.26}$$

It helps here to define the cross product coefficient matrix so that,

$$\dot{\bar{\omega}} \times \bar{\rho}_G = -\bar{\rho}_G \times \dot{\bar{\omega}} = -[\mathrm{cros}(\bar{\rho}_G)]\dot{\bar{\omega}} \tag{2.27}$$

where,

$$[\mathrm{cros}(\bar{\rho}_G)] = \begin{bmatrix} 0 & z_G & -y_G \\ -z_G & 0 & x_G \\ y_G & -x_G & 0 \end{bmatrix} \tag{2.28}$$

Now collecting the mass matrix coefficients into a 6×6 matrix including the inertia cross coupling effects, results in the following equation,

$$M = \begin{bmatrix} \begin{bmatrix} m & 0 & 0 \\ 0 & m & 0 \\ 0 & 0 & m \end{bmatrix} & m\begin{bmatrix} 0 & z_G & -y_G \\ -z_G & 0 & x_G \\ y_G & -x_G & 0 \end{bmatrix} \\ m\begin{bmatrix} 0 & -z_G & y_G \\ z_G & 0 & -x_G \\ -y_G & x_G & 0 \end{bmatrix} & \begin{bmatrix} I_{xx} & I_{xy} & I_{xz} \\ I_{yx} & I_{yy} & I_{yz} \\ I_{zx} & I_{zy} & I_{zz} \end{bmatrix} \end{bmatrix}. \tag{2.29}$$

The remaining terms on the left hand side of the equations of motion arising from the centripetal and coriolis accelerations become,

$$f(x) = \begin{bmatrix} m(\bar{\omega} \times \bar{\omega} \times \bar{\rho}_G + \bar{\omega} \times \bar{v}) \\ \bar{\omega} \times (I_o \omega) + m\{\bar{\rho}_G \times \bar{\omega} \times \bar{v}\} \end{bmatrix}. \tag{2.30}$$

The double vector cross products are nonlinear in the primary velocity variables and hence the need for the nonlinear functional, $f(\bullet)$ The reader can perform the indicated manipulations to express individual equations within the set if so desired.

The components of the hydrodynamic and external forces and moments acting on the vehicle body are separated in the above analysis into six components each acting along the vehicle body fixed coordinate axes and form the total vector of forces and moments as,

$$\bar{F}_h(t) = [X_f(t), Y_f(t), Z_f(t), K_f(t), M_f(t), N_f(t)]', \tag{2.31}$$

where the vector components in order refer to the surge, sway, heave forces, and the roll, pitch, and yaw moments respectively.

The long form of the six degrees of freedom equations of motion can be written as follows,

$$\begin{aligned} &m[\dot{u} - vr + wq - x_G(q^2 + r^2) + y_G(pq - \dot{r}) + z_G(pr + \dot{q})] = \\ &-(W - B)\sin\theta + X_f \end{aligned} \tag{2.32}$$

$$m[\dot{v}+ur-wp+x_G(pq+\dot{r})-y_G(p^2+r^2)+z_G(qr-\dot{p})]= \\ (W-B)\cos\theta\sin\phi+Y_f \tag{2.33}$$

$$m[\dot{w}-uq+vp+x_G(pr-\dot{q})+y_G(qr+\dot{p})-z_G(p^2+q^2)]= \\ (W-B)\cos\theta\cos\phi+Z_f \tag{2.34}$$

$$I_x\dot{p}+(I_z-I_y)qr+I_{xy}(pr-\dot{q})-I_{yz}(q^2-r^2)-I_{xz}(pq+\dot{r})+ \\ m[y_G(\dot{w}-uq+vp)-z_G(\dot{v}+ur-wp)]=(y_GW-y_BB)\cos\theta\cos\phi \\ -(z_GW-z_GB)\cos\theta\sin\phi+K_f \tag{2.35}$$

$$I_y\dot{q}+(I_x-I_z)pr-I_{xy}(qr+\dot{p})+I_{yz}(pq-\dot{r})+I_{xz}(p^2-r^2)- \\ m[x_G(\dot{w}-uq+vp)-z_G(\dot{u}-vr+wq)]=-(x_GW-x_BB)\cos\theta\cos\phi \\ -(z_GW-z_BB)\sin\theta+M_f \tag{2.36}$$

$$I_z\dot{r}+(I_y-I_x)pq-I_{xy}(p^2-q^2)-I_{yz}(pr+\dot{q})+I_{xz}(qr-\dot{p})+ \\ m[x_G(\dot{v}+ur-wp)-y_G(\dot{u}-vr+wp)]=(x_GW-x_BB)\cos\theta\sin\phi \\ +(y_GW-y_BB)\sin\theta+N_f \tag{2.37}$$

while the kinematic relations for the vehicle rate of change of attitude and motion over the ocean bottom require equations 2.11 and 2.8.

10. Adaptation Of The Non-Linear Equations Of Motion To The Vertical Plane

Restricting the motions of the vehicle to the vertical (dive) plane, the only significant motions that must be incorporated to effectively model the vehicle in the dive plane are, the surge velocity (u), the heave velocity (w), the pitch velocity (q), the pitch angle (θ) and the global depth position (Z). This restriction simplifies the twelve previously developed equations to a system of four non-linear equations of motion, which are;

$$m(\dot{w}-uq-z_Gq^2-x_G\dot{q})=Z_f \tag{2.38}$$

$$I_y\dot{q} + mz_G wq - mx_G(\dot{w} - uq) = M_f \tag{2.39}$$

$$\dot{\theta} = q \tag{2.40}$$

$$\dot{Z} = -u\sin\theta + w\cos\theta \tag{2.41}$$

where,

$$Z_f = Z_{\dot{q}}\dot{q} + Z_{\dot{w}}\dot{w} + Z_q uq + Z_w uw -$$
$$\frac{1}{2}\rho\int_{tail}^{nose} C_D b(x)\frac{(w - xq)^3}{|w - xq|}dx + (W - B)\cos\theta + u^2(Z_{\delta_s}\delta_s + Z_{\delta_b}\delta_b) \tag{2.42}$$

and,

$$M_f = M_{\dot{q}}\dot{q} + M_{\dot{w}}\dot{w} + M_q uq + M_w uw$$
$$-\frac{1}{2}\rho\int_{tail}^{nose} C_D b(x)\frac{(w - xq)^3}{|w - xq|}xdx \tag{2.43}$$
$$-(x_G W - x_B B)\cos\theta - (z_G W - z_B B)\sin\theta + u^2(M_{\delta_s}\delta_s + M_{\delta_b}\delta_b)$$

results from expanding the Z_f and the M_f terms from (2.31) in a first order Taylor series expansion and incorporating both hydrostatic and fluid drag forces.

Equations 2.38, 2.39, 2.40 and 2.41 can be linearized for a level flight path when the dive plane angle is zero, i.e. $\delta_o = 0$. By setting all time derivatives to zero, and neglecting for the moment the hydrodynamic drag terms the following are obtained,

$$Z_w uw + (W - B)\cos\theta = 0 \tag{2.44}$$

$$M_w uw - (x_G W - x_B B)\cos\theta - (z_G W - z_B B)\sin\theta = 0 \tag{2.45}$$

$$q = 0 \tag{2.46}$$

$$-u\sin\theta + w\cos\theta = 0 \tag{2.47}$$

If the assumption is made that the vehicle is neutrally buoyant, then it can be said that $x_G = x_B$ and $W = B$. From this equations 2.44 and 2.45 can be reduced to;

$$Z_w uw = 0 \tag{2.48}$$

$$M_w uw - (z_G - z_B)B\sin\theta = 0, \tag{2.49}$$

which yield the nominal position $w_o = q_o = 0$ and $\sin\theta_o = 0$, resulting in the θ_o solution as either $\theta_o = 0$ or $\theta_o = \pi$. Choosing to linearize around the nominal point $\theta_o = 0$ results in;

$$q^2 = 2q_o q = 0 \tag{2.50}$$

$$wq = w_o q + q_o w = 0 \tag{2.51}$$

$$\sin\theta = \cos\theta_o \theta = \theta \tag{2.52}$$

$$w\cos\theta = (-w_o \sin\theta_o)\theta + (\cos\theta_o)w = w. \tag{2.53}$$

The linear equations of motion are then written as;

$$(m - Z_w)\dot{w} - (Z_{\dot{q}} + mx_G)\dot{q} = Z_w uw + (Z_q + m)uq + Z_\delta u^2\delta \tag{2.54}$$

$$(I_y - M_{\dot{q}})\dot{q} - (M_{\dot{w}} + mx_G)\dot{w} = M_w uw + (M_q - mx_G)uq - (z_G - z_B)W\theta + M_\delta u^2\delta \tag{2.55}$$

$$\dot{\theta} = q \tag{2.56}$$

$$\dot{Z} = -u\theta + w. \tag{2.57}$$

As equations 2.42 and 2.43 show, both Z_δ and M_δ are a linear combination of the respective stern and bow hydrodynamic control surface coefficients and the respective input value of δ. This makes the system of equations as a multiple input system. To reduce this system into a single input system the linear combination of control inputs will be modified into the following form;

$$Z_\delta = (Z_{\delta_S} + \alpha Z_{\delta_S}). \tag{2.58}$$

This will allow a single input δ to control both stern planes and bow planes, and will cause the bow planes to be slaved to the stern planes. This technique is known as dual control The value α will range from -1 to 1. The selection of the value of α will allow the planes to operate as desired for the particular maneuvering condition, i.e., $\alpha = 0$ for no

bow plane control, α = -1 for bow plane and stern plane control opposed to each other, yielding the maximum pitch moment, and α = 1 for bow and stern plane control in the same direction, yielding the maximum heave force.

In state space form these equations can be written as;

$$\begin{bmatrix} \dot{\theta} \\ \dot{w} \\ \dot{q} \\ \dot{Z} \end{bmatrix} = \begin{bmatrix} 0 & 0 & 1 & 0 \\ a_{13}z_{GB} & a_{11}u & a_{12}u & 0 \\ a_{23}z_{GB} & a_{21}u & a_{22}u & 0 \\ -u & 1 & 0 & 0 \end{bmatrix} \begin{bmatrix} \theta \\ w \\ q \\ Z \end{bmatrix} + \begin{bmatrix} 0 \\ b_1u^2 \\ b_2u^2 \\ 0 \end{bmatrix} \delta, \tag{2.59}$$

where the coefficients a_{ij} and b_i are given by;

$$D_v = (m - Z_{\dot{w}})(I_y - M_{\dot{q}}) - (mx_G + Z_{\dot{q}})(mx_G + M_{\dot{w}}) \tag{2.60}$$

$$a_{11}D_v = (I_y - M_{\dot{q}})Z_w + (mx_G + Z_{\dot{q}})M_w \tag{2.61}$$

$$a_{12}D_v = (I_y - M_{\dot{q}})(m + Z_q) + (mx_G + Z_{\dot{q}})(M_q - mx_G) \tag{2.62}$$

$$a_{13}D_v = -(mx_G + Z_{\dot{q}})W \tag{2.63}$$

$$b_1D_v = (I_y - M_{\dot{q}})Z_\delta + (mx_G + Z_{\dot{q}})M_\delta \tag{2.64}$$

$$a_{21}D_v = (m - Z_{\dot{w}})M_w + (mx_G + M_{\dot{w}})Z_w \tag{2.65}$$

$$a_{22}D_v = (m - Z_{\dot{w}})(M_q - mx_G) + (mx_G + M_{\dot{w}})(m + Z_q) \tag{2.66}$$

$$a_{23}D_v = -(m - Z_{\dot{w}})W \tag{2.67}$$

$$b_2D_v = (m - Z_{\dot{w}})M_\delta + (mx_G + M_{\dot{w}})Z_\delta \tag{2.68}$$

and $z_{GB} = z_G - z_B$ is the metacentric height.

This linear system of equations becomes the basis for the control law design in the following section.

B. CONTROL LAW DESIGN

1. Introduction

The control design problem can be stated as follows: Given the system;

$$\dot{x} = Ax + B\delta, \tag{2.69}$$

where the state vector equation is,

$$x = \begin{bmatrix} \theta \\ w \\ q \\ Z \end{bmatrix}, \tag{2.70}$$

how do we find δ, such that the system will behave as desired. The type of control that is of interest in this problem is closed loop control, where δ is a function of the state x. Since the state x is used to determine the control effort $\delta(x)$ it is called feedback control.

2. Pole Placement

A linear full state feedback control law is introduced in the form

$$\delta = -Kx, \tag{2.71}$$

where K is the feedback gain vector to be determined such that the closed loop system of equations 2.69 and 2.71 has the desired system dynamics. Substituting equation 2.71 into equation 2.69 yields,

$$\dot{x} = (A - BK)x. \tag{2.72}$$

The actual characteristic equation of this closed loop system is given by

$$det[A - BK - sI] = 0. \tag{2.73}$$

The gain vector K can be chosen such that the actual characteristic equation assumes any desired set of eigenvalues. If the desired locations of the closed loop poles are chosen at $s = s_i$ for $i=1, \ldots, n$, the desired characteristic equation becomes

$$(s - s_1)(s - s_2)\ldots(s - s_n) = 0 \tag{2.74}$$

The required values of K are obtained by matching coefficients in the two polynomials of the actual and desired characteristic equations.

Consider the previously developed linear state matrix equation 2.59. Substituting equation 2.71 into equation 2.59 results in the closed loop system

$$\begin{bmatrix} \dot{\theta} \\ \dot{w} \\ \dot{q} \\ \dot{Z} \end{bmatrix} = \begin{bmatrix} 0 & 0 & 1 & 0 \\ a_{13}z_{GB} - b_1u^2k_1 & a_{11}u - b_1u^2k_2 & a_{12}u - b_1u^2k_3 & -b_1u^2k_4 \\ a_{23}z_{GB} - b_2u^2k_1 & a_{21}u - b_2u^2k_2 & a_{22}u - b_2u^2k_3 & -b_2u^2k_4 \\ -u & 1 & 0 & 0 \end{bmatrix} \begin{bmatrix} \theta \\ w \\ q \\ Z \end{bmatrix} \tag{2.75}$$

The characteristic equation of the closed loop system is given by

$$det \begin{vmatrix} -s & 0 & 1 & 0 \\ a_{13}z_{GB} - b_1u^2k_1 & a_{11}u - b_1u^2k_2 - s & a_{12}u - b_1u^2k_3 & -b_1u^2k_4 \\ a_{23}z_{GB} - b_2u^2k_1 & a_{21}u - b_2u^2k_2 & a_{22}u - b_2u^2k_3 - s & -b_2u^2k_4 \\ -u & 1 & 0 & -s \end{vmatrix} = 0, \tag{2.76}$$

which after some algebra reduces to

$$\begin{aligned} s^4 + (A_2k_2 + A_3k_3 - E_1)s^3 + (-B_1k_1 - B_2k_2 - B_3k_3 - B_4k_4 - E_2)s^2 \\ + (-C_1k_1 - C_2k_2 - C_4k_4 - E_3)s + (-D_1k_4 - D_2k_4) = 0 \end{aligned} \tag{2.77}$$

where ,

$$A_2 = -B_4 = b_1u^2 \tag{2.78}$$

$$A_3 = -B_1 = b_2u^2 \tag{2.79}$$

$$B_2 = (a_{22}b_1 - a_{12}b_2)u^3 \tag{2.80}$$

$$B_3 = C_1 = (a_{11}b_2 - a_{21}b_1)u^3 \tag{2.81}$$

$$C_2 = D_1 = (a_{23}b_1 - a_{13}b_2)z_{GB}u^2 \tag{2.82}$$

$$C_4 = (a_{22}b_1 + b_2 - a_{12}b_2)u^3 \tag{2.83}$$

$$D_2 = (a_{11}b_2 - a_{21}b_1)u^4 \tag{2.84}$$

$$E_1 = (a_{11} + a_{22})u \tag{2.85}$$

$$E_2 = a_{23}z_{GB} + (a_{12}a_{21} - a_{11}a_{22})u^2 \tag{2.86}$$

$$E_3 = (a_{13}a_{21} - a_{11}a_{23})z_{GB}u \tag{2.87}$$

Now if the closed loop poles are placed at $-p_1$, $-p_2$, $-p_3$, and $-p_4$, then the desired characteristic equation is,

$$(s+p_1)(s+p_2)(s+p_3)(s+p_4) = 0, \tag{2.88}$$

or

$$s^4 + \alpha_1 s^3 + \alpha_2 s^2 + \alpha_3 s + \alpha_4 = 0 \tag{2.89}$$

with,

$$\alpha_1 = p_1 + p_2 + p_3 + p_4 \tag{2.90}$$

$$\alpha_2 = p_1p_2 + p_1p_3 + p_1p_4 + p_2p_3 + p_2p_4 + p_3p_4 \tag{2.91}$$

$$\alpha_3 = p_1p_2p_3 + p_1p_2p_4 + p_1p_3p_4 + p_2p_3p_4 \tag{2.92}$$

$$\alpha_4 = p_1p_2p_3p_4 \tag{2.93}$$

The control gains can now be computed by equating coefficients of the actual and desired characteristic equations,

$$A_2k_2 + A_3k_3 = -\alpha_1 - E_1 \tag{2.94}$$

$$B_1k_1 + B_2k_2 + B_3k_3 + B_4k_4 = \alpha_2 + E_2 \tag{2.95}$$

$$C_1k_1 + C_2k_2 + C_4k_4 = \alpha_3 + E_3 \tag{2.96}$$

$$(D_1 + D_2)k_4 = \alpha_4 \tag{2.97}$$

Now that a method for computing the gains of a controllable single input system that will place the poles at any desired location has been developed, the selection of pole location must be accomplished.

3. Pole Location Selection

In a typical second order system control law design the transient response specifications will be given. This results in an allowable region in the s-plane where the desired location of the poles can be obtained. For higher order systems the concept of dominant roots can be employed. In selecting poles for a physical system it is necessary to

look at the physics of the system. If the poles are specified too negative, a very small time constant for the control system will result, and the physical system may not be able to react that fast. The control law $u = -Kx$, implies that for a given state x the larger the gain, the larger the required control input. In practice there are limits typically placed on u (actuator size and saturation). Occasional control saturation is not serious and may even be desired. A system that never saturates is in all likelihood over designed.

Considering the control law design to stabilize the submarine to a level flight path at $\theta = 0$ it will be required that the submarine return to level flight, after a small disturbance in θ or Z, within the time it takes for the vehicle to travel three ship lengths. Since the submarine is about 14 feet long and it travels at 5 ft/sec, the required recovery time is about 10 seconds. This means that the time constant is about 3 seconds, and the closed loop poles should be placed at approximately -0.3.

Control design using pole placement is very easy using ***MATLAB***. The appropriate ***MATLAB*** command is **place**, which accepts as inputs the A and B matrices along with a vector of the desired closed loop poles, and returns the gain vector K. Using equation 2.59 with a nominal speed of 5 ft/sec and the vector $p = [-0.3 \;\; -0.31 \;\; -0.32 \;\; -0.33]$, (**place** does not like poles in the exact same location), the gain vector K was calculated using ***MATLAB*** and by simultaneously solving equations 2.94 through 2.97 yielding the same results. Substituting the gain vector and state variable vector into equation 2.71 results in a control law of

$$\delta = -(-0.9917\theta - 0.8333w - 0.6026q + 0.0351Z). \tag{2.98}$$

Using this control law along with equations 2.38 through 2.43 a simulation program was developed to investigate the vehicle's response to initial disturbances, the results of which will be presented in the following chapter.

III. PROBLEM IDENTIFICATION

A. VEHICLE SIMULATIONS

With the control law developed and the vertical plane equations of motion defined, a vehicle simulation program was developed (see Appendix A). This program was used to simulate the vehicle's response at a variety of speeds and initial disturbances. The simulations were conducted with several simplifications applied to the vertical plane equations of motion (E.O.M.), equations 2.38 through 2.43. The simplifications or constraints applied to the E.O.M. were ;

1) to consider the body drag forces negligible,
2) to consider the vehicle to be neutrally buoyant, i.e., (W=B),
3) to assume that the locations of the center of gravity and center of buoyancy, in the X-Y plane, are coincidental, and
4) that the rudder is restricted to ± 23 degrees.

These assumption resulted in the reduction of equations 2.38 through 2.43 to the following system of equations;

$$\begin{bmatrix} 1 & 0 & 0 & 0 \\ 0 & (m-Z_w) & -Z_{\dot{q}} & 0 \\ 0 & -M_w & I_y - M_q & 0 \\ 0 & 0 & 0 & 1 \end{bmatrix} \begin{bmatrix} \dot{\theta} \\ \dot{w} \\ \dot{q} \\ \dot{Z} \end{bmatrix} = \begin{bmatrix} q \\ m(uq + z_G q^2) + Z_q uq + Z_w uw + u^2 Z_\delta \\ m(-z_G wq) + M_q uq + M_w uw - Bz_{GB} \sin\theta + u^2 M_\delta \\ -u \sin\theta + w \cos\theta \end{bmatrix} \quad (3.1)$$

forming the basis of the initial vehicle simulations.

The vehicle's response to small disturbances, as stated earlier, was investigated over a wide range of speeds. A small sample of these simulations is shown in Figures 3-1 through 3-3.

As Figure 3-1 depicts, the vehicle returns to level flight in approximately 10 seconds. This response is as expected based on the control system design of Chapter II. The simulation results represented in Figure 3-2 also show the vehicle steadying out in a level flight at the desired depth, however the vehicle requires a significant amount of time for this to occur. The reason for this extended amount of time is that the control law gains were set for the nominal operating speed of 5 fps, and the vehicle is being simulated at one-third of that speed. This results in a very slow return to ordered position caused by the reduced hydrodynamic effects at this speed.

The final plot of the sample vehicle simulations, Figure 3-3, illustrates a problem with the vehicle stability. As can be seen, the vehicle does not return to the desired position, but instead steadies out at a pitch angle of eight degrees, with a steady state dive plane value of 23 degrees. This same type of response, but with different pitch angle values, was observed in all the simulations conducted below approximately 1.9 fps. These results indicate that there is a critical point, or speed at which the vehicle stability is affected. Determining this point will be the basis for the remainder of this chapter.

B. CRITICAL SPEED IDENTIFICATION

1. Eigenvalue Analysis

Consider the nonlinear system of state equations 3.1, which can be written in the form,

$$\dot{x} = f(x). \tag{3.2}$$

It is known that the equilibrium points, x_o, of the system are defined by

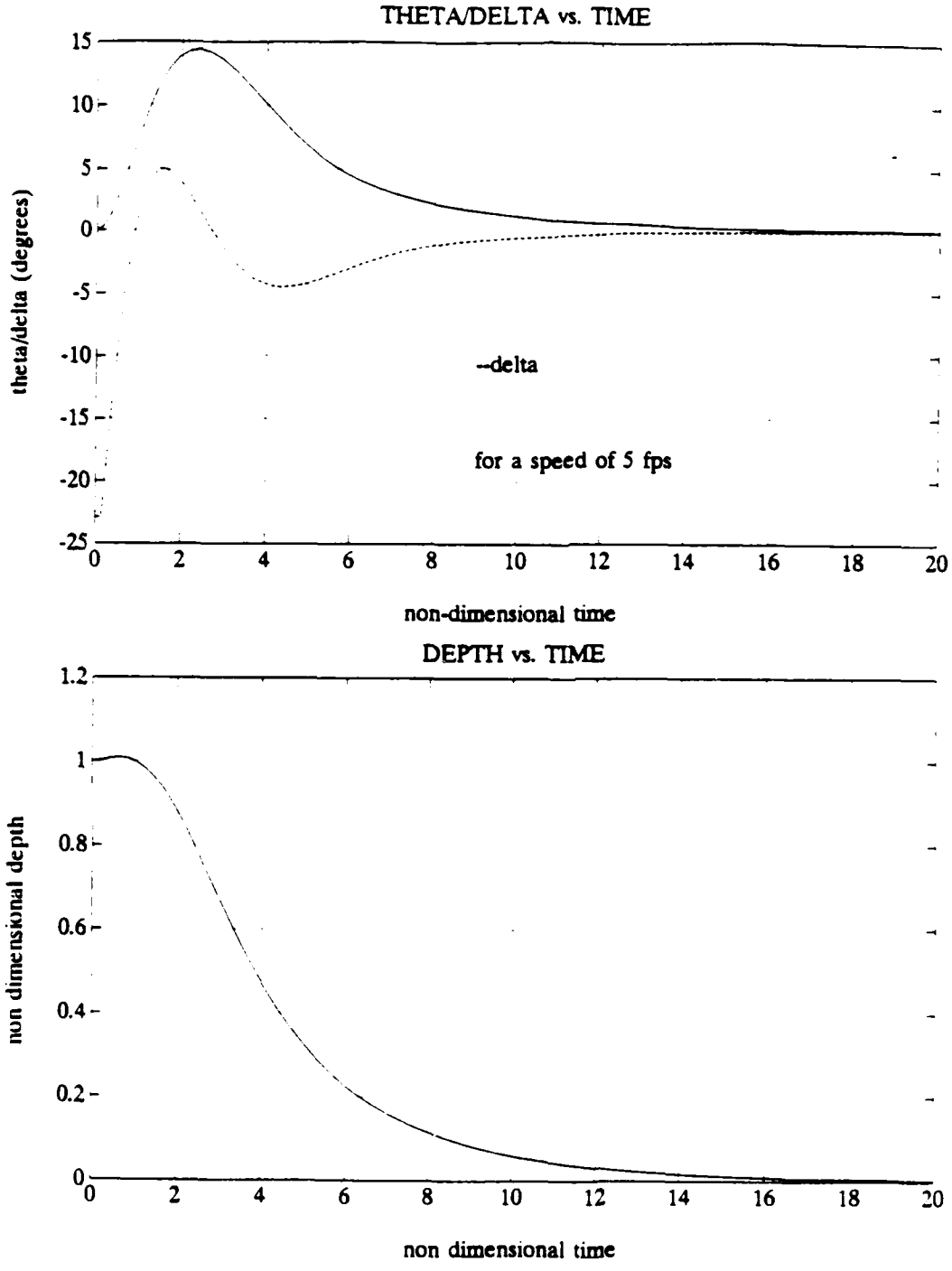

Figure 3-1. Vehicle Response For a Nominal Operating Speed of 5 fps.

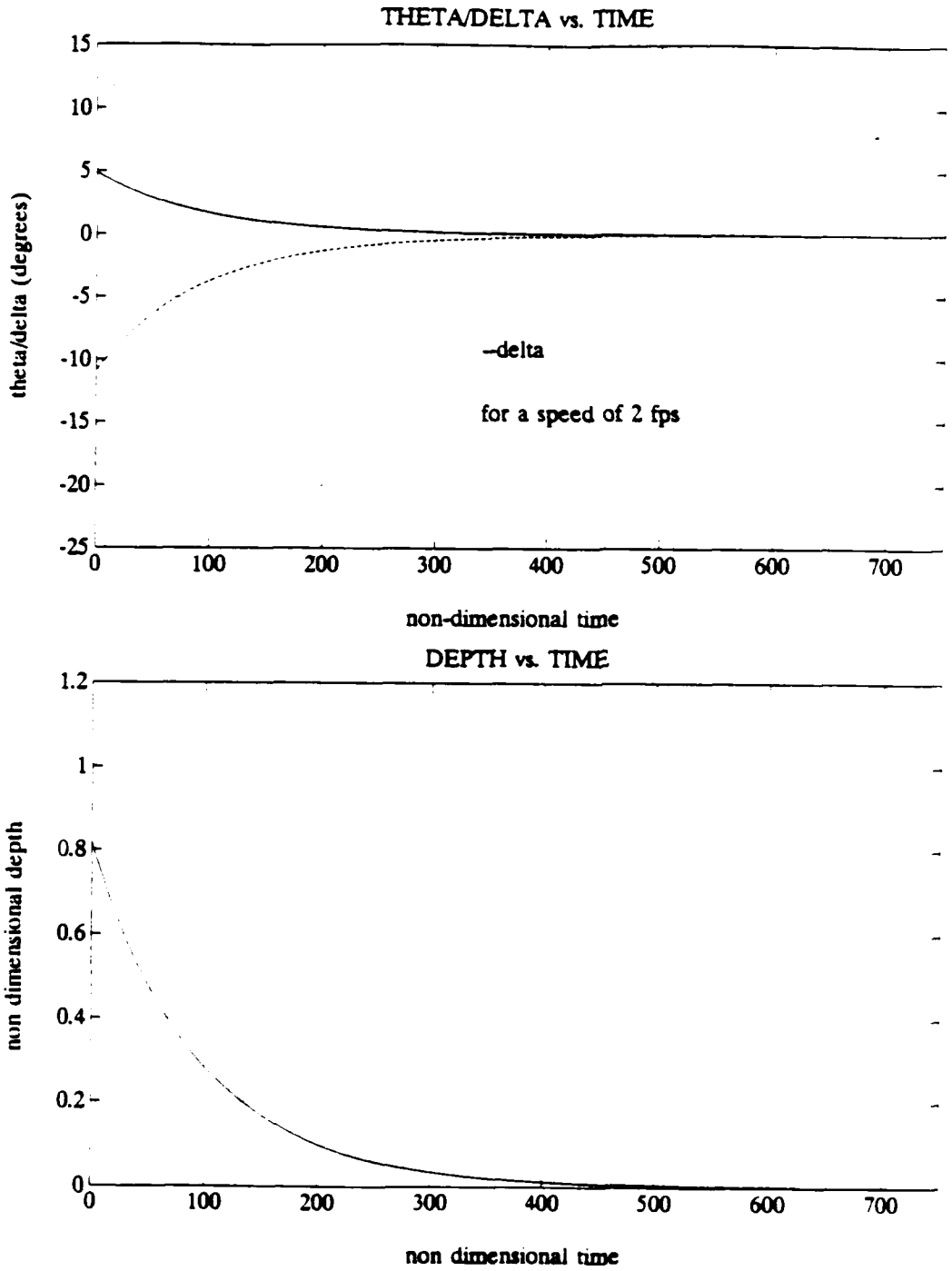

Figure 3-2. Vehicle Response at 2.0 fps.

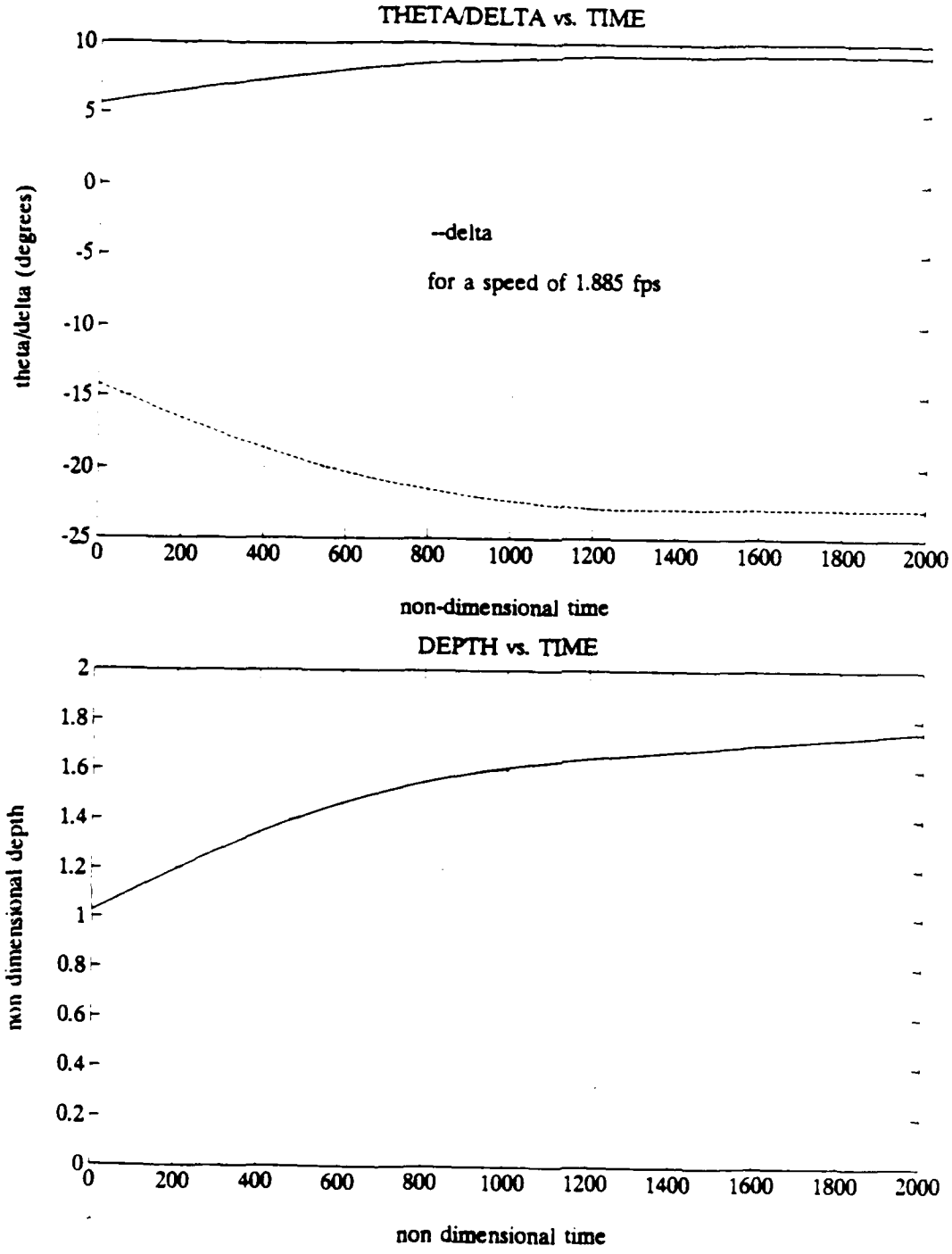

Figure 3-3. Vehicle Response at 1.885 fps.

$$f(x_o) = 0. \tag{3.3}$$

This is a nonlinear system of algebraic equations and it may have multiple solutions in x_o, which means that the nonlinear system of equations may have more than one position of static equilibrium. If one equilibrium value x_o, is selected, the stability properties can be established by linearization. The linearization converts equation 3.2 into the form

$$\dot{x} = Ax, \tag{3.4}$$

where A is the Jacobian matrix of $f(x)$ evaluated at the equilibrium point x_o,

$$A = \left.\frac{\partial f}{\partial x}\right|_{x_o}, \tag{3.5}$$

and the state x has been redefined to designate small deviations from the equilibrium x_o,

$$x \rightarrow x - x_o. \tag{3.6}$$

As long as all eigenvalues of A have negative real parts, the linear system will be stable. This means that the equilibrium x_o will be stable for the nonlinear system as well. This statement is nothing more than Lyapunov's linearization technique.

The question that must be answered is, what happens if one real eigenvalue of the linearized A matrix is zero? The interesting case here is when the rest of the eigenvalues have all negative real parts, otherwise x_o is unstable and the problem is solved. If the case of a zero eigenvalue appears too specialized to be of any practical use, consider this: Assume that $f(x)$ depends on one physical parameter and that physical parameter is allowed to vary over some range. Then clearly A will depend on that parameter and as the parameter varies, it is possible that one real eigenvalue of A will become zero for a specific value of the parameter. The problem is then to establish the dynamics of the nonlinear system as one real eigenvalue of A crosses zero, i.e., goes from negative to positive. As the solution evolves in time, things are interesting only along the direction of the eigenvector that corresponds to the critical eigenvalue. Along the rest of the directions in

the state space, everything should converge back to the equilibrium; remember it was assumed that all remaining eigenvalues of A have real negative parts. Although, strictly speaking, this is a true statement for linear systems, there are technical reasons that force it to be true for nonlinear systems as well, the only difference is that the corresponding directions in the state space are curved instead of straight.

By taking the previously developed characteristic equation 2.77, and remembering that the roots of this equation are the eigenvalues of interest, it is easy to see that if α_4 of equation 2.93, is set equal to zero, then one eigenvalue will be zero. If this is done, and recalling that k_4 holds a non-zero value. equation 2.97 reduces to

$$(a_{11}b_2 - a_{21}b_1)u^2 + z_{GB}(a_{13}b_2 - a_{23}b_1) = 0. \tag{3.7}$$

Since all parameters of equation 3.7 have a fixed value with the exception of u, there must be some value of u that causes the linear A matrix to become unstable. Recognizing this fact will allow equation 3.7 to be solved in terms of u yielding

$$u = \left[\frac{z_{GB}(a_{23}b_1 - a_{13}b_2)}{(a_{11}b_2 - a_{21}b_1)}\right]^{1/2}. \tag{3.8}$$

Using equations 2.60 through 2.68, equation 3.8 can be simplified into the following form;

$$u = \left[\frac{z_{GB}Z_\delta B}{(M_w Z_\delta - Z_w M_\delta}\right]^{1/2}. \tag{3.9}$$

Substituting the appropriate values from Appendix B, equation 3.9 can be solved for the value of u that causes the systems to become unstable. This results in a value of u = 1.8979 fps using an $\alpha = 0$. This value corresponds very closely to the value of 1.9 fps obtained by vehicle simulations.

As a check to this solution, a ***MATLAB*** program was written to compute the closed loop eigenvalues of the matrix equation 2.59 as a function of the speed u Figure 3-4 shows a plot of the real parts of the eigenvalues versus speed. It can be seen that the real part of the eigenvalue, represented by the dash-dot line, becomes positive at speeds less than approximately 1.9 fps supporting the earlier findings. (For clarity purposes, the values of the eigenvalue represented by the dash-dot line were scaled by a factor of ten.)

2. Steady State Analysis

To determine the existence of multiple steady state solutions, for the system represented by equation 2.59, it is necessary to perform a steady state analysis on the system of equations which models the vehicle dynamics. Using matrix equation 3.1, and setting all time derivatives equal to zero, results in the following set of equations;

$$q = 0, \tag{3.10}$$

$$Z_q uq + Z_w uw + u^2 Z_\delta \delta = m(-uq - z_G q^2), \tag{3.11}$$

$$M_q uq + M_w uw - Bz_{GB} \sin\theta + u^2 M_\delta \delta = mz_G wq, \tag{3.12}$$

$$-u \sin\theta + w \cos\theta = 0 \tag{3.13}$$

Simplifying these four equations yields the following two equations in terms of θ, u, and the physical parameters of the vehicle;

$$Z_w u^2 \tan\theta + u^2 Z_\delta \delta = 0 \tag{3.14}$$

$$M_w u^2 \tan\theta - Bz_{GB} \sin\theta + u^2 M_\delta \delta = 0 \tag{3.15}$$

Now if equation 3.14 is multiplied by M_δ, equation 3.15 is multiplied by Z_δ and the two resulting equations are set equal to each other and simplified, the following single equation is obtained,

$$[(Z_w M_\delta - M_w Z_\delta)u^2 + Z_\delta Bz_{GB} \cos\theta] \sin\theta = 0 \tag{3.16}$$

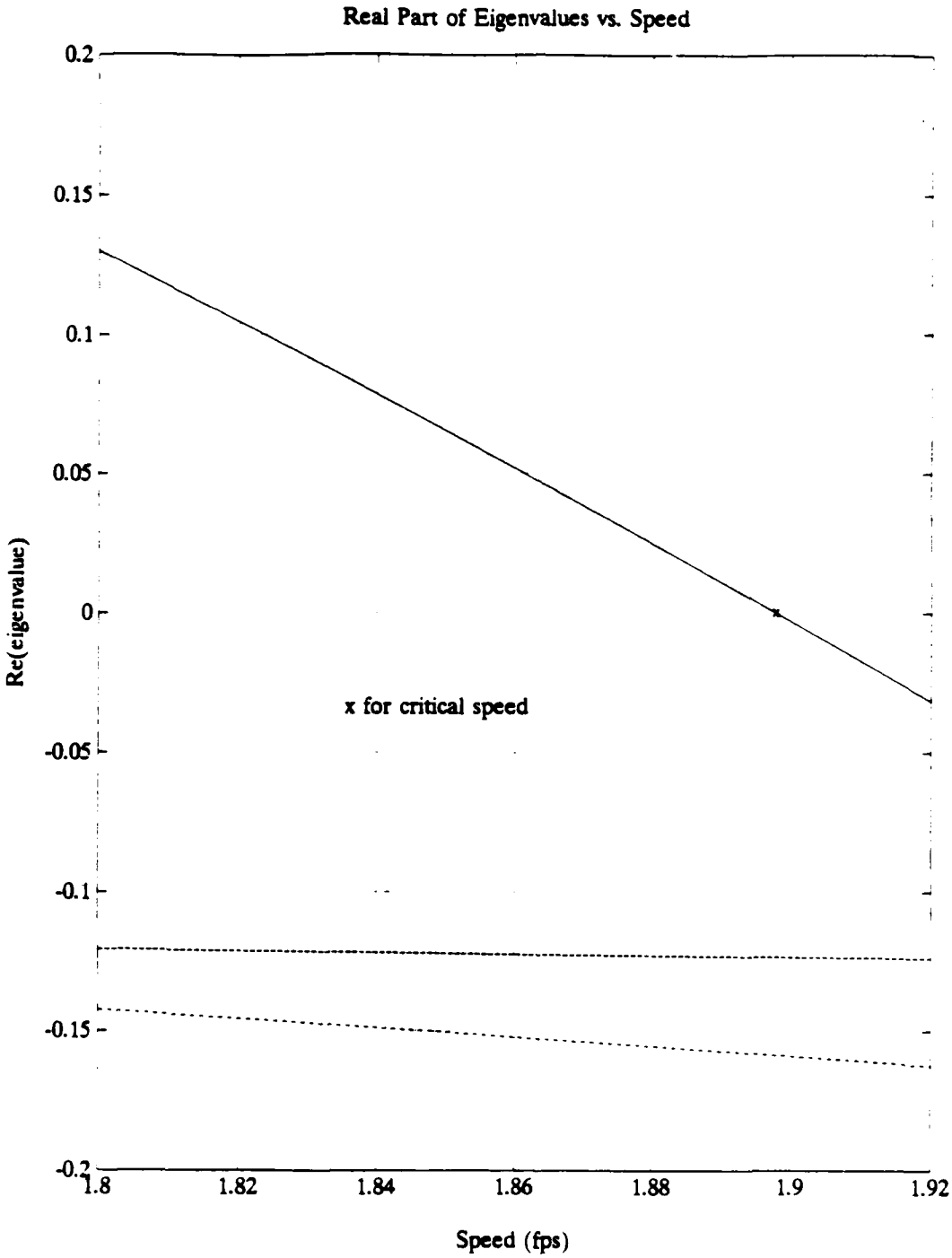

Figure 3-4. Real Part of Closed Loop System Eigenvalues as a Function of Speed.

Through inspection it can be seen that equation 3.16 could have multiple solutions in θ, besides the trivial solution of $\theta = 0$. So, if this equation is rearranged and solved for $\theta \neq 0$, solutions occur when

$$cos\theta = \frac{u^2(M_w Z_\delta - Z_w M_\delta)}{Z_\delta B z_{GB}}. \tag{3.17}$$

Therefore, the steady state value of θ is represented by

$$\theta_{ss} = cos^{-1}\left[\frac{u^2(M_w Z_\delta - Z_w M_\delta)}{Z_\delta B z_{GB}}\right], \tag{3.18}$$

which may have multiple solutions based on the value of the speed u. As discussed previously, these multiple solutions were evident in the simulations conducted earlier in this chapter.

Knowing that the maximum value for $cos\theta$ is equal to one, the right-hand side of equation 3.17 will be true for values less than or equal to one. If this constraint is imposed on 3.17, then the equation may be manipulated into the following form

$$u^2 \leq \frac{Z_\delta B z_{GB}}{(M_w Z_\delta - Z_w M_\delta)}. \tag{3.19}$$

Rearranging this equation and solving for the upper limiting case yields the same results as equation 3.9. Again this supports the critical speed values discussed earlier.

Equation 3.19 can be expressed in a non-dimensional Froude number form by dividing the equation by both the gravitational constant g and the physical parameter z_{GB} and taking the square root of the result. This will convert equation 3.19 into the non-dimensional form given below;

$$Fn = \sqrt{\frac{u^2}{g z_{GB}}} \leq \sqrt{\frac{Z_\delta B}{g(M_w Z_\delta - Z_w M_\delta)}} \tag{3.20}$$

With the steady state θ solution derived, equations for both the steady state value of δ and steady state value of Z can be determined. Using equation 3.14 and substituting the steady state value of θ will allow the steady state δ equation to be obtained;

$$\delta_{ss} = \frac{-Z_w}{Z_\delta} tan\theta_{ss}. \tag{3.21}$$

To achieve the steady state solution of Z, begin by writing equation 2.71 in expanded general form as

$$\delta = -(k_1\theta + k_2 w + k_3 q + k_4 Z). \tag{3.22}$$

Then by applying the same conditions to equation 3.22 that resulted in equations 3.14 and 3.15, and using the previously developed steady state equations for θ and δ, an equation of the form

$$Z_{ss} = \frac{\frac{-Z_w}{Z_\delta} tan\theta_{ss} + k_1\theta_{ss} + k_2 u\, tan\theta_{ss}}{-k_4} \tag{3.23}$$

is obtained.

The loss of stability of an equilibrium and the generation of additional equilibrium states, is called a pitchfork bifurcation and is very common in nature. The buckling of a beam is one such example. Using equations 3.18, 3.21, and 3.23 as a basis for another ***MATLAB*** program, the steady state solutions of θ, δ, and Z versus Froude number were investigated with the results displayed in Figures 3-5 through 3-7. These three plots are referred to as supercritical pitchforks, so named because upon the loss of stability of the trivial equilibrium the additional nearby equilibrium states are stable. Graphically, this can be represented in Figures 3-5 through 3-7, where the solid curves represent stable and dotted curves represent unstable equilibria [Ref. 17]. These three figures also demonstrate the control input saturation. Upon control surface saturation, the

steady state equations for θ, δ and Z are no longer valid due to the limit placed on the maximum plane angle. The steady state equations that hold for this region of saturation are given below;

$$\delta_{ss} = \pm\ 22.9^{\circ}\ (0.4 \text{ radians}), \tag{3.24}$$

$$w_{ss} = \frac{-uZ_{\delta}\delta_{ss}}{Z_{w}}, \tag{3.25}$$

and,

$$\theta_{ss} = sin^{-1}\left[\frac{M_{\delta}u^{2}\delta_{ss} - M_{w}uw_{ss}}{z_{GB}B}\right]. \tag{3.26}$$

As can be seen in Figures 3-5 and 3-6, at an approximate Froude number of 1.05 the control surfaces saturate resulting in the linear solutions displayed below that *saturation* Froude number. In Figure 3-7 there is no steady state solution because if the steady state values of δ and θ are placed into the $\dot{Z}$ equation, $\dot{Z}$ is non-zero below the saturation Froude number.

A parameter introduced in Chapter II was α, which allowed us to go from a multiple input system to a single input system. This parameter has a significant effect on the location of the critical speed and/or Froude number. Figure 3-8 shows the relationship been the critical speed u_{cr} and the metacentric height z_{GB} for different values of α.

These three curves shown in Figure 3-8 can be converted into a single curve by plotting α versus Froude number, and is shown in Figure 3-9. As can be seen in this plot the critical Froude number varies from 0.81 to 1.22 over the allowable range of α

In addition to the effect that α has on the location of the critical Froude number, it also effects the magnitude of the steady state values at a given Froude number and the

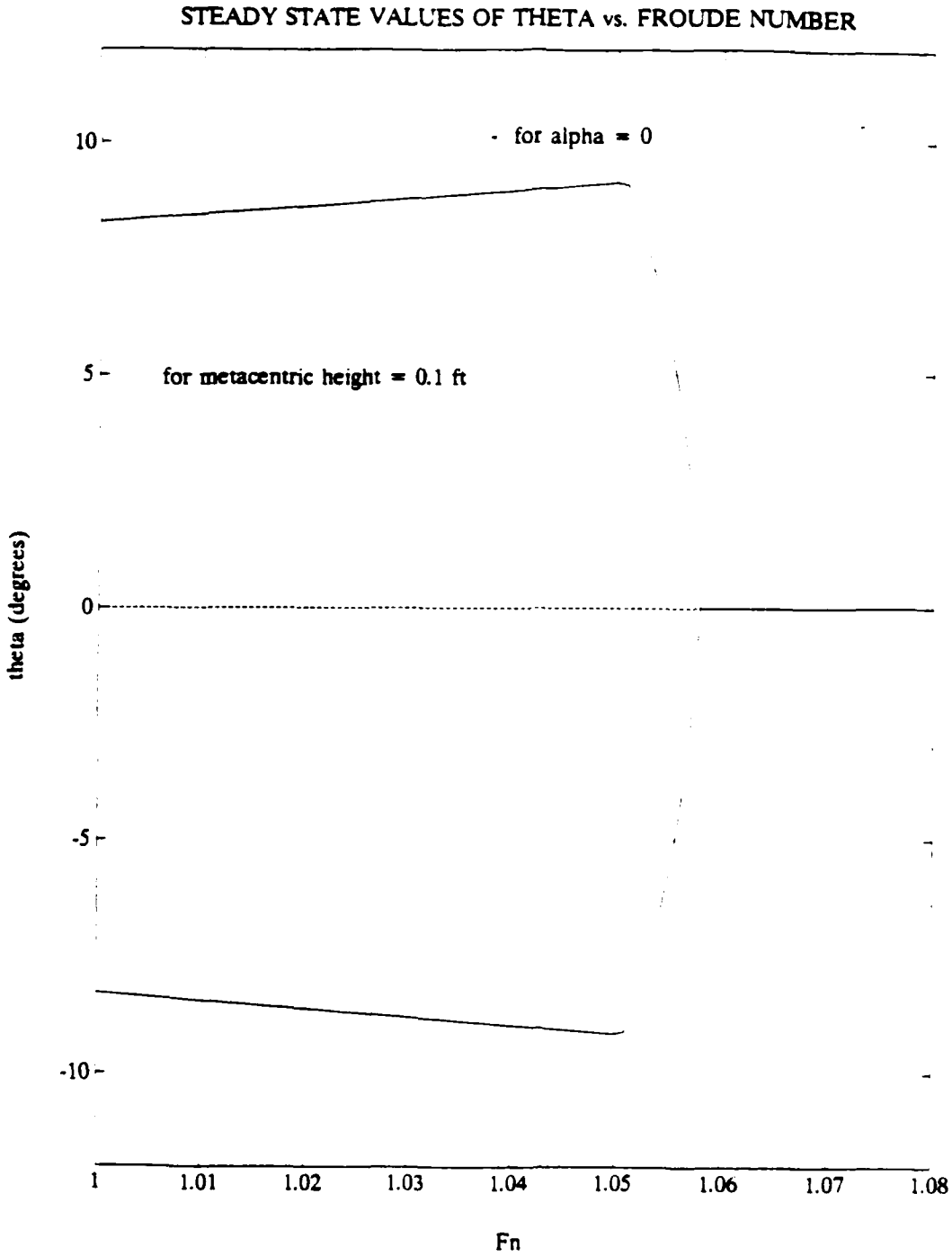

Figure 3-5. Steady State Values of θ vs Froude Number.

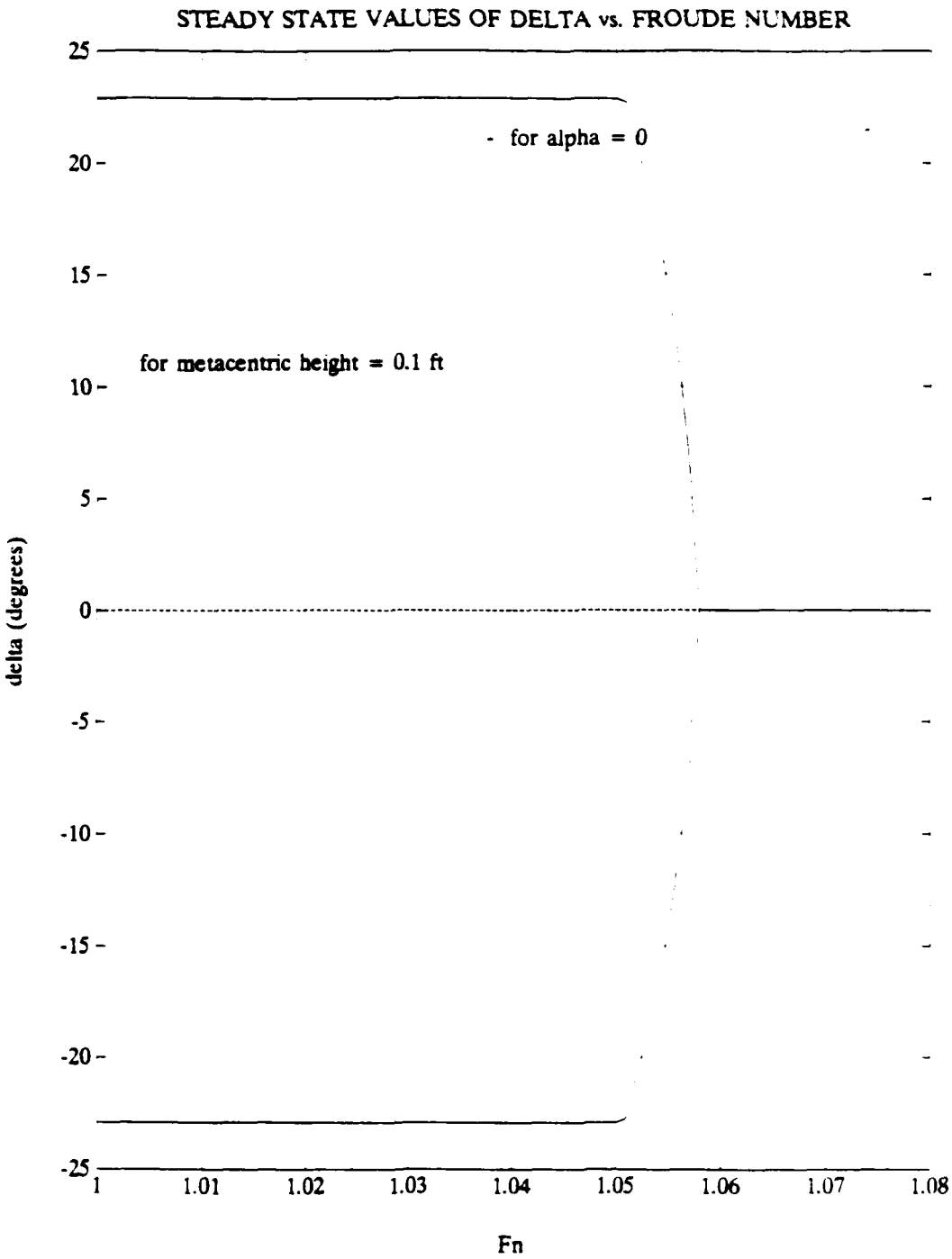

Figure 3-6. Steady State Values of δ vs Froude Number.

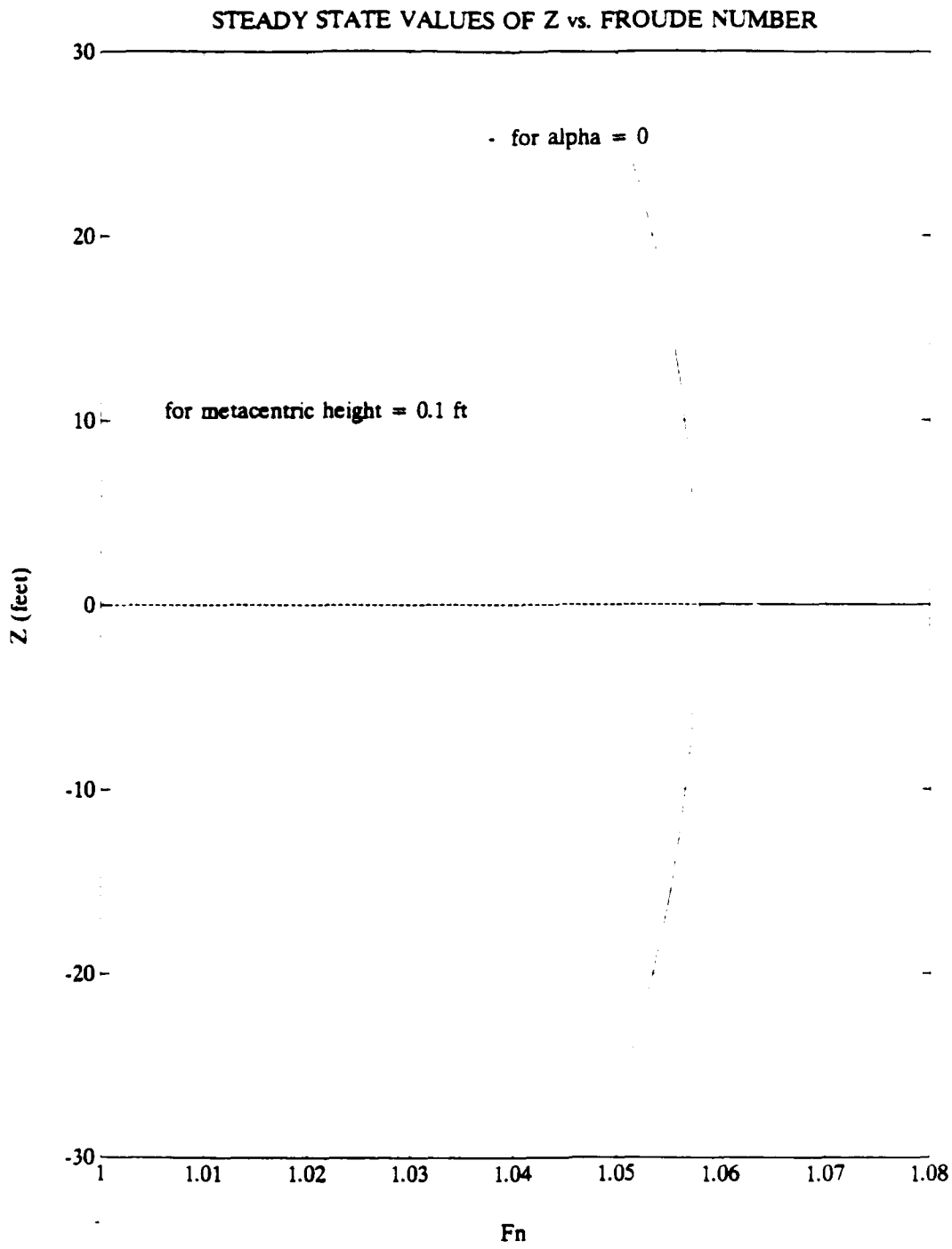

Figure 3-7. Steady State Values of Z vs Froude Number.

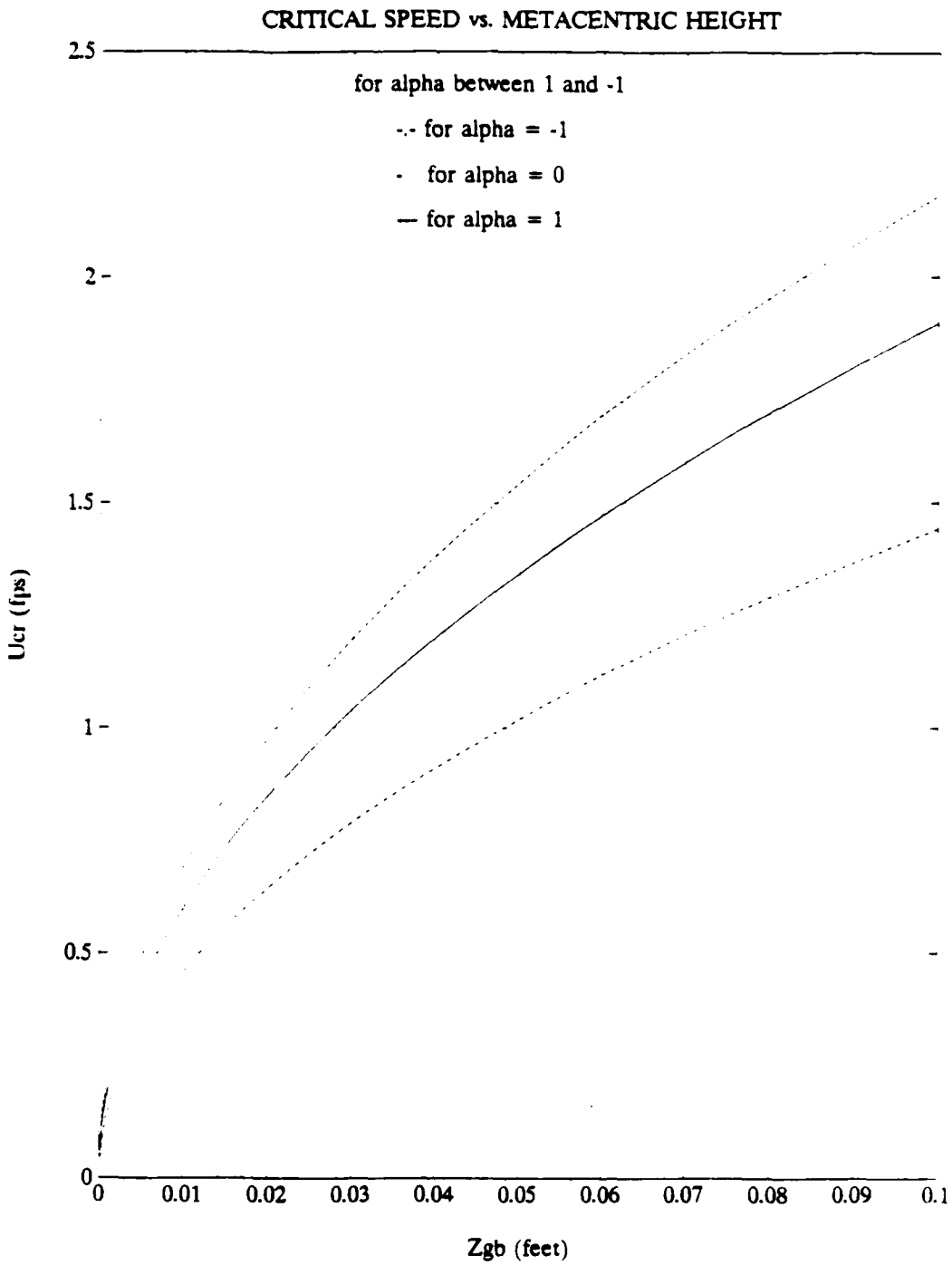

Figure 3-8. Relationship Between Critical Speed and Metacentric Height For Various Values of α.

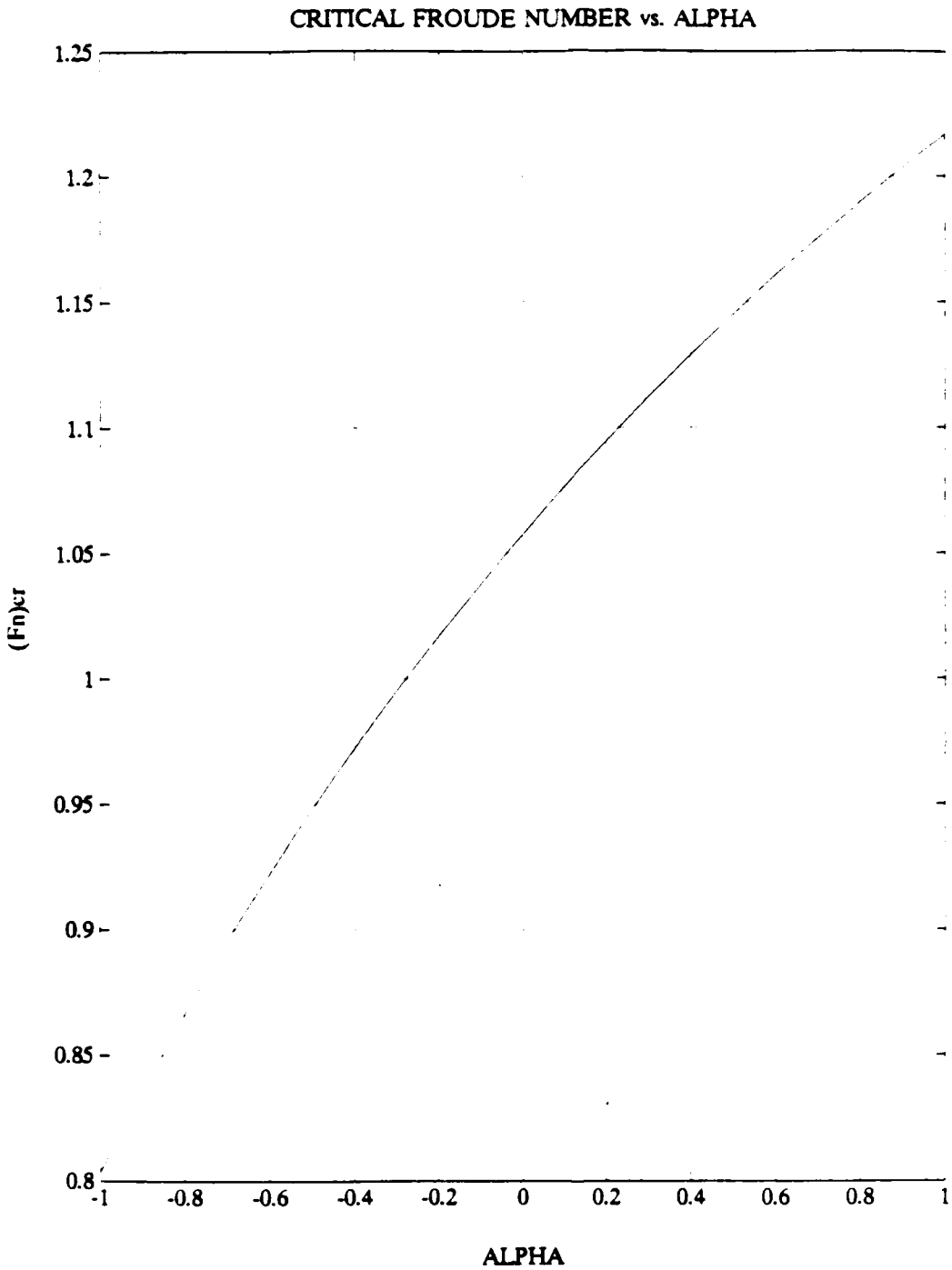

Figure 3-9. Froude Number as a Function of α.

location at which the control surfaces saturate. When comparisons are made, it can be shown that as the value of α becomes more positive the location of the critical Froude number and steady state values of θ and Z become greater. Comparing the changes in the δ steady state solutions, the shape of the δ pitchfork does not change however, the location of the critical point moves in the direction of increasing Froude number as α increases. The results of this discussion are shown graphically in Figures 3-10 through 3-12.

An interesting result is displayed in Figure 3-13. This figure depicts the relationship between α and the critical or saturation Froude number. At the lower Froude numbers, there is very little difference between the critical Froude number and the saturation Froude number. This demonstrates that upon reaching a low critical Froude number the control surface immediately saturates attempting to keep the vehicle stable. At the higher Froude numbers there is a significant difference between the critical Froude number and the saturation Froude number. This is because as the Froude number approaches 2.78, the value used in the control law design conducted in Chapter II, the control surfaces will not have to saturate to maintain stability.

3. Controllability Analysis

In general, every system of the form,

$$\begin{aligned} \dot{x} &= Ax + Bu, \\ y &= Cx, \end{aligned} \tag{3.27}$$

can be divided through a series of transformations into four subsystems:

1) A controllable and observable part.
2) An uncontrollable and observable part.
3) A controllable and unobservable part.
4) An uncontrollable and unobservable part.

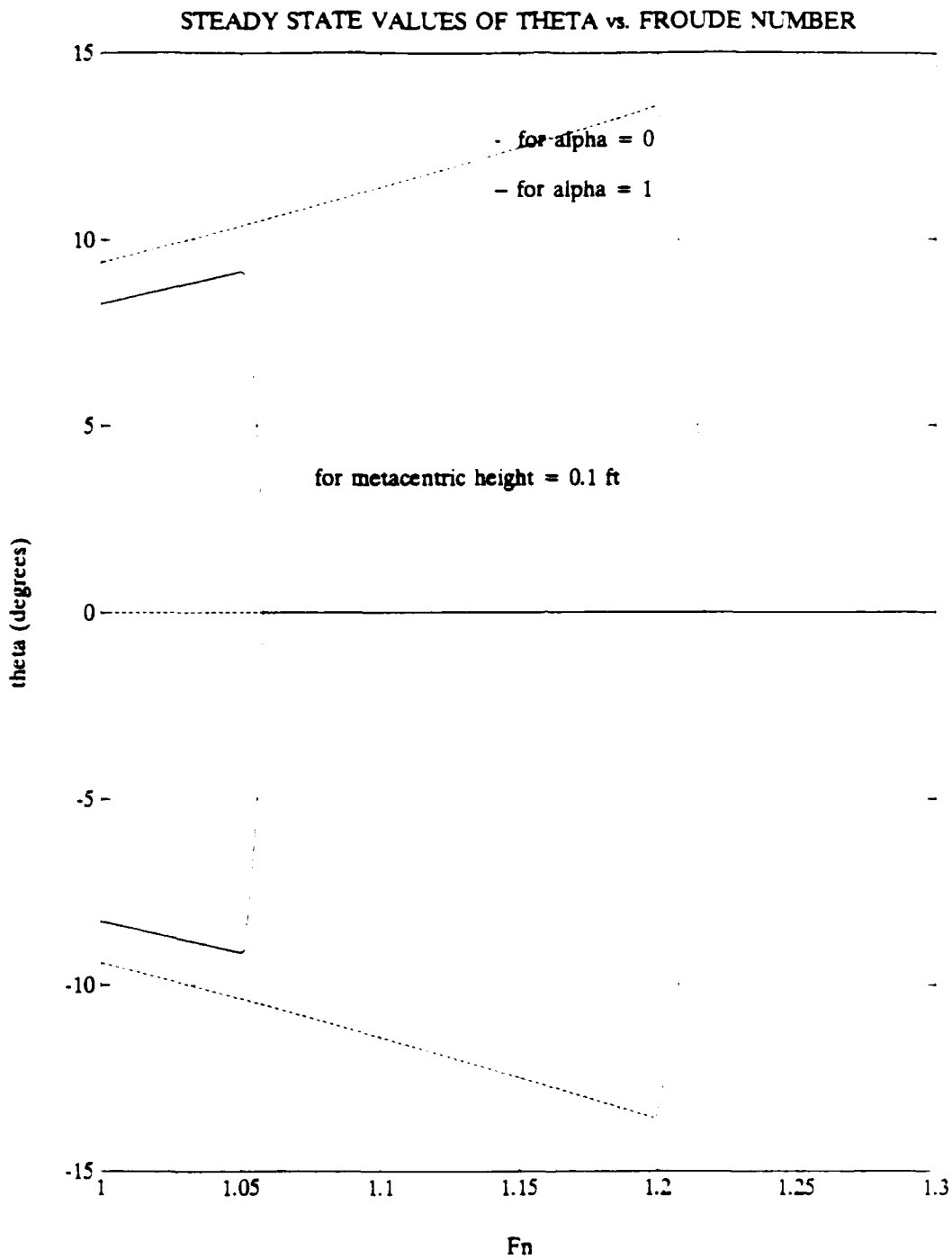

Figure 3-10. Comparison of Steady State Values of θ for Different Values of α.

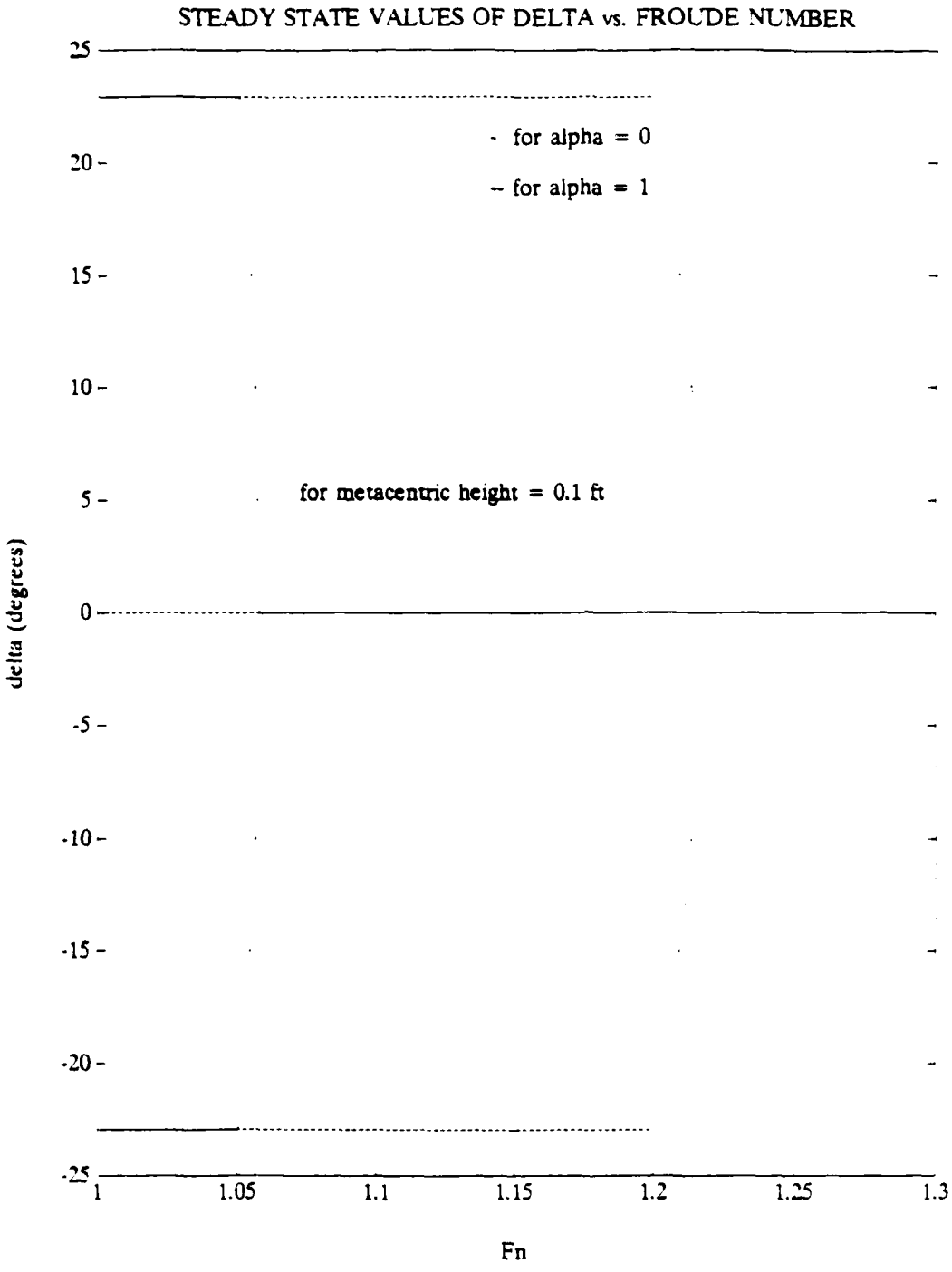

Figure 3-11. Comparison of Steady State Values of δ for Different Values of α.

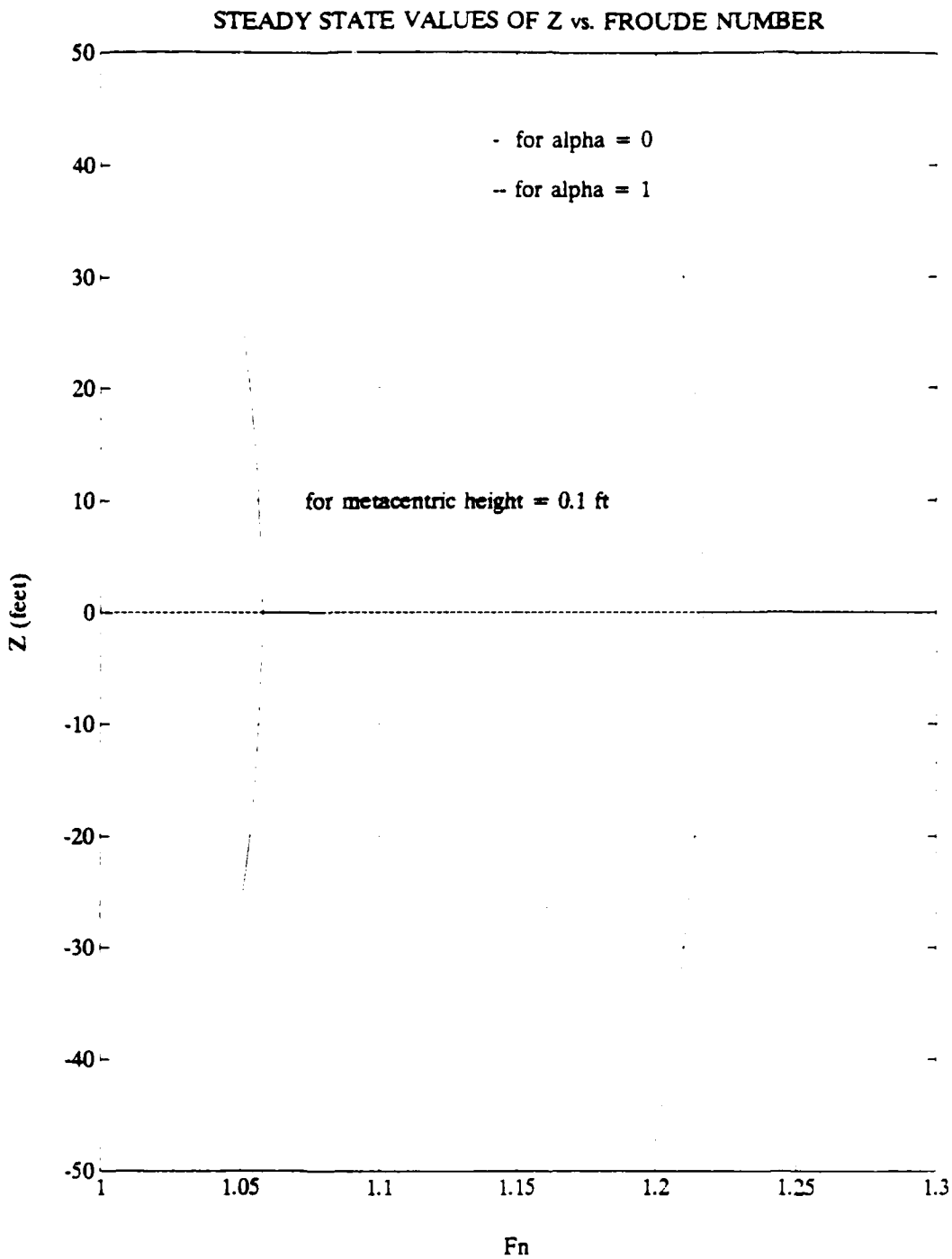

Figure 3-12. Comparison of Steady State Values of Z for Different Values of α.

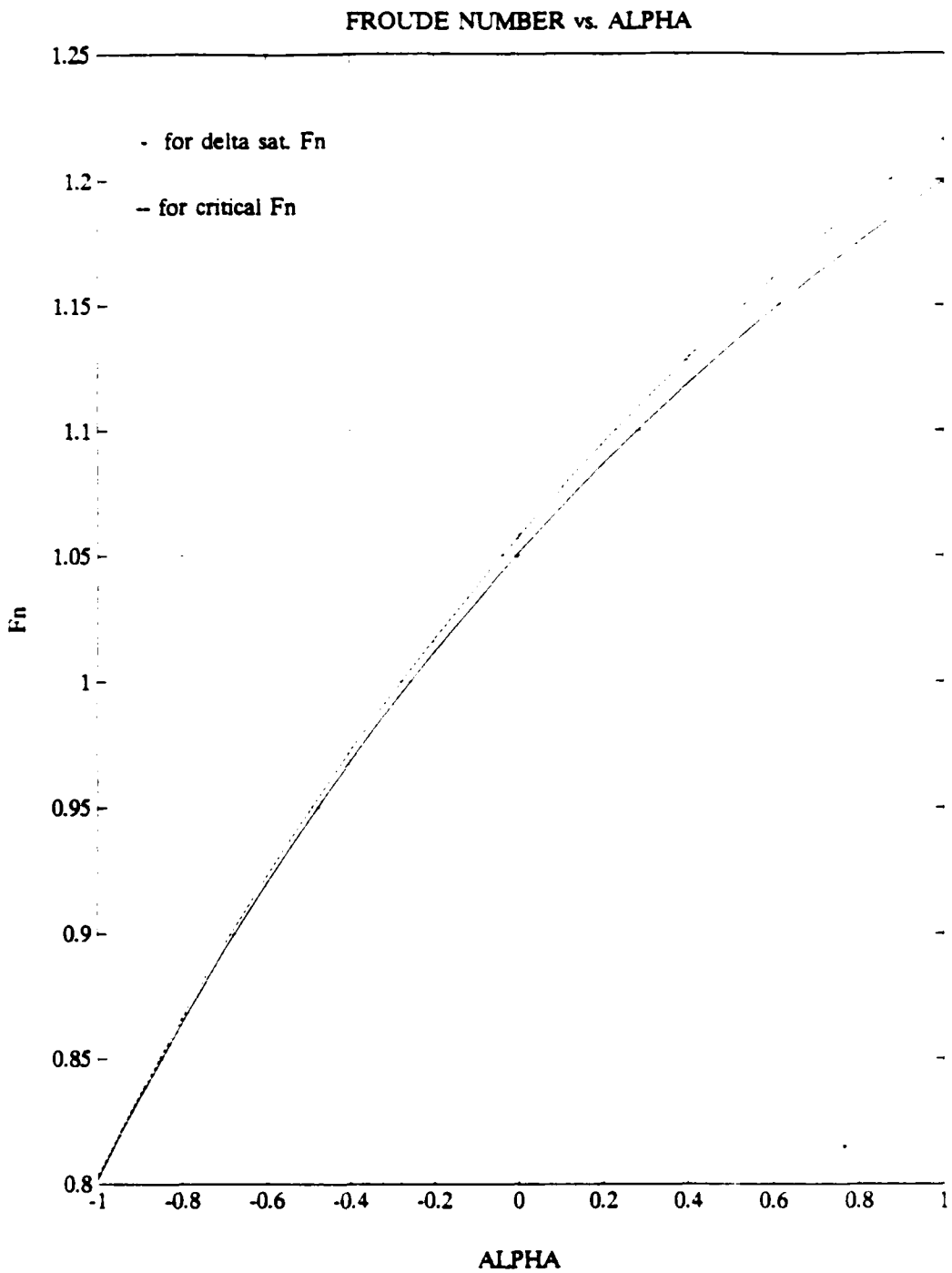

Figure 3-13. Relationship Between Critical/Saturation Froude Number and α.

This is known as Kalman's decomposition theorem. Now, since the transfer function of any system is determined by the controllable and observable subsystems only, then the transfer function may contain less information than is actually needed to model the complete system. The precise definition of controllability is:

A system is said to be *controllable* if any initial state $x(t_o)$ can be driven to any final state $x(t_f)$ using possibly unbounded control $u(t)$ in finite time $t_o < t < t_f$

From the state equations 3.27, this should depend only on A and B, where A is a $n \times n$ square matrix. The criterion for controllability is as follows: Compute the controllability matrix

$$c = [B, AB, A^2B, \ldots, A^{n-1}B], \tag{3.28}$$

and the system is controllable if and only if the rank of c (the number of linearly independent rows or columns) is n. Roughly speaking, c shows how possible it is to change the state of a system using the input. For a single input system B is $n \times 1$ and c is a square matrix. The test is then that c be nonsingular

$$det(c) \neq 0. \tag{3.29}$$

Now, if the controllability matrix is formed using the A and B matrices from equation 2.59 then the following matrix results;

$$c = \begin{bmatrix} c_{11} & c_{12} & c_{13} & c_{14} \\ c_{21} & c_{22} & c_{23} & c_{24} \\ c_{31} & c_{32} & c_{33} & c_{34} \\ c_{41} & c_{42} & c_{43} & c_{44} \end{bmatrix}, \tag{3.30}$$

where,

$$c_{11} = 0, \tag{3.31}$$

$$c_{12} = b_2 u^2, \tag{3.32}$$

$$c_{13} = a_{21} u^3 b_1 + a_{22} u^3 b_2, \tag{3.33}$$

$$c_{14} = b_1u^2(a_{11}a_{21}u^2 + a_{21}a_{22}u^2) + b_2u^2(a_{23}z_{GB} + a_{21}a_{12}u^2 + a_{22}{}^2u^2), \tag{3.34}$$

$$c_{21} = b_1u^2, \tag{3.35}$$

$$c_{22} = a_{11}u^3b_1 + a_{12}u^3b_2, \tag{3.36}$$

$$c_{23} = b_1u^2(a_{11}{}^2u^2 + a_{21}a_{12}u^2) + b_2u^2(a_{13}z_{GB} + a_{11}a_{12}u^2 + a_{12}a_{22}u^2), \tag{3.37}$$

$$\begin{aligned} c_{24} = {} & b_1u^2(a_{11}u(a_{11}{}^2u^2 + a_{12}a_{21}u^2) + a_{21}u(a_{13}z_{GB} + a_{11}a_{12}u^2 + a_{12}a_{22}u^2)) + \\ & b_2u^2(a_{13}z_{GB}a_{11}u + a_{12}a_{23}z_{GB}u + a_{12}u(a_{11}{}^2u^2 + a_{12}a_{21}u^2) + \\ & a_{22}u(a_{23}z_{GB} + a_{12}a_{21}u^2 + a_{22}{}^2u^2)), \end{aligned} \tag{3.38}$$

$$c_{31} = b_2u^2, \tag{3.39}$$

$$c_{32} = a_{21}u^3b_1 + a_{22}u^3b_2, \tag{3.40}$$

$$c_{33} = b_1u^2(a_{11}a_{21}u^2 + a_{21}a_{22}u^2) + b_2u^2(a_{23}z_{GB} + a_{21}a_{12}u^2 + a_{22}{}^2u^2), \tag{3.41}$$

$$\begin{aligned} c_{34} = {} & b_1u^2(a_{11}u(a_{11}a_{21}u^2 + a_{12}a_{22}u^2) + a_{21}u(a_{23}z_{GB} + a_{12}a_{21}u^2 + a_{22}{}^2u^2)) + \\ & b_2u^2(a_{13}z_{GB}a_{21}u + a_{22}a_{23}z_{GB}u + a_{12}u(a_{11}a_{21}u^2 + a_{12}a_{22}u^2) + \\ & a_{22}u(a_{23}z_{GB} + a_{12}a_{21}u^2 + a_{22}{}^2u^2)), \end{aligned} \tag{3.42}$$

$$c_{41} = 0, \tag{3.43}$$

$$c_{42} = b_1u^2, \tag{3.44}$$

$$c_{43} = a_{11}u^3b_1 + (a_{12}u - u)b_2u^2, \tag{3.45}$$

and $c_{44} = b_1u^2(a_{11}{}^2u^2 + a_{21}u(a_{12}u - u)) + b_2u^2(a_{13}z_{GB} + a_{11}a_{12}u^2 + a_{22}u(a_{12}u - u))$. (3.46)

Now, if the determinant of the controllability matrix is computed as a function of Froude number, then it can be shown that the system becomes uncontrollable at the critical Froude number. The graphical results of this computation are shown in Figure 3-14 for different values of the parameter α.

With the critical parameter that causes the vehicle to lose stability identified, i.e., the Froude number, and the effect that the parameter α has on the location of this critical value understood, the simplifications discussed at the beginning of this chapter can be removed from the E.O.M. and an analysis on the effects of incorporating these additional parameters can be conducted. This detailed analysis will be the topic of Chapter IV.

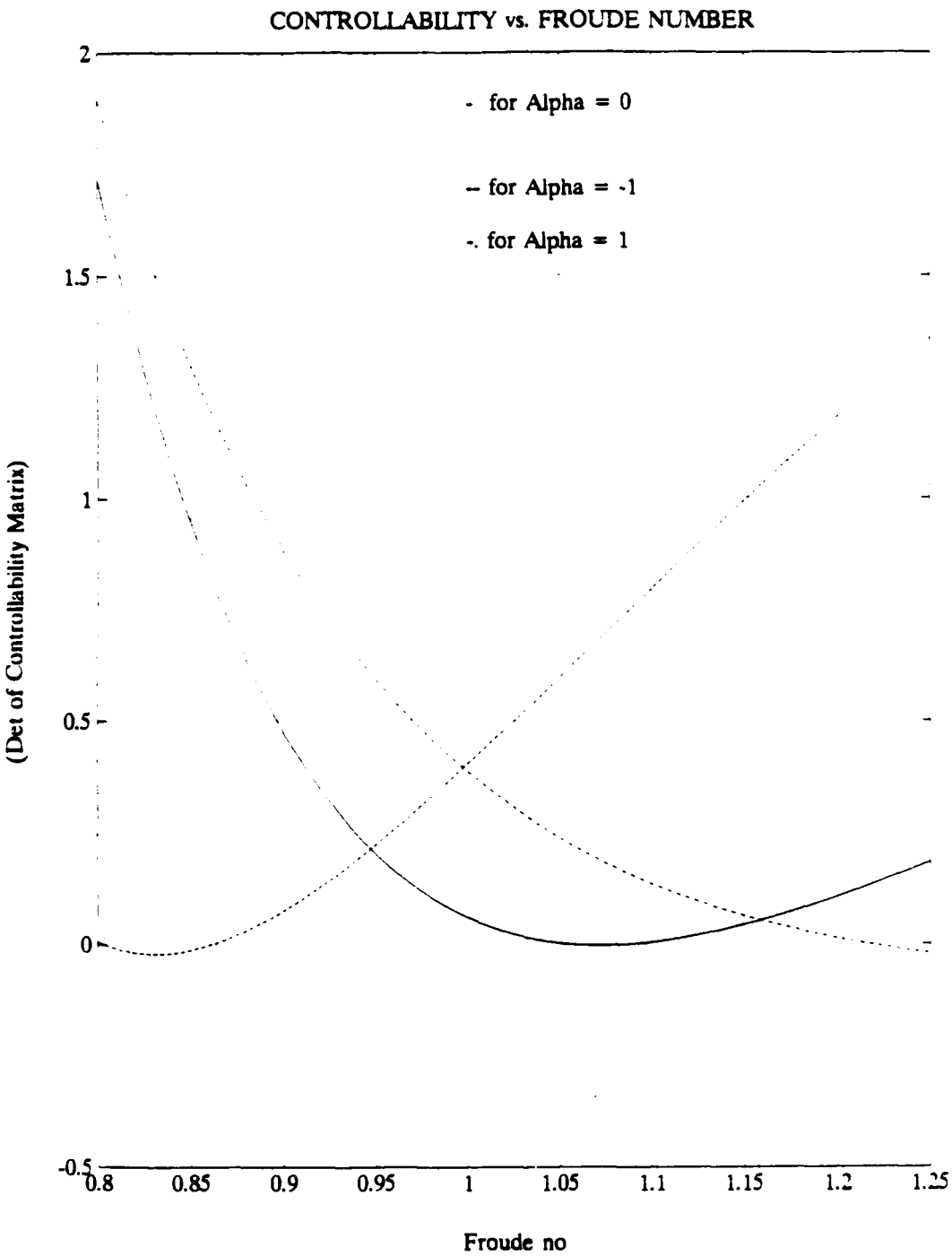

Figure 3-14. System Controllability vs Froude Number.

IV. BIFURCATION ANALYSIS

A. ASYMMETRIC PITCHFORK

Now that the critical parameter, the Froude number, has been identified, the simplifications applied to the E.O.M. in the previous chapter can be removed. The resulting system of equations is given by equations 2.38 through 2.43. To determine the existence of multiple steady state solutions for this new system of equations it is, once again, necessary to perform a steady state analysis as conducted in Section B.2 of the previous chapter. This analysis will reduce the system of equations into the following;

$$Z_w uw - \frac{1}{2}\rho C_D A w|w| + (W - B)\cos\theta + Z_\delta u^2\delta = 0 \tag{4.1}$$

$$M_w uw - \frac{1}{2}\rho C_D x_A A w|w| - (x_G W - x_B B)\cos\theta - (z_G W - z_B B)\sin\theta + M_\delta u^2\delta = 0, \tag{4.2}$$

with equation 3.13 also obtained from the steady state Z equation. By multiplying equation 4.1 by M_δ and equation 4.2 by Z_δ and setting the resulting equations equal to each other the following equation is obtained;

$$\begin{gathered}(Z_w M_\delta - M_w Z_\delta)uw - (\frac{1}{2}\rho A C_D)(M_\delta - x_A Z_\delta)w|w| + \\ ((W - B)M_\delta + (x_G W - x_B B)Z_\delta)\cos\theta + Z_\delta(z_G W - z_B B)\sin\theta = 0\end{gathered} \tag{4.3}$$

This equation, along with,

$$w = u\tan\theta, \tag{4.4}$$

from equation 3.13 is the exact steady state solution set with all parameters included.

Figure 4-1 shows the results obtained when equation 4.3 is solved numerically, using the FORTRAN program in Appendix A, for a small value of x_{GB} (the difference in the location of the center of gravity and buoyancy), with the submarine neutrally buoyant ($W = B$). This small value of x_{GB} perturbs the pitchfork, as seen, from the symmetric pitchfork displayed earlier in Figure 3-5. This comparison shows that the critical or bifurcation point has moved to a lower Froude number, with the stable solutions represented by the solid lines and the unstable solutions represented by the dashed lines in both cases. The stable steady state solution, that the vehicle will acquire, is dependent on the initial conditions that are given to the vehicle. Using the results displayed in Figure 4-1 as an indication that x_{GB} may also be a critical parameter, the subsequent task is to determine the relationship between the critical Froude number and x_{GB} or $f(Fn, x_{GB})$.

B. BIFURCATION GRAPHS

The first order of business in the attempt to identify $f(Fn, x_{GB})$ is to simplify the exact pitchfork equation. This can be accomplished by replacing the $cos\theta$ and $sin\theta$ terms in equation 4.3 with the following Taylor series expansions

$$sin\theta = \frac{w}{u} - \frac{1}{2}\frac{w^3}{u^3} = \frac{2wu^2 - w^3}{2u^3} \tag{4.5}$$

$$cos\theta = 1 - \frac{1}{2}\frac{w^2}{u^2} = \frac{2u^2 - w^2}{2u^2}, \tag{4.6}$$

which will allow the exact solution to be represented as follows:

$$\begin{aligned} &Z_\delta(z_G W - z_B B)w^3 + 2u^3 C_D A(M_\delta - x_A Z_\delta)w|w| \\ &-(2u^4(Z_w M_\delta - M_w Z_\delta) + 2u^2 Z_\delta(z_G W - z_B B))w - 2u^2((W - B)M_\delta, \\ &+(x_G W - x_B B)Z_\delta + ((W - B)M_\delta + (x_G W - x_B B)Z_\delta)w^2 = 0 \end{aligned} \tag{4.7}$$

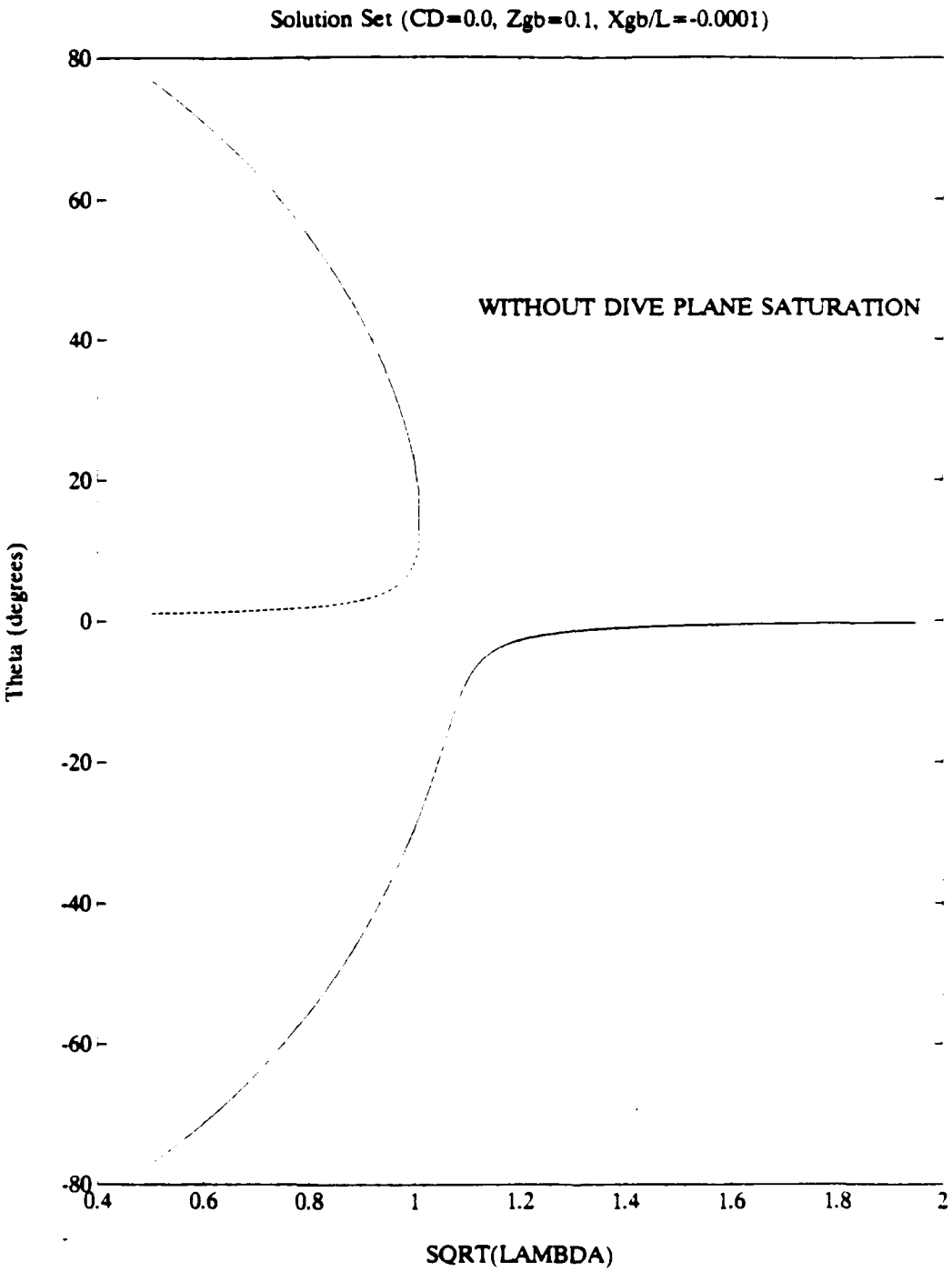

Figure 4-1. Exact Solution Set for Xgb/L=-0.0001.

where C_D now equals the terms $\frac{1}{2}\rho C_D$ present in equation 4.3. Defining the following parameters

$$\delta_B = B - W, \tag{4.8}$$

$$x_{GB} = x_G - x_B, \tag{4.9}$$

$$z_{GB} = z_G - z_B, \tag{4.10}$$

$$z_G W - z_B B = z_{GB} W - z_B \delta_B \equiv \delta_z, \tag{4.11}$$

$$x_G W - x_B B = x_{GB} W - x_B \delta_B \equiv \delta_x, \tag{4.12}$$

$$\lambda = 1 \quad Fn^2, \tag{4.13}$$

and substituting them into equation 4.7 will allow the coefficients in front of the various powers of w to be written as follows;

$$w^3\text{: } A_4 = Z_\delta(z_{GB}W - z_B\delta_B) = Z_\delta(\lambda u^2 W - z_B\delta_B), \tag{4.14}$$

$$w|w|\text{: } A_3 = 2u^3 C_D A(M_\delta - x_A Z_\delta), \tag{4.15}$$

$$w\text{: } A_2 = -2u^2(u^2(Z_w M_\delta - M_w Z_\delta) + Z_\delta(\lambda u^2 W - z_B\delta_B)), \tag{4.16}$$

$$w^0\text{: } A_1 = -2u^2(-\delta_B M_\delta - Z_\delta(x_{GB}W - x_B\delta_B)) \tag{4.17}$$

$$w^2\text{: } A_0 = (-\delta_B M_\delta - Z_\delta(x_{GB}W - x_B\delta_B)). \tag{4.18}$$

The resulting form of equation 4.7 can be written

$$A_4 w^3 + A_3 w|w| + A_2 w + A_1 + A_1 w^2 = 0, \tag{4.19}$$

which is a generic pitchfork equation. If it is assumed that the submarine is neutrally buoyant, and equation 4.19 is divided by $Z_\delta z_{GB} W$, then the above coefficients can be redefined as;

$$A_4 = 1, \tag{4.20}$$

$$A_3 = 2uC_D A(M_\delta - x_A Z_\delta)\frac{g}{Z_\delta W}\frac{u^2}{g z_{GB}}, \tag{4.21}$$

$$A_2 = -2u^2\left(\frac{u^2}{gz_{GB}}\frac{g(Z_w M_\delta - M_w Z_\delta)}{Z_\delta W} + 1\right), \tag{4.22}$$

$$A_1 = \frac{u^2}{gz_{GB}} 2g, \tag{4.23}$$

$$A_0 = -\frac{u^2}{gz_{GB}}\frac{x_{GB}g}{u^2}. \tag{4.24}$$

Letting the critical parameter λ be defined as

$$\lambda = \frac{u^2}{gz_{GB}}, \tag{4.25}$$

will allow equation 4.19 to be put into the following pitchfork solution form;

$$w^3 + \gamma\lambda w|w| - 2u^2(1+\zeta\lambda)w + 2\beta u^2\lambda + \beta\lambda w^2 = 0, \tag{4.26}$$

where,

$$\beta = -\frac{x_{GB}g}{u^2}, \tag{4.27}$$

$$\zeta = \frac{g(Z_w M_\delta - M_w Z_\delta)}{Z_\delta W}, \tag{4.28}$$

$$\gamma = 2uC_D A(M_\delta - x_A Z_\delta)\frac{g}{Z_\delta B}. \tag{4.29}$$

To determine if the above manipulation and definitions are correct and valid, take the symmetric case that was developed in the previous chapter, i.e., $x_{GB} = 0$. This causes equation 4.26 to reduce to

$$w(w^2 + \gamma\lambda|w| - 2u^2(1+\zeta\lambda)) = 0, \tag{4.30}$$

resulting in a solution always occurring at w=0, with two more solutions appearing at the bifurcation value

$$1 + \zeta\lambda_o = 0. \tag{4.31}$$

Rearranging and substituting the appropriate values into equation 4.31 will yield

$$\frac{u^2}{z_{GB}} = \frac{Z_\delta W}{M_w Z_\delta - Z_w M_\delta}, \tag{4.32}$$

which is identical to equations 3.9 and 3.20, thus verifying the manipulation.

To find the relationship between Fn and x_{GB} the function $h(w,\lambda,\beta)$, and its partial derivative $h_w(w,\lambda,\beta)$, must be determined. These two functions must then be set equal to zero and to each other in order to obtain a function independent of w. As seen, equation 4.30 is much too complex to complete these requirements, but by neglecting the terms $\lambda w|w|$ and λw^2 in equation 4.26 a simplified pitchfork of the form,

$$w^3 - 2u^2(1+\zeta\lambda)w + 2\beta u^2\lambda = 0, \tag{4.33}$$

or in general terms $h(w,\lambda,\beta) = 0$, can be obtained which can be manipulated to meet the above mentioned requirements, thereby determining the critical (λ,β) curve. By taking the partial derivative, h_w, of equation 4.33, the following equation results;

$$h_w = 3w^2 - 2u^2(1+\zeta\lambda). \tag{4.34}$$

This equation can be set equal to zero, yielding

$$w^2 = \frac{2}{3}u^2(1+\zeta\lambda), \tag{4.35}$$

which can be substituted into equation 4.33 to obtain the value of w where the function and it's partial derivative is equal to zero;

$$w = \frac{3\beta\lambda}{2(1+\zeta\lambda)}. \tag{4.36}$$

This value of w can now be substituted back into equation 4.35 to obtain the desired $f(\lambda,\beta)$, or

$$27\beta^2\lambda^2 = 8u^2(1+\zeta\lambda)^3. \tag{4.37}$$

Attempting to solve this equation analytically for λ as a function of β, to determine the shape of this curve is difficult. Therefore, an approximation to this equation is needed for small values of β. By rearranging equation 4.37 into the form

$$\beta^2 = \frac{8u^2(1+\zeta\lambda)^3}{27\lambda^2}, \tag{4.38}$$

an equation that determines β as a function of λ is now produced. If this function is represented in a Taylor series expansion and simplified, then equation 4.38 can be written as

$$\lambda = \lambda_o + \frac{3}{2}(\beta^2 \quad (u^2\zeta^4))^{1/3}, \tag{4.39}$$

which can be considered as an approximation to the (λ,β) curve, with equation 4.37 as the exact (λ,β) curve. Through inspection it can be seen that the general shape of this curve is that of a cusp.

Figure 4-2 shows a comparison of four bifurcation curves. The curves represent the relationship between the critical speed U, which can be converted into the non dimensional parameter λ using equation 4.25, and the value of x_{GB}, which also can be converted into a non dimensional parameter β using equation 4.27. The curves labeled exact bifurcation set, pitchfork bifurcation set, exact cusp and approximate cusp come from the numerical solution to equations 4.7, 4.26, 4.37 and 4.39 respectively. Observe that in the general vicinity of x_{GB}=0 and near the critical speed the shape of each of these curves is indeed that of a cusp, with the peak occurring at the critical speed of 1.9 fps. Now, with the comparison conducted in Figure 4-2 complete, equation 4.7, the exact pitchfork solution will be used for the remainder of this analysis.

Returning to equation 4.7, it can be seen that there is only one additional parameter, C_D, that the cusp curve produced using equation 4.39 does not incorporate (because z_{GB} and x_{GB} are incorporated into the non dimensional parameters λ and β). It is therefore necessary to conduct a sensitivity analysis to determine the effect that C_D has on the shape of the cusp curve. Figure 4-3 displays the results obtained when this sensitivity analysis was conducted.

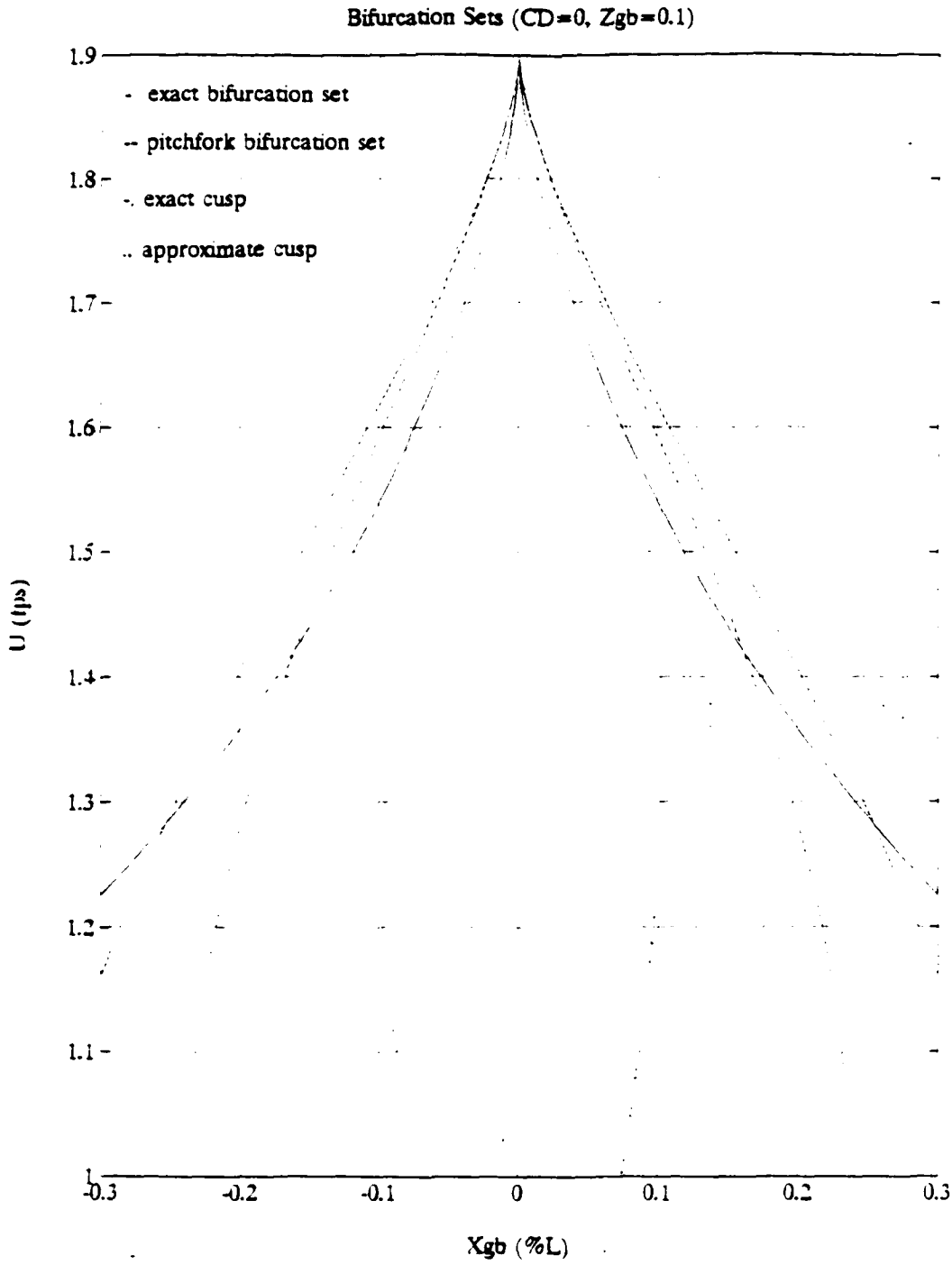

Figure 4-2. Comparison of Bifurcation Curves.

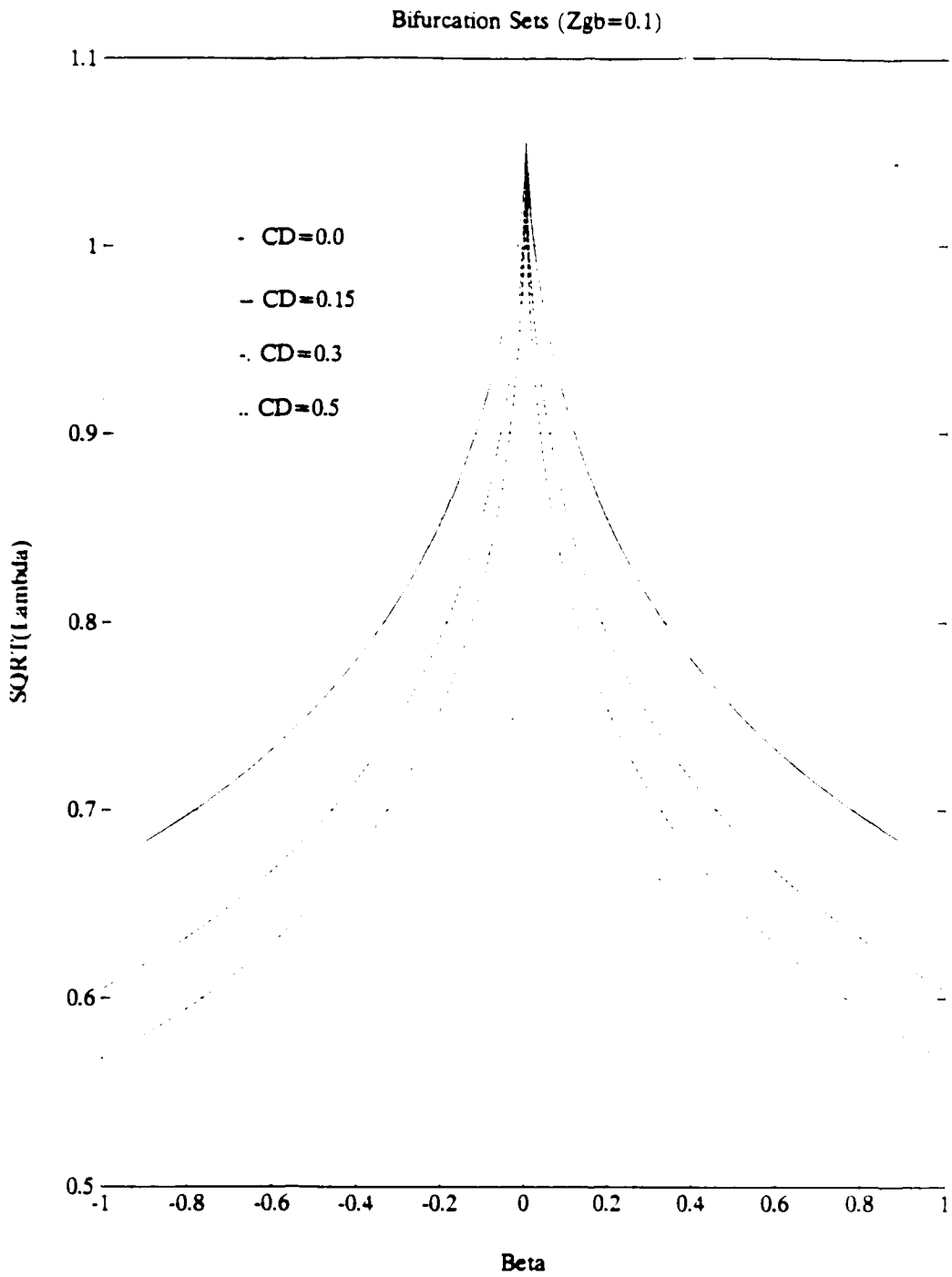

Figure 4-3. Comparison of Exact Bifurcation Set for Different Values of Drag Coefficient.

As seen in the plot, the drag coefficient has no effect on the location of the peak of the cusp. The drag coefficient, however, does modify the slope of the cusp as displayed by the four cases shown in Figure 4-3.

C. SOLUTION SETS

In this section, the equilibrium solutions to equations 4.3 and 4.5 will be investigated. As determined in the previous section, the critical parameters that control the location and shape of the pitchfork solution sets are λ, β and the drag coefficient C_D. By running the FORTRAN program of Appendix A for several values of x_{GB} L the shape and trend of the solution sets can be determined. The result of this comparison, for a $C_D = 0.0$, is displayed in Figure 4-4. This plot supports the symmetry about $x_{GB} = 0$ displayed in the earlier cusp curves. Observe that the critical or bifurcation point moves to a lower value of λ as x_{GB} increases, and that for low values of λ the equilibrium solutions converge to the same value independent of the value of x_{GB}.

When the comparison is made regarding the effect that the drag coefficient has on the solution sets, for a given value of x_{GB}, Figure 4-5 is produced. This variation in drag coefficient for a constant value of x_{GB} has a similar effect on the movement of the bifurcation point as fixing the drag coefficient and varying x_{GB}. The difference is, however, evident by studying the stable solutions. The stable solutions for non-zero drag coefficients become more linear as the value of C_D increases. This results from the increased effect of the $w|w|$ term in equation 4.3 as the value of C_D increases.

Although Figure 4-5 shows the actual solution to the exact pitchfork equation it is not realistic since the effect of dive plane saturation is not considered. Once the dive planes saturate, the equations used to obtain the steady state solutions displayed in

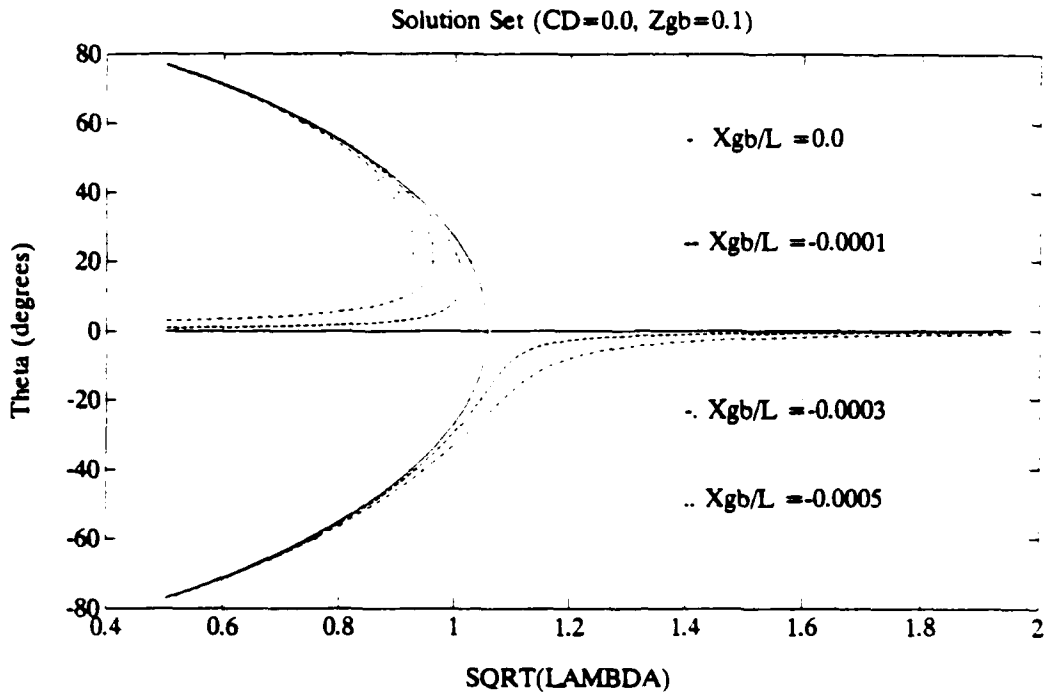

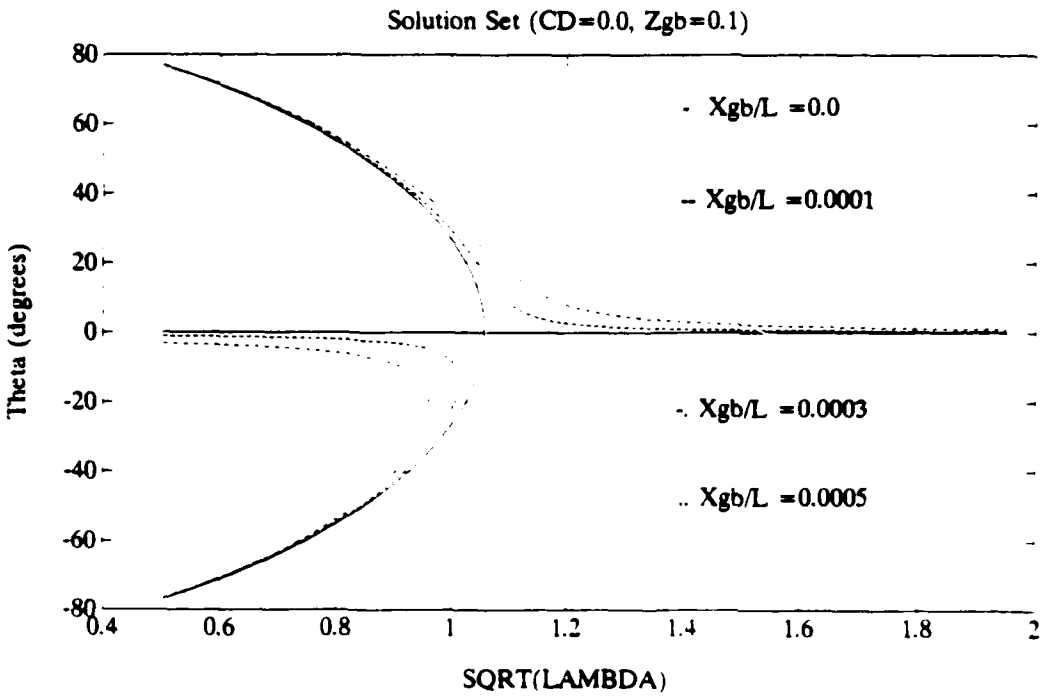

Figure 4-4. Comparison of Exact Solution Set for Different Values of Xgb/L.

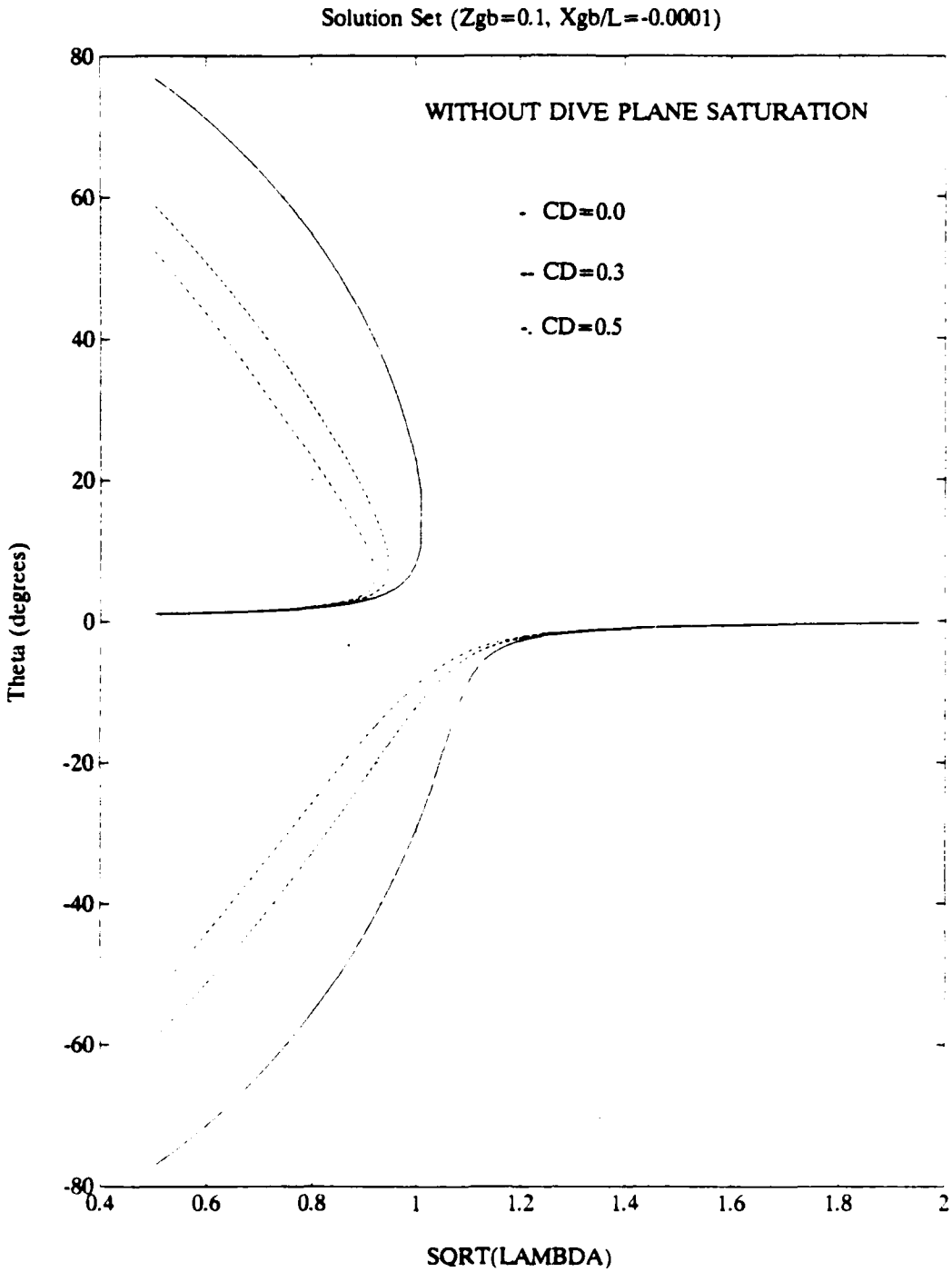

Figure 4-5. Comparison of Exact Solution Set for Different Values of C_D.

Figures 4-4 and 4-5 are no longer valid. Instead, equations 4.1 and 4.2 are modified, still remembering that the assumption of neutral buoyancy remains in affect, resulting in the following two equations;

$$Z_w uw - C_D Aw|w| + u^2 Z_\delta \delta_{sat} = 0, \tag{4.40}$$

$$M_w uw - C_D x_A Aw|w| - Wx_{GB} \cos\theta - z_{GB} W \sin\theta + M_\delta u^2 \delta_{sat} = 0. \tag{4.41}$$

To obtain an equation that can be used to compute the steady state θ solution while taking into consideration dive plane saturation requires solving equation 4.40 for w and then substituting this value into equation 4.41 which should yield an equation independent of w. The ability to perform this manipulation is hindered by the inclusion of the absolute value term in both of the above equations. However, if the absolute value terms are neglected by considering the case of C_D=0.0, then a single equation for the steady state value of θ may be obtained.

Neglecting the drag affects, and performing the algebra will yield an equation of the following form;

$$(M_w Z_\delta - M_\delta Z_w) u^2 \delta_{sat} + Z_w W (x_{GB} \cos\theta + z_{GB} \sin\theta) = 0, \tag{4.42}$$

which may be used to determine the values of θ once the dive planes have saturated. The validity of neglecting the drag terms is questionable, and an analysis that incorporates C_D will be conducted later in this section once the effect of varying x_{GB} is determined. Figure 4-6 displays the changes that occur to the solution set of Figure 4-1 when saturation is considered. Notice that saturation occurs when the solution set is at approximately nine degrees, and that when multiple solutions occur, the stable equilibrium states are represented by the saturation portions of the solution set.

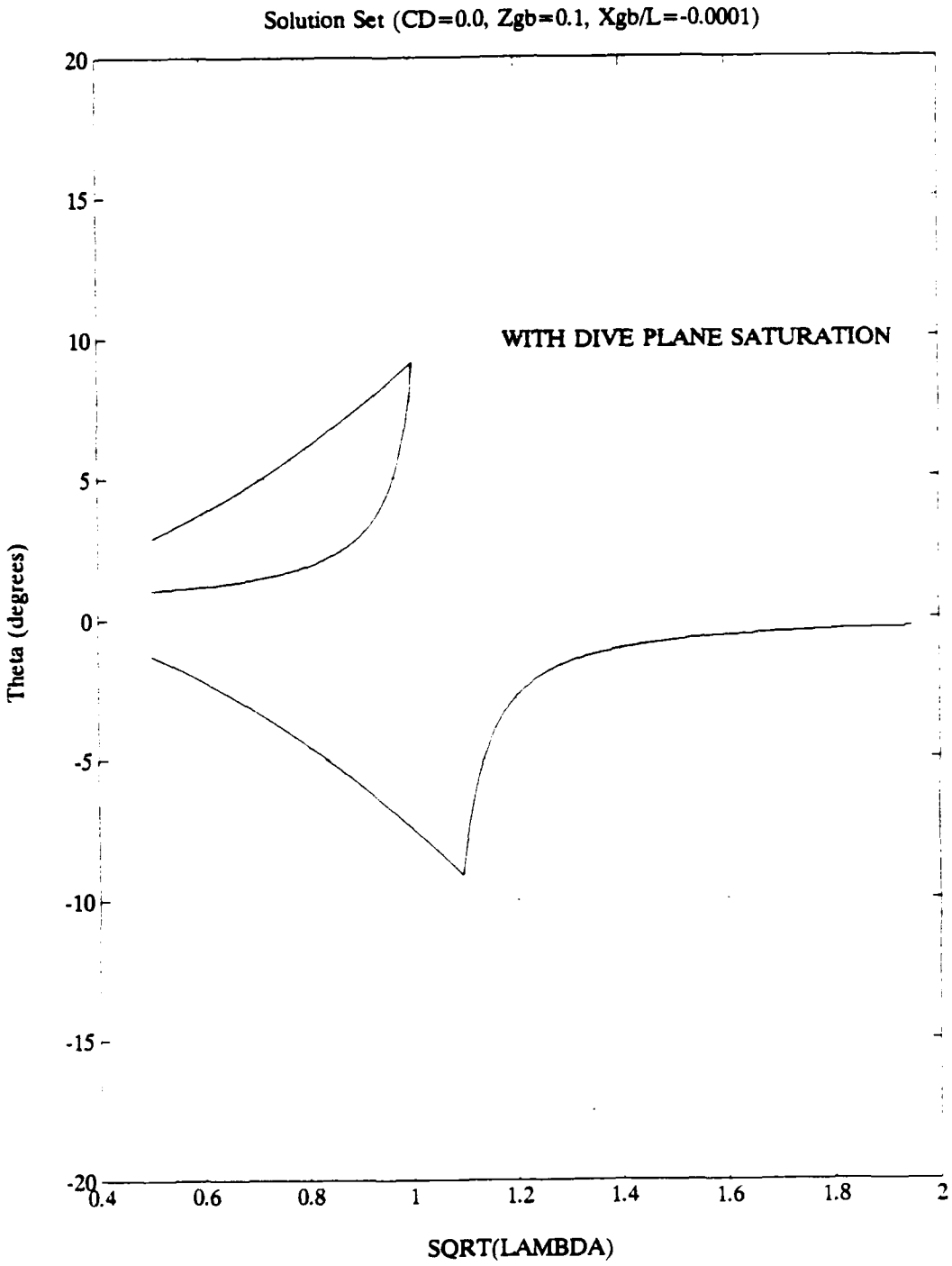

Figure 4-6. Exact Solution Set for Xgb/L=-0.0001 With Saturation Included.

When the saturation condition is applied to the previously displayed solution sets for different values of x_{GB} (Figure 4-4), the results shown in Figure 4-7 are produced. Items of interest in Figure 4-7 are that:

1) The bifurcation point on each solution set moves to a lower value of λ as the absolute value of x_{GB} increases.
2) The range where multiple solutions exist decreases as the absolute value of x_{GB} increases.
3) The amount of trim produced, in still water, by the given value of x_{GB} can be obtained from the point where the upper an lower solution branches converge.

Incorporating the saturation condition into the solution sets raises some additional concerns. To begin, what if the point of dive plane saturation occurs after the bifurcation points identified in Figure 4-4? If this condition did occur, referring to Figure 4-1 which displays the stable and unstable solution branches, there would be at least one value of λ where there were three stable solution branches. To determine if this condition is possible a comparison of solution sets with and without saturation is necessary. This comparison is shown in Figure 4-8. As this plot depicts, the range between the bifurcation point and saturation point increases as the value of x_{GB} increases. This result will allow the fore mentioned concern, of three stable solution branches, to be disregarded.

A second concern is the validity of the previously developed bifurcation cusp curves. Since the exact bifurcation equation, equation 4-7, does not include saturation, the cusp curves produced using this equation will not accurately predict the occurrence of multiple solutions. However, if equation 4.42 is expanded in a Taylor series, it can be manipulated into a form that will allow a cusp curve, which includes saturation, to be developed.

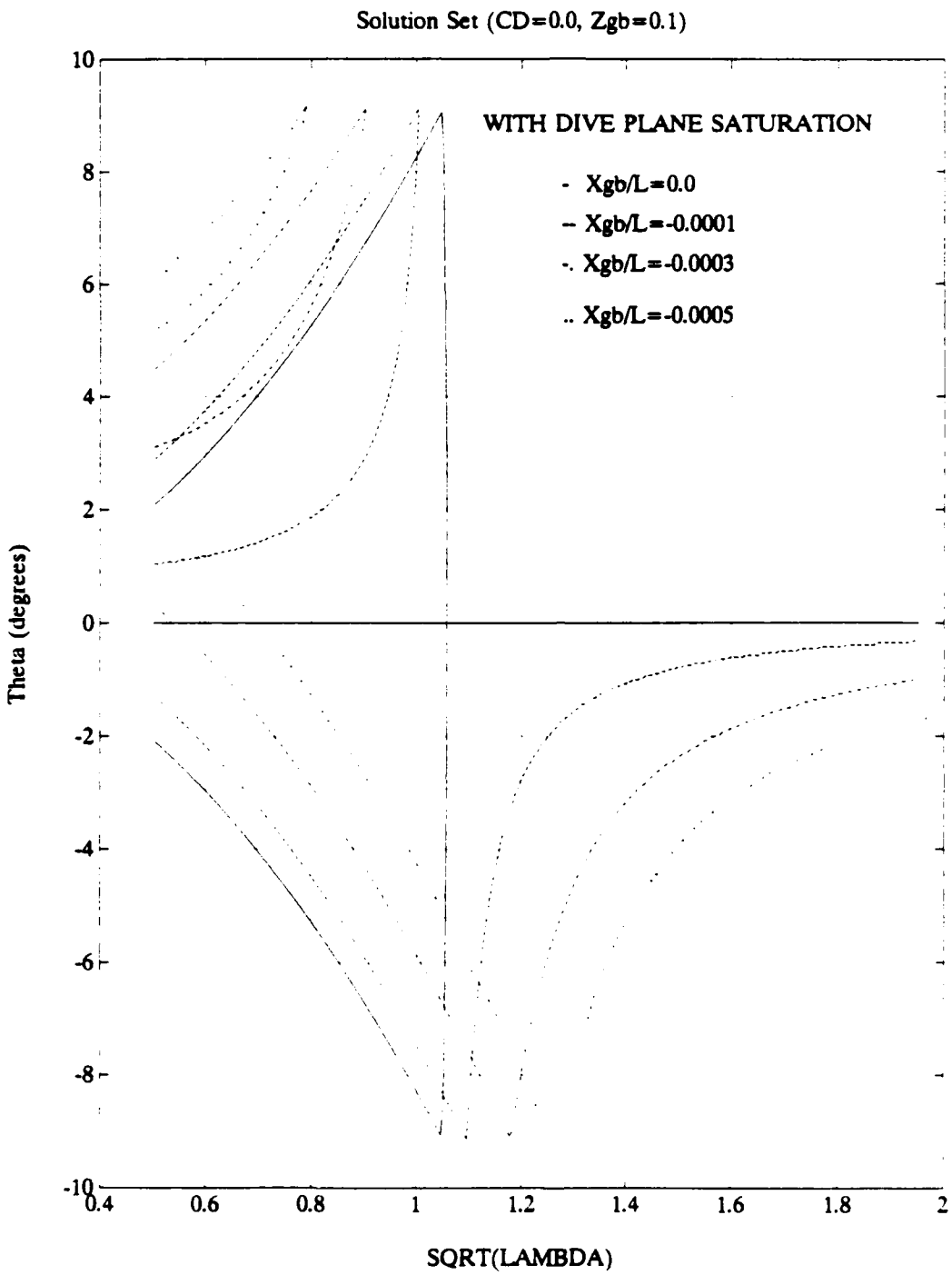

Figure 4-7. Comparison of Exact Solution Set for Different Values of Xgb/L With Saturation Included.

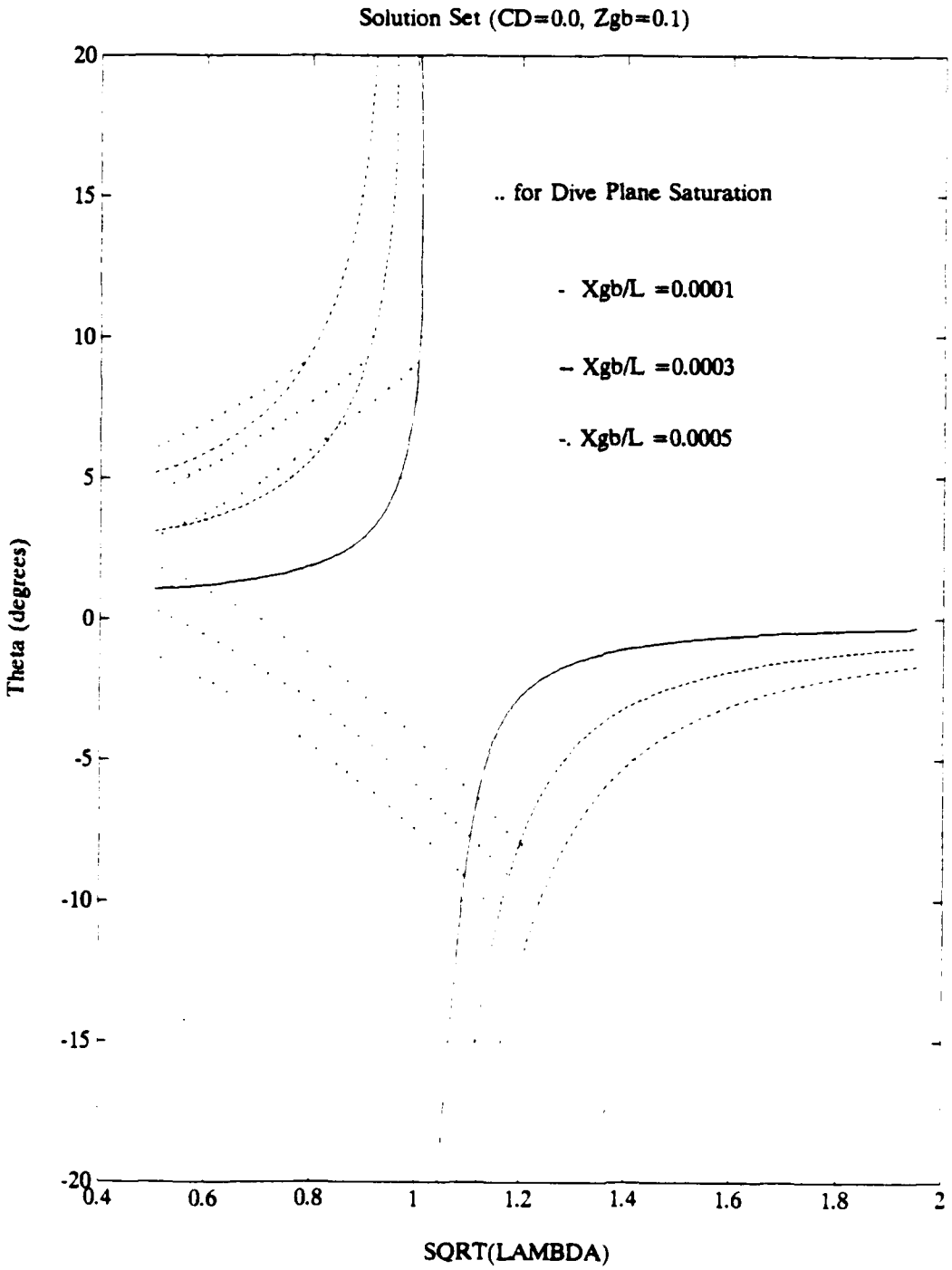

Figure 4-8. Comparison of Bifurcation Points and Dive Plane Saturation Points.

Performing this manipulation will produce the following equation;

$$u^2 = \frac{-x_{GB}Z_w W + z_{GB}WZ_\delta\delta_{sat}}{(Z_\delta M_w - M_\delta Z_w)(\delta_{sat}(1+(Z_\delta - Z_w)^2\delta_{sat})^{1/2})} \tag{4.43}$$

By converting u^2 and x_{GB} into the non dimensional parameters λ and β the cusp curve shown in Figure 4-9 can be produced. This cusp displays the saturation point for both solution branches, and as seen it differs quite extensively from the exact bifurcation cusp without saturation. If Figure 4-9 is replotted to allow the peak area of the cusp to be more accurately represented, then Figure 4-10 is produced. By using these two cusp curves then the general form of the resulting solution set for any path through the cusp can be predicted. It is this prediction that the subsequent section will address.

D. PATH FORMULATION

The ability to accurately predict how the vessel will respond to various changes in operating conditions is critical for proper control of the vessel. It is this prediction that necessitates the need for path analysis to be conducted. If the ballast condition on the vessel is held constant, x_{GB} =*-0.0001*, and the speed of the vessel is varied, path *A* of Figure 4-11 is obtained. Neglecting for the moment the saturation cusp shown in Figure 4-11, it would be expected that a single steady state solution would exist for all values, of the parameter *sqrt(*λ*)*, greater than the point where the path intersects the solid cusp curve. At the speed where the path intersects the cusp the bifurcation point occurs, and for speed values which place the path inside the cusp multiple steady state solutions occur. The results of this path analysis are depicted in Figure 4-1, presented earlier in this chapter.

If attention is returned to the path through the saturation cusp of Figure 4-11, then the same type of predictions made for the path through the solid cusp can be made for the this cusp, with some slight differences. As the speed decreases the path intersects the

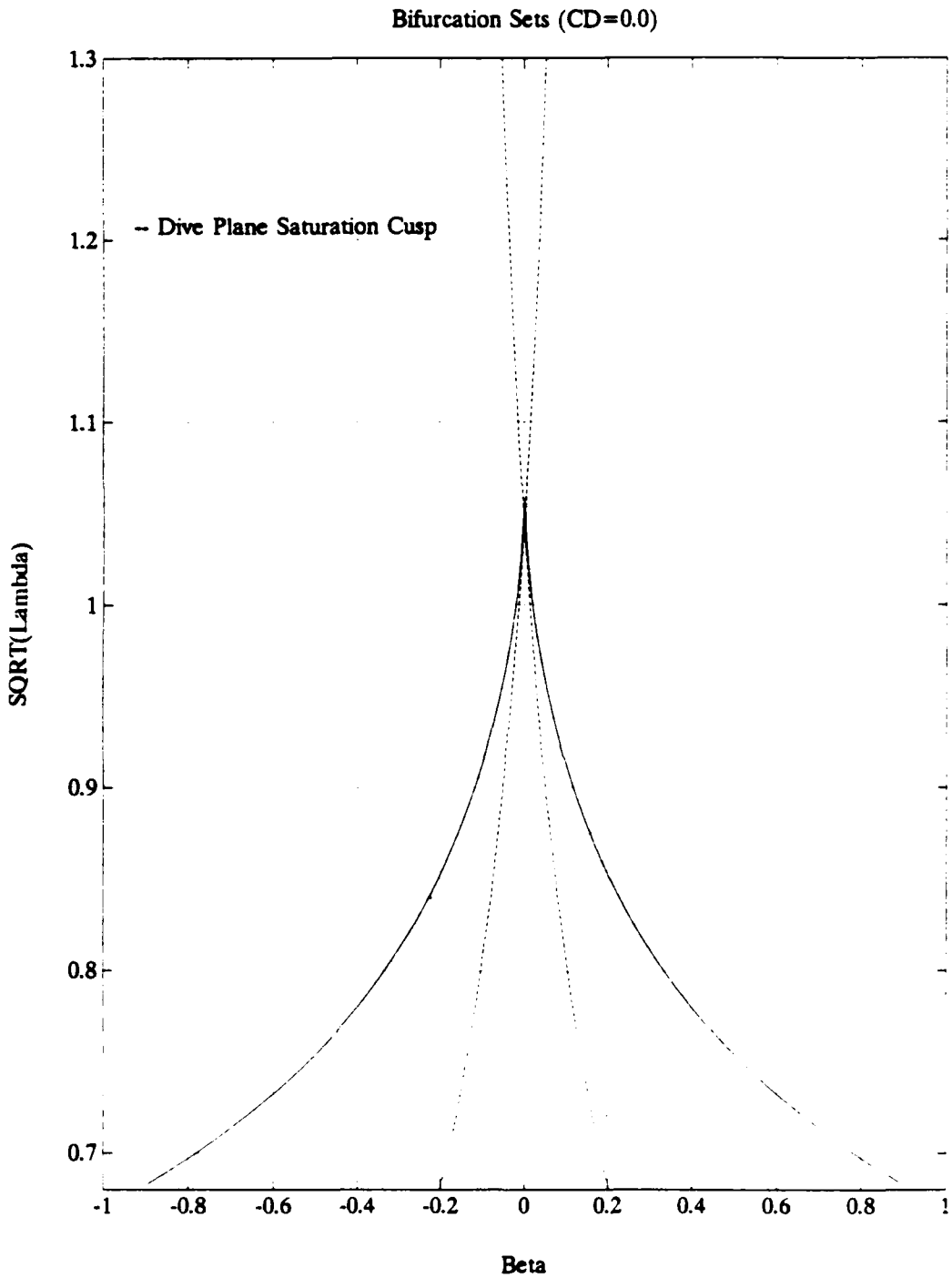

Figure 4-9. Bifurcation Cusp With Dive Plane Saturation Included.

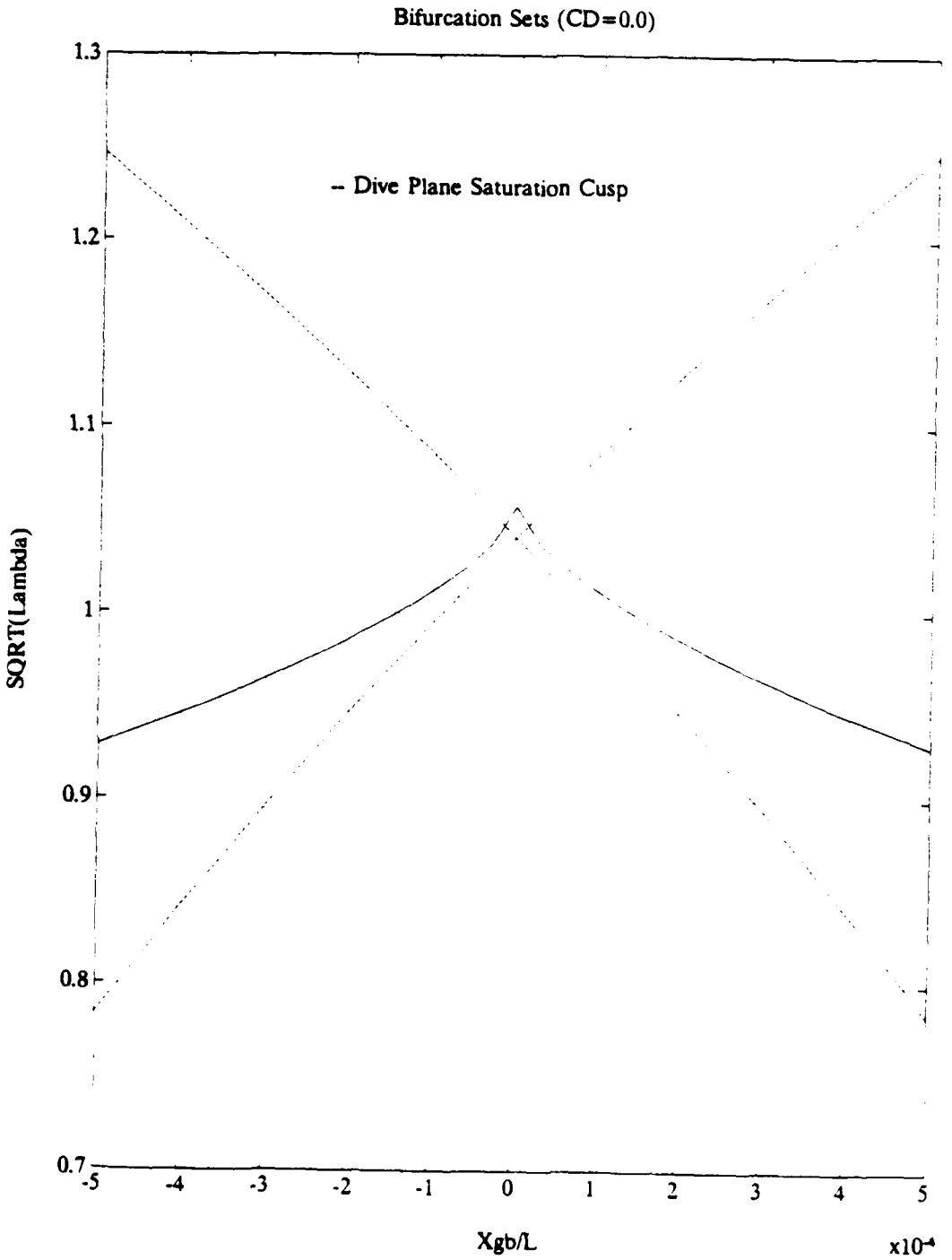

Figure 4-10. Expanded Bifurcation Cusp With Saturation Included.

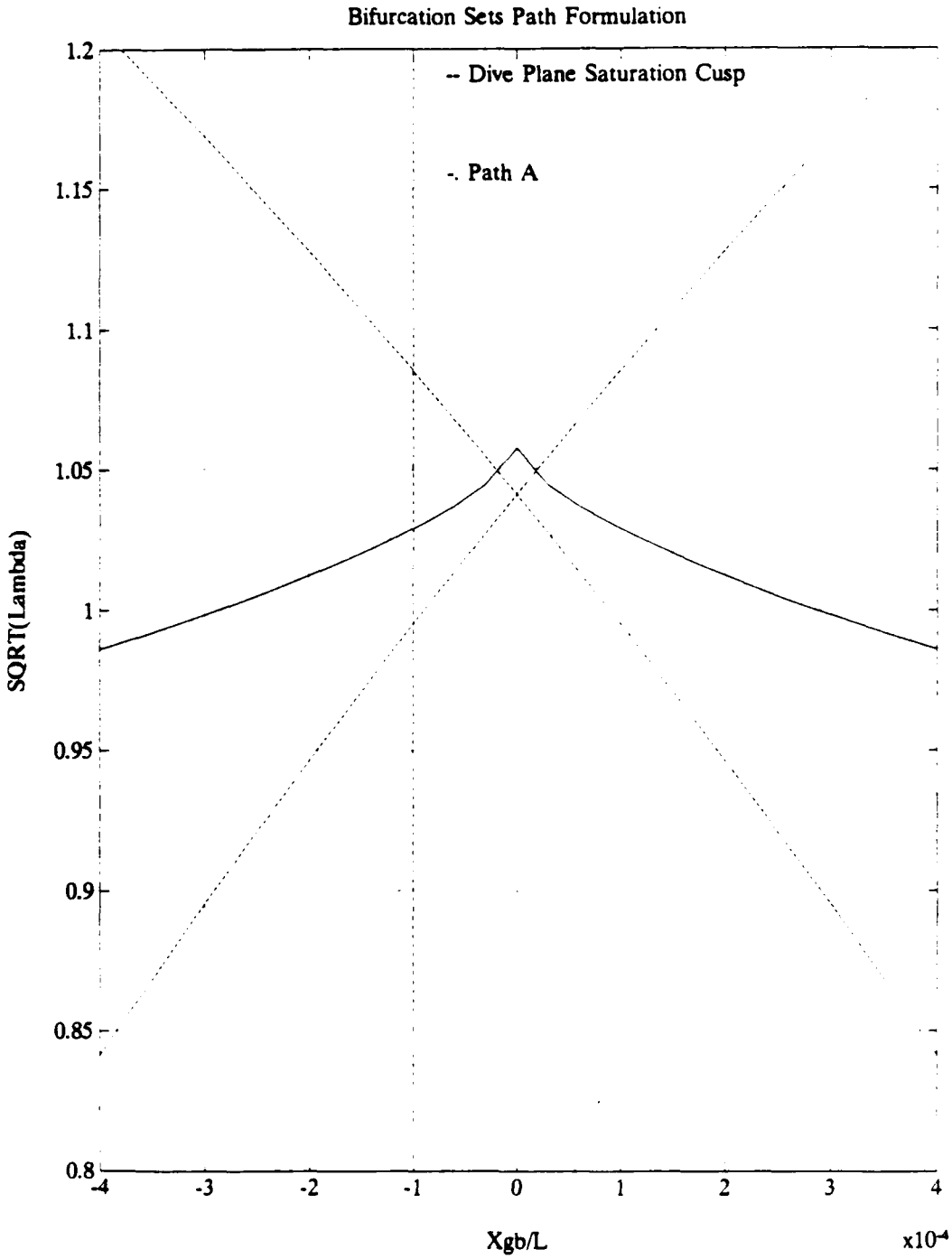

Figure 4-11. Path Formulation for Xgb/L=-0.0001.

upper portion of the dotted cusp at an approximate value of 1.08. At this value saturation occurs on one of the solution branches but there remains only one steady state solution since the path has not yet entered the cusp. As the speed continues to decrease, the path intersects and enters the saturation cusp at an approximate value of 0.99 with saturation of the other solution branch and the existence of multiple steady state solutions occurring. These results are evident in Figure 4-6.

Now, if the speed of the vessel is held constant, and the loading conditions on the hull are changed, then the paths shown in Figure 4-12 are obtained. Path B, at a Froude Number of 1.1, is outside the cusp, therefore only a single steady state solution for each value of x_{GB}/L should exist. While path C, at a Froude Number of 1.0, passes through the cusp at $\pm$ 0.0001 values of x_{GB}/L resulting in single steady state solutions for values less than or greater than $\pm$ 0.0001, while values between $\pm$ 0.0001 result in multiple steady state solutions. Through numerical computation the solution set as a function of x_{GB}/L is obtained with the results shown in Figure 4-13.

As seen in Figure 4-13, path B, represented by the dotted line, does in fact result in a single steady state solution throughout the range of x_{GB}/L, however, for path C this is not the case. Path C, represented by the solid line, exhibits multiple solutions between the x_{GB}/L values of $\pm$ 0.0001, as predicted. This is a hysteresis curve, with the unstable solutions occurring between the corners of the curve. If the value of x_{GB}/L began at -0.0005 and progressed to the positive value of 0.0001, the solution set would remain on the curve with θ taking on the values shown. Once the value of x_{GB}/L becomes greater than 0.0001 the solution jumps from -9° to 7.5°. This same jump would be evident if the value of x_{GB}/L began positive and progressed negative. These jumps indicate that if the dive planes are held constant, then the vessel will instantaneously change its pitch angle.

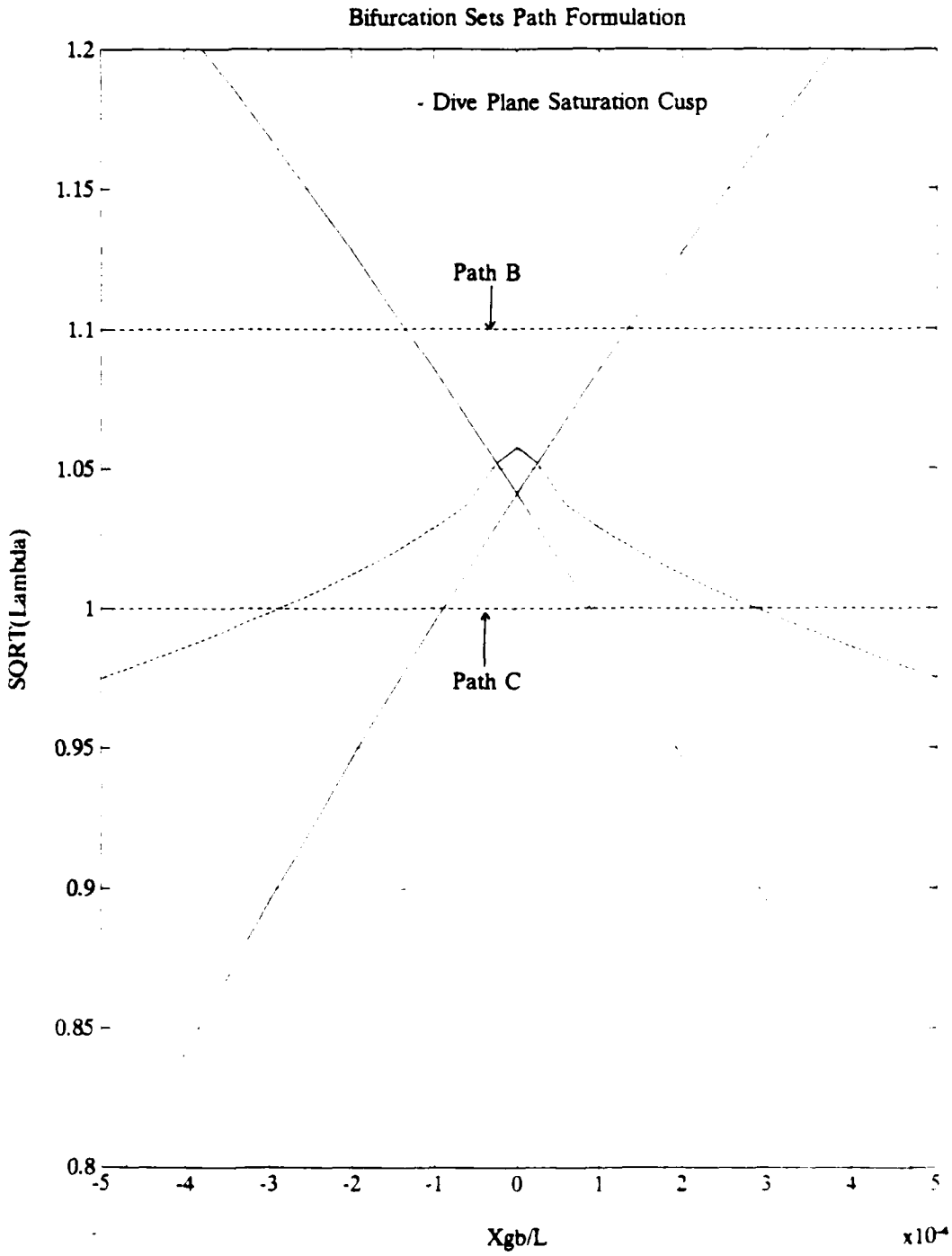

Figure 4-12. Path Formulation at a Constant Speed With Xgb/L Varying.

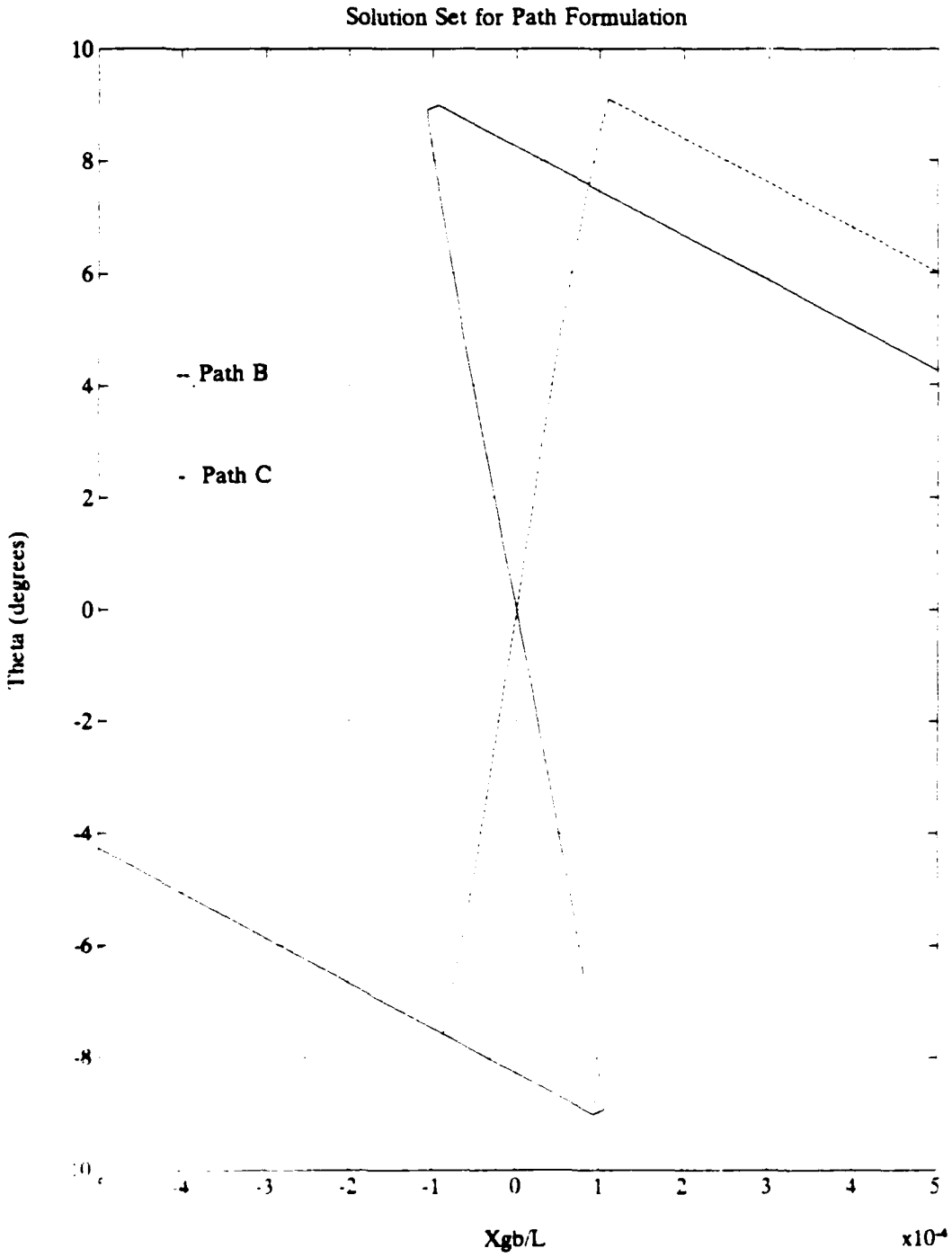

Figure 4-13. Solution Set for Path Formulation.

To counter this effect the dive plane angle must be reversed. It is this dive plane reversal that the following chapter will discuss.

Before proceeding to the next chapter it is necessary to determine the effect that drag has on the previously developed bifurcation cusps. Using equations 4.40 and 4.41, and substituting equation 4.4 into both equations will result in the following two equations;

$$Z_w u^2 \tan\theta - C_D A u^2 \tan\theta|\tan\theta| + Z_\delta u^2 \delta_{sat} = 0, \tag{4.44}$$

$$M_w u w - C_D x_A A u^2 \tan\theta|\tan\theta| - W x_{GB} \cos\theta - z_{GB} W \sin\theta + M_\delta u^2 \delta_{sat} = 0. \tag{4.45}$$

By using the **MATLAB** function *fzeros* contained in the program of Appendix A, the value of θ that solves equation 4.44 can be determined as a function of speed. This relationship can then be used to solve equation 4.45 to obtain the relationship between x_{GB} and u.

With this relationship obtained the cusp curves of Figure 4-14 can be plotted. It can be seen that for a given value of x_{GB}/L increasing the drag coefficient forces the bifurcation point to a lower speed. An interesting item to note is the diamond shape peak on these cusps. This is a result of saturation not occurring, for a small range of speeds, in the small region around $x_{GB}/L=0$. Path formulation through these cusps can be developed as shown earlier in this section.

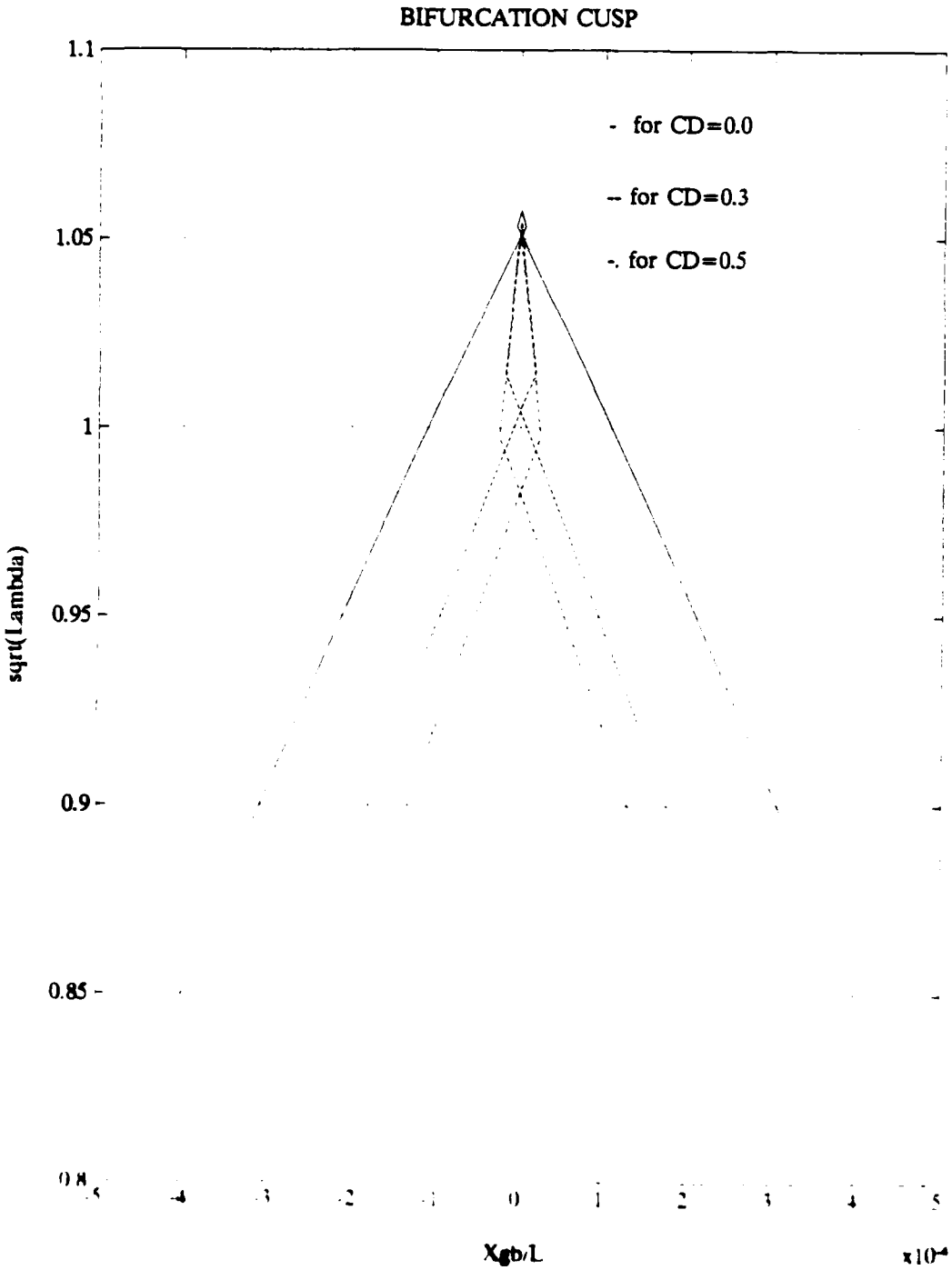

Figure 4-14. Bifurcation Cusp With Saturation Included for Different Values of C_D.

V. DIVE PLANE REVERSAL

A. STERN PLANE REVERSAL

The ability of a submarine to avoid detection and perform its mission is dependent on its ability to maintain ordered depth. Modern asymmetric submarines exhibit an inherent phenomenon known as dive plane reversal, which is difficult to deal with. To introduce this physical occurrence, refer to Figure 5-1 [Ref. 14] and consider the case of wanting to dive the vehicle to a deeper depth. At moderate to high speeds the stern planes would be deflected by an angle δ_s, this would in turn cause a force and moment to be developed due to the angle of attack of the planes. The vessel will respond by pitching downward, and will assume some angle of attack to the fluid flow causing hull forces and moments to develop. The stern plane and hull forces bring the ship to some steady state pitch angle which is obtained when the restoring moment and pitching moments balance. The vessel now has the ability to *fly* itself to the ordered depth with the normal hull force assisting in pushing the vessel to a deeper depth.

At low speed we would expect the same to be true, however it is not. If the stern planes are set to an angle δ_s, this would cause a force and moment to be developed due to the angle of attack of the planes, the vessel will pitch downward creating a pressure field around the vessel due to the angle of attack with the fluid resulting in hull forces and moments to develop The vessel once again steadies out at some steady state pitch angle when the restoring moment and pitching moments balance Since the speed of the vessel is not as great as in the previous case, the hull forces and moments are not as large, therefore

$Z_w W$ NORMAL FORCE DUE TO ANGLE OF ATTACK ON HULL

$Z_{\delta_s} \delta_s$ NORMAL FORCE DUE TO STERNPLANE DEFLECTION ANGLE (δ_s)

$M_w W$ PITCH MOMENT DUE TO ANGLE OF ATTACK ON HULL

$M_{\delta_s} \delta_s$ PITCH MOMENT DUE TO STERNPLANE DEFLECTION ANGLE (δ_s)

$M_\theta \theta$ METACENTRIC PITCH MOMENT DUE TO PITCH ANGLE (θ)

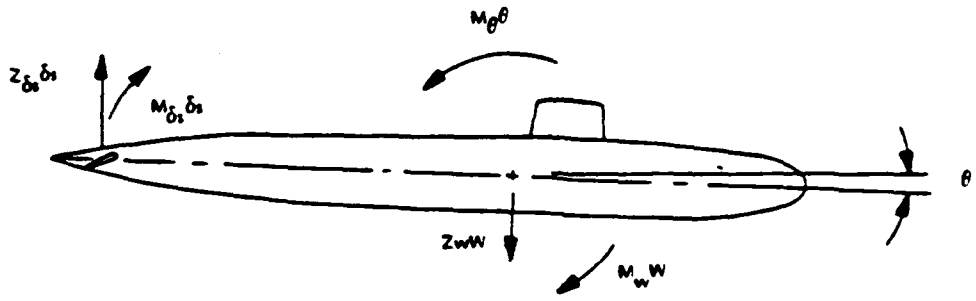

VERY LOW SHIP SPEED

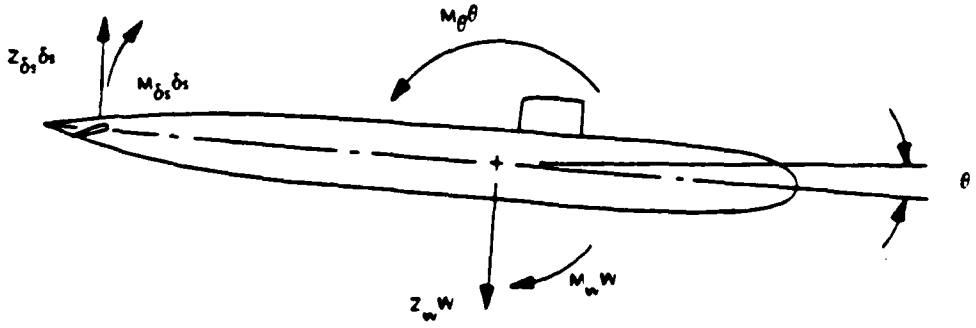

MODERATE AND HIGH SHIP SPEED

Figure 5-1. Stern plane Reversal.

instead of the vessel *flying* itself to the ordered depth with the hull force assisting, the stern plane force actual pushes the vessel upward causing it to rise instead of dive, with some non-zero pitch angle. [Ref. 14] This condition was evident in the simulation shown in Figure 3.3.

With this description of the vehicle response complete, it is obvious that to dive the vessel at low speeds, the opposite stern plane angle must be ordered. This will result in the vessel being pushed to the ordered depth at some bow up attitude. This required shift in dive plane angle is what is known as **STERN PLANE REVERSAL**.

To tie together the previously completed bifurcation analysis with the physical occurrence just discussed, Figure 5-2 is produced. Figure 5-2 presents the pitch angle and stern plane angle required for straight and level flight with the bow planes centered. As the vessel's speed decreases, the metacentric moment ($M_\theta\theta$) makes it increasingly difficult to maintain a positive pitch angle on the hull. The stern plane angle is negative trying to produce a pitch-up moment, but the downward force of the stern planes requires an even larger pitch angle [Ref. 14]. Between the speeds of 1.08 and 1.18 knots, the required stern plane angle is beyond the normal operating range and the vessel cannot be flown straight and level. Below the critical speed, the stern plane and vessel pitch angle must reverse sign to maintain neutral trim.

In a final effort to show the physical significance of stern plane reversal, the force input to the stern planes is plotted. If the control gains are allowed to change as the speed of the vessel changes, Figure 5-3 is produced. This plot shows the non-dimensional force per unit depth error input to the stern plane as a function of speed. It is basically the control system gain used to set the stern plane angle. As can be seen, as the critical speed

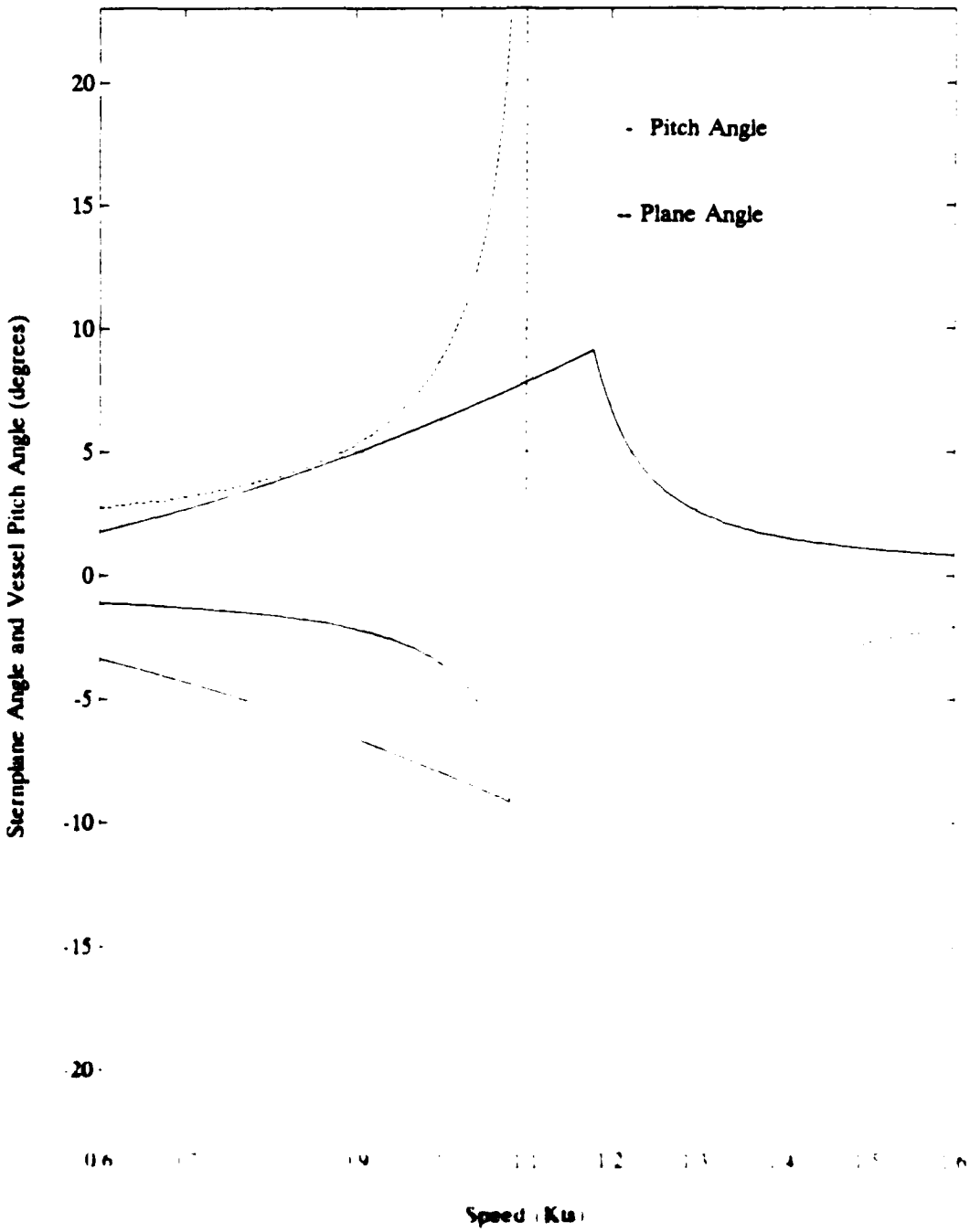

Figure 5-2 Variation of Pitch and Stern plane Angles as a Function of Speed

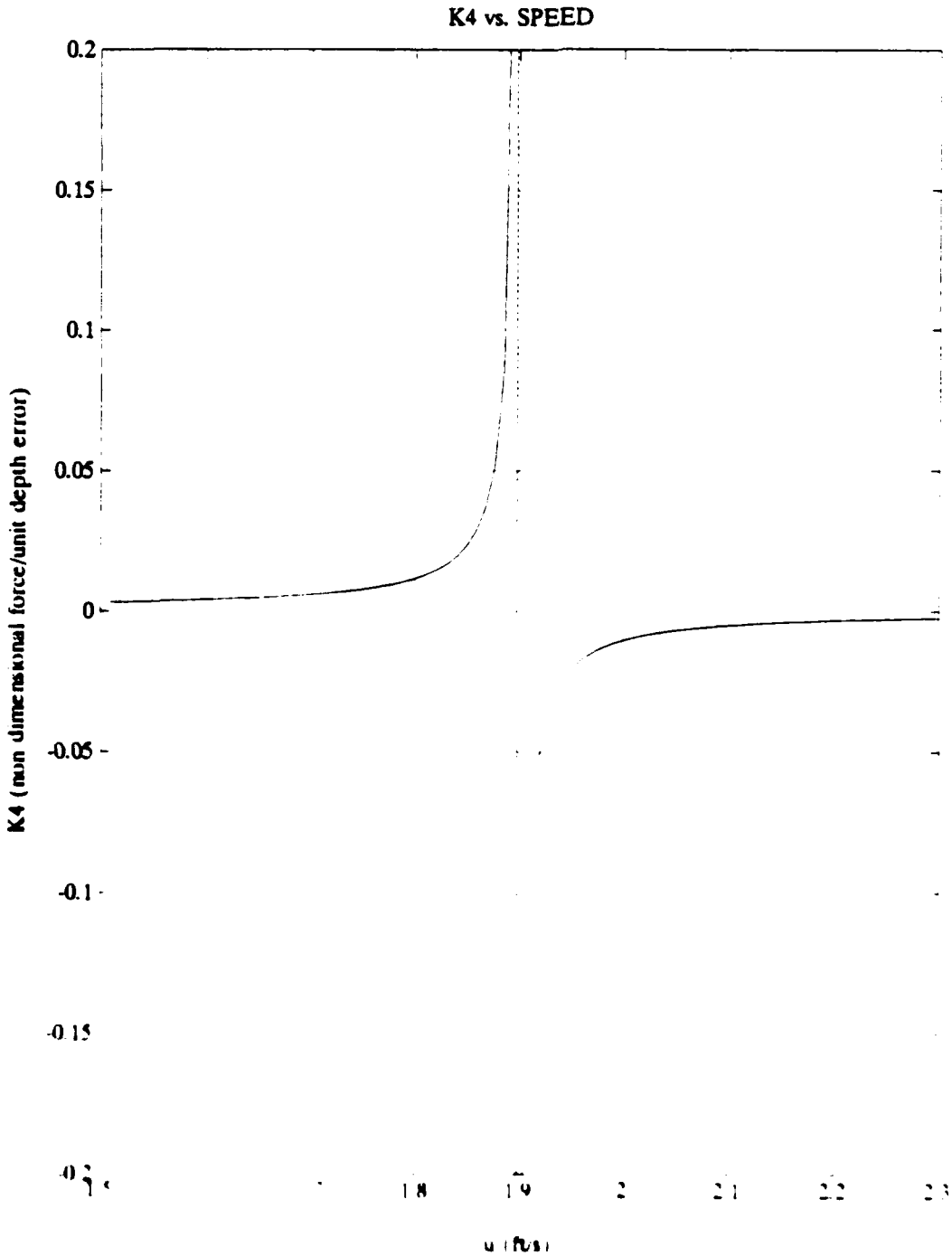

Figure 5-3 Control System Force Input to the Stern planes.

is approached the value of input tends to infinity requiring the stern planes to operate outside normal values. As the speed passes the critical value the sign of this input changes requiring the stern planes to operate in the opposite direction. This reversal in sign is evident of the stern plane reversal phenomenon shown and discussed earlier in this chapter.

B. BOW PLANE REVERSAL

The reversal effect that was shown to occur with the stern planes can also be shown to occur with the bow planes. If the value of α is allowed to tend to ∞, indicating no stern plane control and only bow plane control, then the same analysis conducted throughout this thesis for stern plane reversal can be performed for bow plane reversal. If the critical Froude number, (sqrt(λ)), is plotted as a function of α, then the results shown in Figure 5-4 are produced. This plot shows that for bow plane control only, the critical value approaches 2.05 as α approaches ∞.

To show that the same type of results can be obtained for the bow plane analysis, the case of neutral buoyancy, $x_{GB} = 0$ and dive plane saturation, with bow plane control only was investigated. Referring to Figure 5-5, it can be seen that at a Froude number of 2.05 multiple steady state solutions occur. These results are similar to the results displayed in Figure 3-5. The major differences are that the critical point occurs at a Froude number of 2.05 vice 1.05, and the maximum value of θ is only $\pm$ 4.5° vice $\pm$ 9.5°. The reason for these changes is due to the values of Z_{δ_s} and M_{δ_s} being only one-half the respective value for the stern planes.

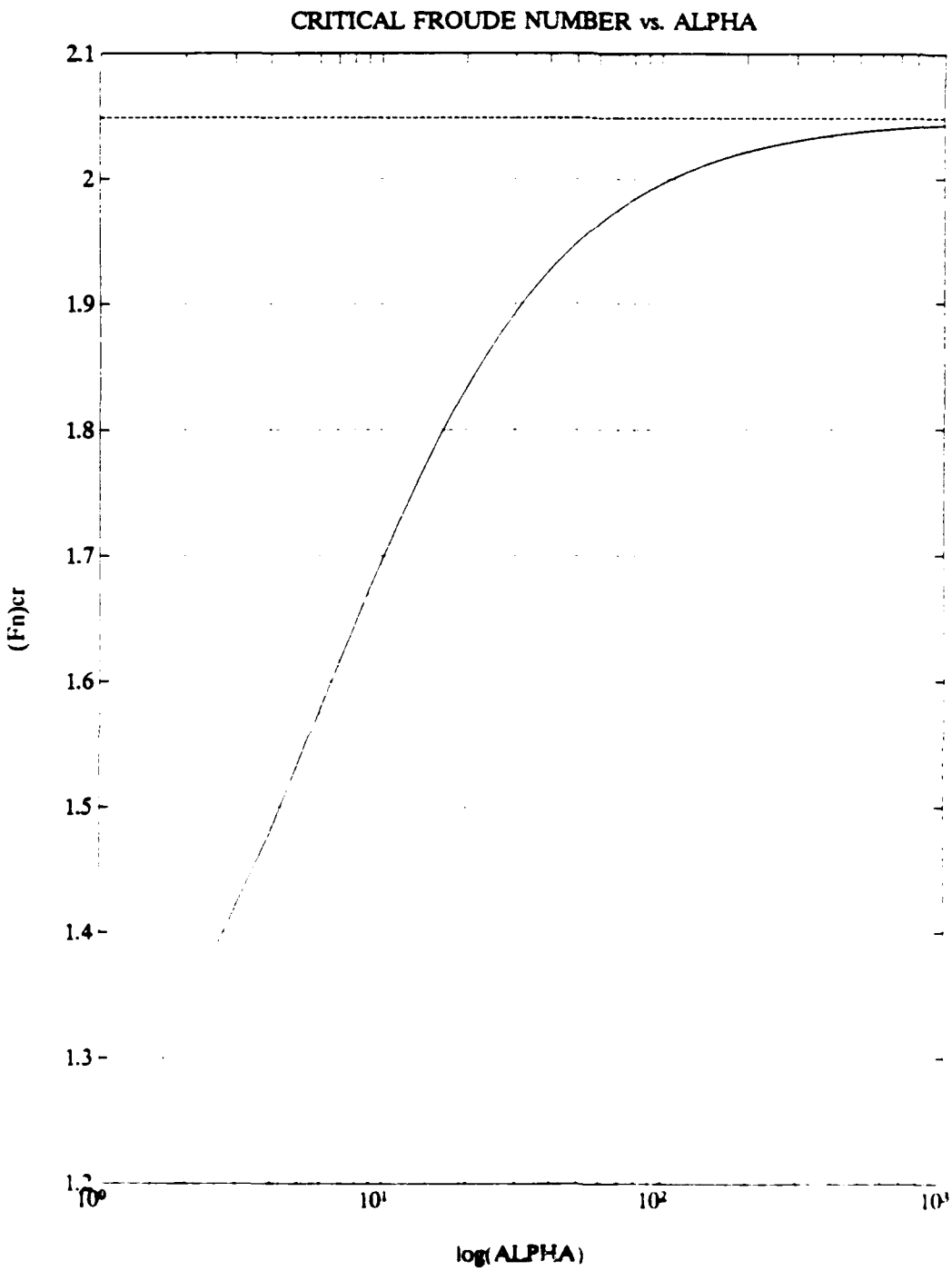

Figure 5-4. Identification of Critical Froude Number for Bow plane Control.

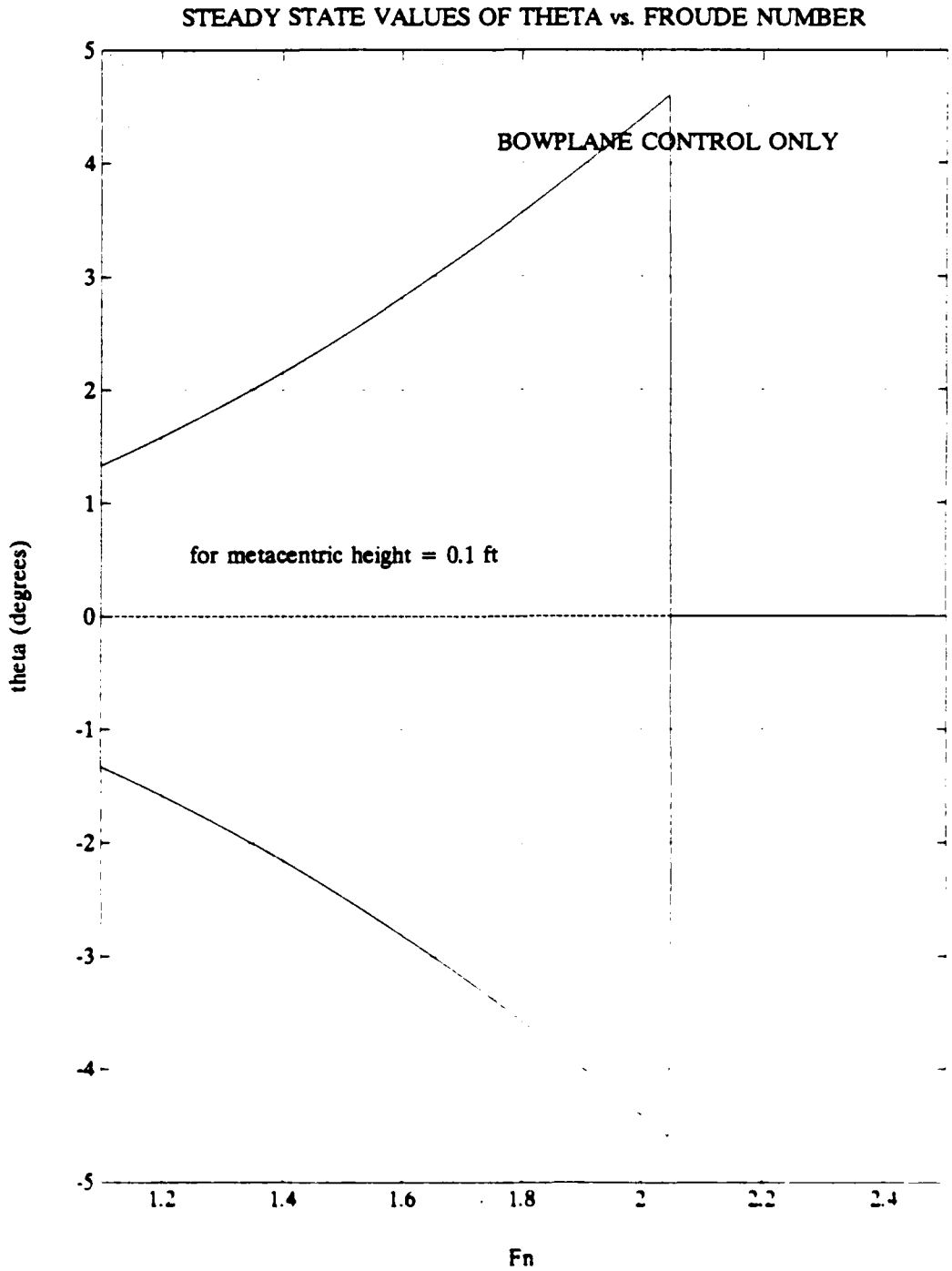

Figure 5-5. Steady State Values of θ for Bow plane Control.

C. BIAS EFFECTS

As a final area of analysis, the condition of operating near the surface, such as during periscope operations, must be investigated to determine the effects this will have on the previously developed bifurcation cusps. Operating near the surface will require the incorporation of a suction force and moment into the equations of motion. This force and moment is a function of the distance away from the surface, and the angle the vessel makes with the surface. Therefore, as a simple model of suction effects consider the case of operating with excess buoyancy. To conduct the analysis requires the use of equations 4.1, 4.2 and 4.4. Performing the same substitution and solution technique as was used in Chapter V to obtain the saturation curves that incorporated the drag coefficient will result in solving the following equations to obtain the bifurcation cusps that would quasi-model surface effects;

$$Z_w uw - \frac{1}{2}\rho C_D A u^2 \tan\theta|\tan\theta| + (W - B)\cos\theta + Z_\delta u^2 \delta_{sat} = 0, \tag{5.1}$$

$$\begin{aligned} M_w uw - \frac{1}{2}\rho C_D x_A A u^2 \tan\theta|\tan\theta| - (x_G W - x_B B)\cos\theta \\ - (z_G W - z_B B)\sin\theta + M_\delta u^2 \delta_{sat} = 0 \end{aligned} \tag{5.2}$$

If the value of C_D is set equal to zero then the saturation cusp produced in Figure 4-10 can be compared to the results obtained for several cases of excess buoyancy. Since it is the saturation cusp that controls the location of the bifurcation point, as shown in previous the chapter, the non saturation cusp will be neglected for the remainder of the analysis. Figure 5-6 shows the results obtained as excess buoyancy is increased. As can be seen the cusp peak moves to down and to the right occurring at a lower speed and at a non zero value of x_{cp}/l. The body of the cusp also shifts to the right as seen with the

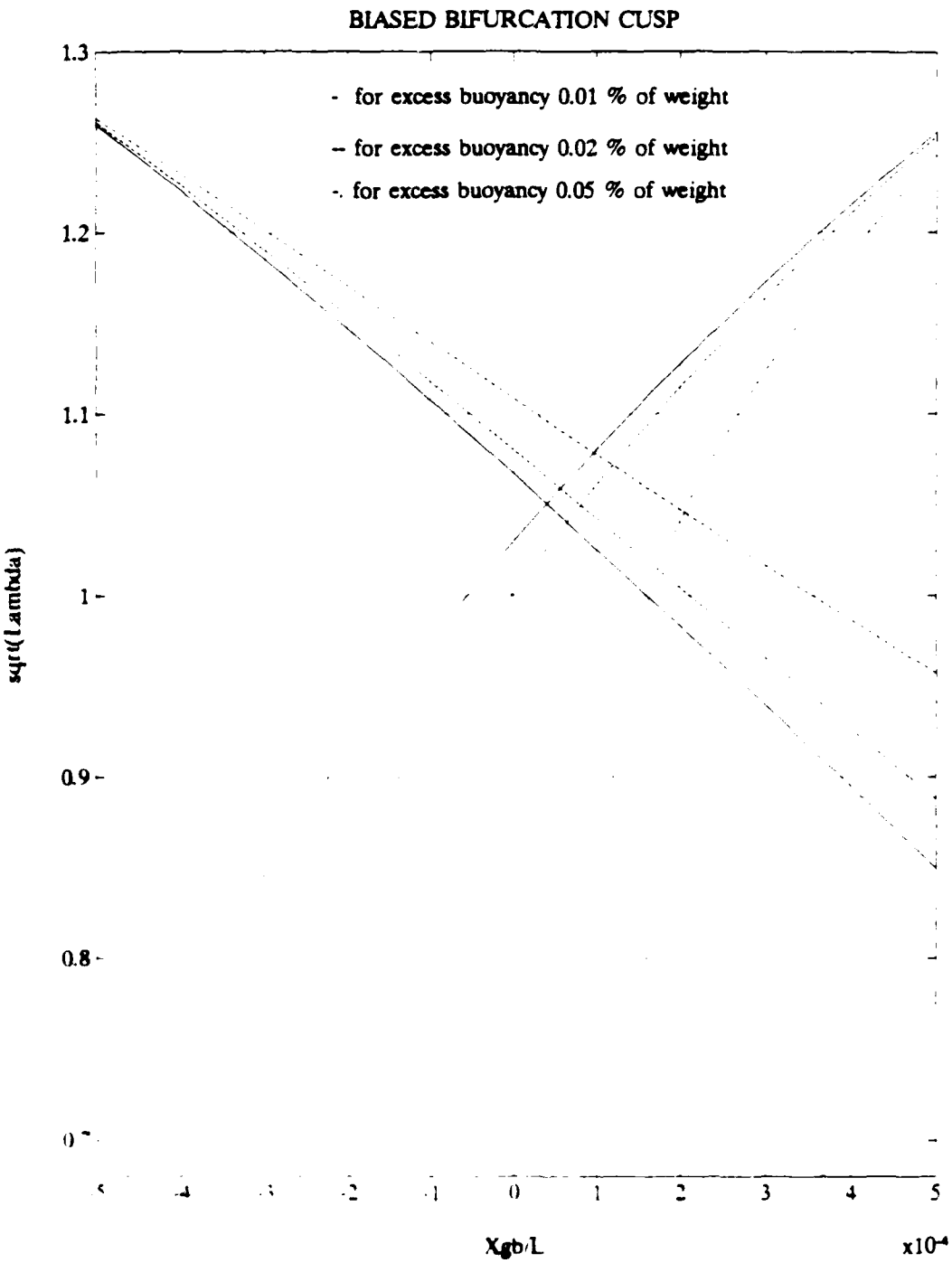

Figure 5-6. Bias Effects Caused by Operating Near the Surface.

entire cusp occurring in the positive region of the x_{CB}/L range for a value of 0.05 % excess buoyancy

To determine how the value of drag coefficient effects the cusp curves, consider the case of $C_D = 0.3$ shown in Figure 5-7. These cusps were produced for the same values of excess buoyancy used in Figure 5-6. Notice that the cusp curves shift to the right by the same value seen in Figure 5-6, but the peak value now occurs at an even a lower speed.

In order to observe the sensitivity of the biased cusp to drag only, consider the case of setting the excess buoyancy to 0.01 % and varying the drag coefficient, shown Figure 5-8. These results indicate that increased drag causes the critical speed to occur at a lower value. They also show that drag tends to counter the biasing effect that excess buoyancy was previously show to have. This is evident by the peak point drifting to the left as the value of drag coefficient increases.

In summary, it can be stated that operating near the surface will tend to reduce the critical speed determined in previous chapters and the vessel will have to be placed in a different trim condition to counter surface effects, and that increasing drag will reduce the critical speed but tends to counter the trim condition required.

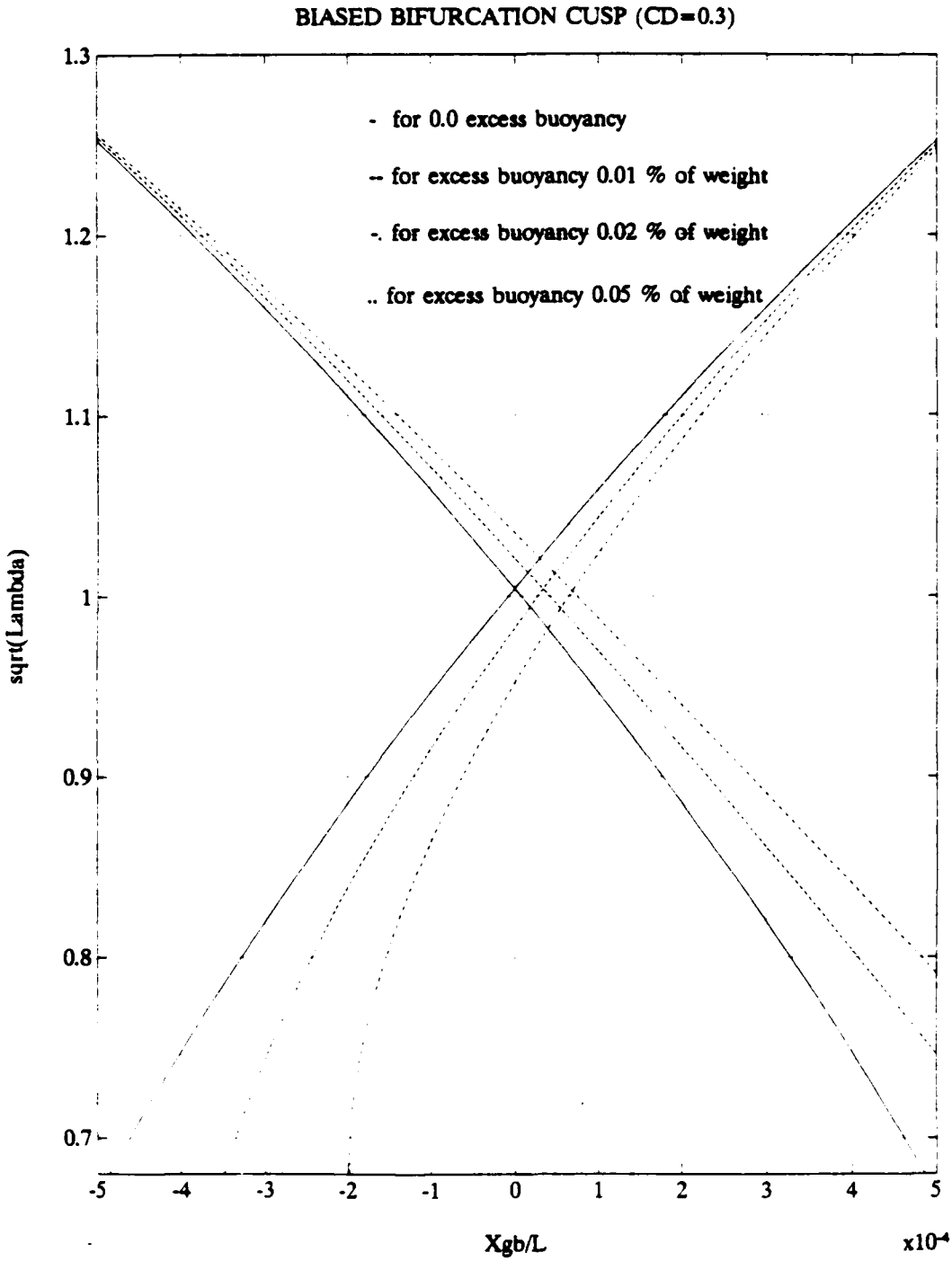

Figure 5-7. Bias Effects Caused by Operating Near the Surface Considering Drag.

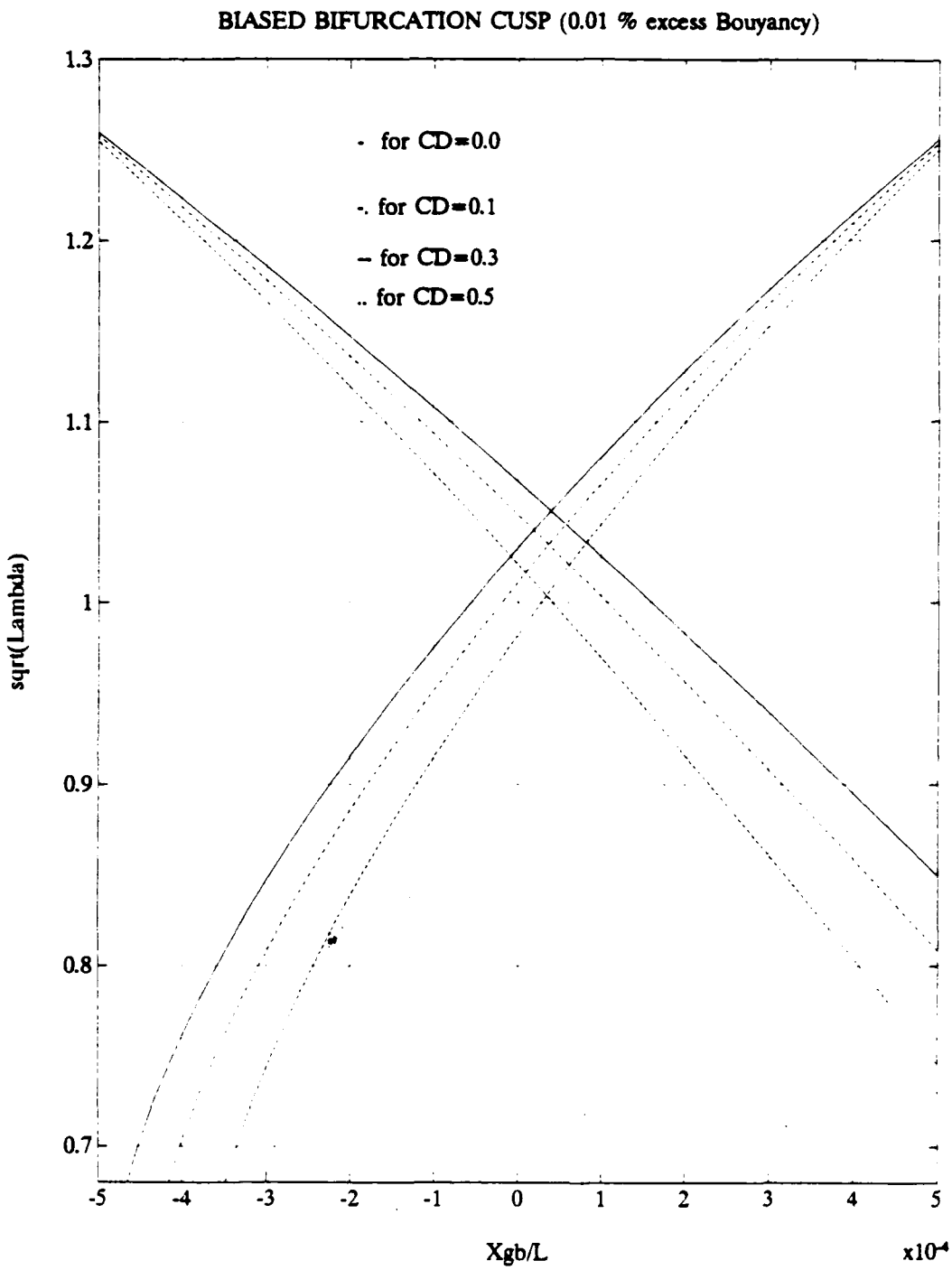

Figure 5-8. Bias Effects Caused by Drag While Operating Near the Surface.

VI. CONCLUSIONS AND RECOMMENDATIONS

A. CONCLUSIONS

- A method for analyzing submarine depth keeping and dive plane reversal has been developed and presented. This analysis identified the three phenomena, a positive real eigenvalue, a steady state pitchfork bifurcation, and an uncontrollable system, that lead to vessel instability.

- The critical parameters have been identified that control the bifurcation. These parameters combine speed, loading conditions and hydrodynamic coefficients into non-dimensional values that may be applied to other models or vessels.

- Since the non-dimensional Froude numbers are based on the metacentric height and LCG-LCB separation, Froude scaling can be used to apply this analysis to full scale vessels, allowing for the reduction of model testing during design phases.

B. RECOMMENDATIONS

Some recommendations for further research are as follows:

- Develop and incorporate into the bifurcation analysis a more complete expression for the free-surface effects.

- Conduct a Hopf bifurcation analysis to identify the critical parameters that lead to vehicle instability at high speeds.

APPENDIX A

COMPUTER PROGRAMS

```
% THIS PROGRAM IS THESIS1.M. IT SIMULATES THE RESPONSE OF THE
DTRC SUBOFF
% MODEL. IT PLACES THE POLES, CALCULATES THE CRITICAL SPEED, AND
USES
% PROGRAM THESISDE.M TO SIMULATE THE VERTICAL PLANE REPONSE.

clg;
global zg m zgb u U Zq Zw Zdlt Mq Mw B1 Mdlt K1 M bm xL Zval Mval rho

% ESTABLISH GEOMETRIC PARAMETERS
W=1556.2363;B1=1556.2363;
Iy=561.32;
g=32.2;
m=W/g;
rho=1.94;
L=13.9792;
xg=0;zg=0.1;
zgb=0.1;

% BEAM AND LENGTH DEFINITION FOR TRAPAZIODAL RULE USE
bm=[0 .485 .658 .778 .871 .945 1.01 1.06 1.18 1.41 1.57 1.66 1.67 1.67 1.67 1.63...
 1.37 .919 .448 .195 .188 .168 .132 .053 0];

x1=[0 .1 .2 .3 .4 .5 .6 .7 1 2 3 4 7.7143 10 15.1429 16 17 18 19 20 20.1...
 20.2 20.3 20.4 20.4167];
xl=(L/20)*x1;
xL=xl-L/2;

% FACTORS TO CONVERT FROM NON-DIMENSIONAL VALUES TO
DIMENSIONAL VALUES
nd1=.5*rho*L^2;
nd2=.5*rho*L^3;
nd3=.5*rho*L^4;
nd4=.5*rho*L^5;
```

```
Alpha=0;

% NON-DIMENSIONAL HYDRODYNAMIC COEFFICIENTS
Zqdnd=-6.33e-4;Zwdnd=-1.4529e-2;Zqnd=7.545e-3;Zwnd=-1.391e-2;
Zds=(-5.603e-3);Zdb=0.5*(-5.603e-3);Zdltnd=(Zds+Alpha*Zdb);
Mqdnd=-8.8e-4;Mwdnd=-5.61e-4;Mqnd=-3.702e-3;Mwnd=1.0324e-2;
Mds=(-0.002409);Mdb=0.5*(0.002409);Mdltnd=(Mds+Alpha*Mdb);

% CONVERTION OF COEFFICENTS INTO DIMENSIONAL VALUES
Zqd=nd3*Zqdnd;Zwd=nd2*Zwdnd;Zq=nd2*Zqnd;Zw=nd1*Zwnd;
Zdlt=nd1*Zdltnd;

Mqd=nd4*Mqdnd;Mwd=nd3*Mwdnd;Mq=nd3*Mqnd;Mw=nd2*Mwnd;
Mdlt=nd2*Mdltnd;

% FORMULATION OF A AND B MATRIX ELEMENTS
Dv=(m-Zwd)*(Iy-Mqd)-(m*xg+Zqd)*(m*xg+Mwd);
a11Dv=(Iy-Mqd)*Zw+(m*xg+Zqd)*Mw;
a12Dv=(Iy-Mqd)*(m+Zq)+(m*xg+Zqd)*(Mq-m*xg);
a13Dv=-(m*xg+Zqd)*W;
b1Dv=(Iy-Mqd)*Zdlt+(m*xg+Zqd)*Mdlt;
a21Dv=(m-Zwd)*Mw+(m*xg+Mwd)*Zw;
a22Dv=(m-Zwd)*(Mq-m*xg)+(m*xg+Mwd)*(m+Zq);
a23Dv=-(m-Zwd)*W;
b2Dv=(m-Zwd)*Mdlt+(m*xg+Mwd)*Zdlt;

a11=a11Dv/Dv;a12=a12Dv/Dv;a13=a13Dv/Dv;
a21=a21Dv/Dv;a22=a22Dv/Dv;a23=a23Dv/Dv;
b1=b1Dv/Dv;b2=b2Dv/Dv;

% ESTABLISHMENT OF POLE LOCATIONS
p1=[-3 -31 -32 -33];

% CALCULATION OF CRITICAL SPEED
Ucr=sqrt(-(a13*b2-a23*b1)*zgb/(a11*b2-a21*b1))

% INPUT OF SPEED WHICH THE VESSEL WILL USE IN THE SIMULATION
U=input('enter speed of vehicle ')

% CALCULATION OF FROUDE NUMBER
Fn=sqrt(U^2/(zgb*g))
```

```
% CALCULATION OF MATRICIES FOR POLE PLACEMENT AND
CONTROLABILLITY ANALYSIS
u=5;
a=[0 0 1 0;a13*zgb a11*u a12*u 0;a23*zgb a21*u a22*u 0;...
-u 1 0 0];
a1=[0 0 1 0;a13*zgb a11*Ucr a12*Ucr 0;a23*zgb a21*Ucr a22*Ucr 0;...
-Ucr 1 0 0];

b=[0;b1*u^2;b2*u^2;0];
b1=[0;b1*Ucr^2;b2*Ucr^2;0];

K1=place(a,b,p1);
C=rank(ctrb(a1,b1));
H=(Mw*Zdlt-Zw*Mdlt)/(zgb*B1*Zdlt);
theta1=acos(H*U^2)*180/pi;
Dss=-(Zw/Zdlt)*tan(acos(H*U^2))*180/pi;
Z=(Dss+K1(1)*acos(H*U^2)+K1(2)*U*tan(acos(H*U^2)))/...
(-K1(4));

% ESTABISHES VEHICLE MASS MATRIX
M=[1 0 0 0,0 (m-Zwd) -Zqd 0 ;0 -Mwd (Iy-Mqd) 0 ;0 0 0 1];

% SET TIME LIMITS AND INITIAL CONDITIONS FOR ODE SOLUTION
t0=0;tf1=2500*L/U;
x0=[0 0 0 1];

% SOLVES VEHICLE SIMULATION ODE'S
[t1,X1]=ode45('thesisde',t0,tf1,x0);

% REDEFINE THE OUTPUT VECTOR ELEMENTS AND FORM DIVE PLANE
RESPONSE
w1=X1(:,2);q1=X1(:,3);z1=X1(:,4);th1=X1(:,1);
d=-(K1(1)*th1+K1(2)*w1+K1(3)*q1+K1(4)*z1);
l1=length(d);

for n=1:l1,
 if d(n)> 4,
   d(n)= 4;
 elseif d(n)<- 4,
   d(n)=- 4;
 end;
end;
```

```
% PLOT THE RESULTS
subplot(211);
plot(t1*U/L,th1*180/pi,t1*U/L,d*180/pi,'--');title('THETA/DELTA vs. TIME ');
xlabel('non-dimensional time ');ylabel('theta/delta (degrees)');grid;
gtext('--delta');gtext(['for a speed of ' num2str(U) ' fps']);

plot(t1*U/L,z1/L);title('DEPTH vs. TIME');xlabel('non dimensional time');
ylabel('non dimensional depth ');grid;
pause;
subplot(111);

% THIS IS PROGRAM THESISDE.M. IT CONTAINS THE SUBOFF MODEL
SYSTEM OF
% EQUATIONS TO BE SOLVED BY PROGRAM THESIS1.M

% SET SYSTEM OF EQUATIONS FUNCTION
function X1dot=thesisde(t1,X1);

% SET CONTROL LAW
d1=-K1(1)*X1(1)-K1(2)*X1(2)-K1(3)*X1(3)-K1(4)*X1(4);

% APPLY DIVE PLANE SATURATION
if d1>.4,
   d1=.4;
 elseif d1<-.4,
   d1=-.4;
 end;

% INCLUDE DRAG TERMS AND CALCULATE AREA AND CENTROID
CD=0;

if X1(2)==0,
  X1(2)=1e-5;
end;

if X1(3)==0,
  X1(3)=1e-5;
end;

Zval=bm.*((X1(2)-xL.*X1(3)).^3)./(abs(X1(2)-xL.*X1(3)));
Mval=bm.*(((X1(2)-xL.*X1(3)).^3).*xL)./(abs(X1(2)-xL.*X1(3)));

ZDragval=0;MDragval=0;
```

```
% trapaziodal integration
for n=1:length(xL)-1,

Zdragval=0.5*(Zval(n)+Zval(n+1))*(xL(n+1)-xL(n));
Mdragval=0.5*(Mval(n)+Mval(n+1))*(xL(n+1)-xL(n));
ZDragval=ZDragval+Zdragval;
MDragval=MDragval+Mdragval;

end;

Zdr=(0.5)*rho*CD*ZDragval;
Mdr=(0.5)*rho*CD*MDragval;

% VEHICLE SYSTEM OF EQUATIONS
F1=[X1(3); m*(U*X1(3)+zg*X1(3)^2)+Zq*U*X1(3)+Zw*U*X1(2)+U^2*Zdlt*d1-Zdr;
  m*(-zg*X1(2)*X1(3))+Mq*U*X1(3)+Mw*U*X1(2)-
B1*zgb*sin(X1(1))+U^2*Mdlt*d1-Mdr;
  -U*sin(X1(1))+X1(2)*cos(X1(1))];

mpr=inv(M);
X1dot=mpr*F1;
```

```
C   PROGRAM STEADY
C
C   STEADY STATE SOLUTIONS OF SUBMARINES
C   IN THE DIVE PLANE AT LOW SPEEDS
C
C   INPUT DATA
C
C   ICON  = 1 : COMPUTATION OF SOLUTION SETS (S.S)
C         2 : COMPUTATION OF BIFURCATION GRAPHS (B.G.)
C
C   IVAR  = 1 : Fn VARIATION
C         2 : Xgb VARIATION
C
    REAL MW,LENGTH,MASS,MDS,MDB,MD,LAMBDA
C
    DIMENSION B(25),X(25),BX(25)
C
C   GEOMETRIC PROPERTIES AND HYDRODYNAMIC COEFFICIENTS
C
    RHO   = 1 94
    LENGTH= 13 9792
    WRITE (*,*) ' ENTER CDZ'
    READ  (*,*) CDZ
    CDZ   = CDZ*0 5*RHO
    BUO= 1556 2363
    WRITE(*,*) 'ENTER VALUE OF EXCESS BUO'
    READ (*,*) FAC
    WEIGHT=FAC*BUO
    MASS  = WEIGHT/32.2
    XB    = 0 0
    ZB    = 0.0
    WRITE (*,*) 'ENTER THE METACENTRIC HEIGHT ZGB'
    READ (*,*) ZG
    ZW    =-0.013910*0.5*RHO*LENGTH**2
    ZDS   =-0.005603*0.5*RHO*LENGTH**2
    ZDB   =-0.005603*0.25*RHO*LENGTH**2
    MW    = 0.010324*0.5*RHO*LENGTH**3
    MDS   =-0.002409*0.5*RHO*LENGTH**3
    MDB   = 0.002409*0.25*RHO*LENGTH**3
C
    WRITE (*,*) 'ENTER THE VALUE OF ALPHA'
    READ (*,*) ALPHA
    ZD=ZDS+ALPHA*ZDB
```

```
      MD=MDS+ALPHA*MDB
C
C     DEFINE THE LENGTH X AND BREADTH B TERMS FOR THE
INTEGRATION
C
      X( 1)=20.4167
      X( 2)=20.4000
      X( 3)=20.3
      X( 4)=20.2
      X( 5)=20.1
      X( 6)=20.0
      X( 7)=19.0
      X( 8)=18.0
      X( 9)=17.0
      X(10)=16.0
      X(11)=15.1429
      X(12)=10.0
      X(13)=7.7143
      X(14)=4.0
      X(15)=3.0
      X(16)=2.0
      X(17)=1.0
      X(18)=0.7
      X(19)=0.6
      X(20)=0.5
      X(21)=0.4
      X(22)=0.3
      X(23)=0.2
      X(24)=0.1
      X(25)=0.0
C
      B( 1)=0.00000
      B( 2)=0.03178
      B( 3)=0.07920
      B( 4)=0.10074
      B( 5)=0.11243
      B( 6)=0.11724
      B( 7)=0.26835
      B( 8)=0.55025
      B( 9)=0.81910
      B(10)=0.97598
      B(11)=1.00000
      B(12)=1.00000
```

```
      B(13)=1.00000
      B(14)=0.99282
      B(15)=0.94066
      B(16)=0.84713
      B(17)=0.70744
      B(18)=0.63514
      B(19)=0.60352
      B(20)=0.56627
      B(21)=0.52147
      B(22)=0.46600
      B(23)=0.39396
      B(24)=0.29058
      B(25)=0.00000
C
      DO 1 I=1,25
         B(I)=B(I)*1.6667
         X(I)=(-X(I)+10.0)*LENGTH/20.0
         BX(I)=B(I)*X(I)
    1 CONTINUE
      CALL TRAP(18,B,X,AREA)
      CALL TRAP(18,BX,X,CH)
      XA=CH/AREA
C      WRITE(*,*) 'AREA EQUALS ',AREA
C      WRITE(*,*) 'XA EQUALS ',XA
      IFC=0
C
C      OPEN RESULTS FILES
      OPEN (10,FILE='R10 RES',STATUS='NEW')
      OPEN (11,FILE='R11 RES',STATUS='NEW')
      OPEN (12,FILE='R12 RES',STATUS='NEW')
      OPEN (13,FILE='R13 RES',STATUS='NEW')
      OPEN (14,FILE='R14 RES',STATUS='NEW')
      OPEN (15,FILE='R15 RES',STATUS='NEW')
      OPEN (16,FILE='R16 RES',STATUS='NEW')
      OPEN (20,FILE='C20 RES',STATUS='NEW')
      OPEN (21,FILE='S21 RES',STATUS='NEW')
      OPEN (22,FILE='S22 RES',STATUS='NEW')
      OPEN (23,FILE='S23 RES',STATUS='NEW')
      OPEN (24,FILE='S24 RES',STATUS='NEW')
      OPEN (31,FILE='S31 RES',STATUS='NEW')
      OPEN (32,FILE='S32 RES',STATUS='NEW')
      OPEN (33,FILE='S33 RES',STATUS='NEW')
      OPEN (34,FILE='S34 RES',STATUS='NEW')
```

```
      OPEN (41,FILE='C41.RES',STATUS='NEW')
      OPEN (42,FILE='C42.RES',STATUS='NEW')
      OPEN (43,FILE='C43.RES',STATUS='NEW')

C
C     READ DATA INTERACTIVELY
C
      WRITE (*,1001)
      READ (*,*)  ICON
      IF (ICON.EQ.2) GO TO 331
      WRITE (*,1009)
      READ (*,*)  IVAR
      GO TO (331,332), IVAR
  331 WRITE (*,1002)
      READ (*,*)  UMIN
      WRITE (*,1003)
      READ (*,*)  UMAX
      WRITE (*,1004)
      READ (*,*)  ITER
      JU=ITER
      IF (ICON.EQ.2) GO TO 332
      WRITE (*,1010)
      READ (*,*)  XG
      XG=XG*LENGTH
      GO TO 300
  332 WRITE (*,1005)
      READ (*,*)  XGMIN
      WRITE (*,1006)
      READ (*,*)  XGMAX
      WRITE (*,1004)
      READ (*,*)  ITER
      JXG=ITER
      XGMIN=XGMIN*LENGTH
      XGMAX=XGMAX*LENGTH
      IF (ICON.EQ.2) GO TO 334
      WRITE (*,1012)
      READ (*,*)  U
  334 CONTINUE
      GO TO 300
  300 WRITE (*,1013)
      READ (*,*)  ISET
      IF (ICON.EQ.2) GO TO 370
      GO TO (350,360,400), ISET
```

```
C
C    EXACT SOLUTION SET
C
 350 DO 2 I=1,ITER
       WRITE (*,2000) I,ITER
       GO TO (351,352), IVAR
 351   U=UMIN+(UMAX-UMIN)*(I-1)/(ITER-1)
       GO TO 355
 352   XG=XGMIN+(XGMAX-XGMIN)*(I-1)/(ITER-1)
 355   A1= ZW*MD-MW*ZD
       A2=-CDZ*AREA*(MD-XA*ZD)
       A3=-(XG-XB)*WEIGHT*ZD
       A4= (ZG-ZB)*WEIGHT*ZD
       CALL
EXSOLS(IVAR,LL,IFC,U,XG,A1,A2,A3,A4,CDZ,AREA,ZW,ZD,ZG,MW,
   & MD,BUO,XA)
       IF (LL.GT.1) IFC=1
   2 CONTINUE
    GO TO 5000
C
C    PITCHFORK SOLUTION SET
C
 360 DO 3 I=1,ITER
       WRITE (*,2000) I,ITER
       GO TO (361,362), IVAR
 361   U=UMIN+(UMAX-UMIN)*(I-1)/(ITER-1)
       GO TO 365
 362   XG=XGMIN+(XGMAX-XGMIN)*(I-1)/(ITER-1)
 365   A1= ZD*(ZG-ZB)*WEIGHT
       A2= 2.0*U*U*U*CDZ*AREA*(MD-XA*ZD)
       A3=-2*U*U*(U*U*(ZW*MD-MW*ZD)+ZD*(ZG-ZB)*WEIGHT)
       A4= 2.0*U*U*ZD*(XG-XB)*WEIGHT
       A5=-ZD*(XG-XB)*WEIGHT
       CALL PITSLS(IVAR,LL,IFC,U,XG,A1,A2,A3,A4,A5)
       IF (LL.GT.1) IFC=1
   3 CONTINUE
    GO TO 5000
C
C    SIMPLE PITCHFORK SOLUTION SET
C
 400 DO 401 I=1,ITER
       WRITE (*,2000) I,ITER
       GO TO (402,403), IVAR
```

```
402  U=UMIN+(UMAX-UMIN)*(I-1)/(ITER-1)
     GO TO 405
403  XG=XGMIN+(XGMAX-XGMIN)*(I-1)/(ITER-1)
405  A1= ZD*(ZG-ZB)*WEIGHT
     A3=-2*U*U*(U*U*(ZW*MD-MW*ZD)+ZD*(ZG-ZB)*WEIGHT)
     A4= 2.0*U*U*ZD*(XG-XB)*WEIGHT
     CALL SIMSLS(IVAR,LL,IFC,U,XG,A1,A3,A4)
     IF (LL GT 1) IFC=1
401 CONTINUE
   GO TO 5000
370 GO TO (380,390,410,430), ISET
C
C    EXACT BIFURCATION SET
C
380 DO 4 I=1,JXG
     WRITE (*,2000) I,JXG
     XG=XGMIN+(XGMAX-XGMIN)*(I-1)/(JXG-1)
     IHS=0
     DO 5 J=1,JU
      U=UMIN+(UMAX-UMIN)*(J-1)/(JU-1)
      A1= ZW*MD-MW*ZD
      A2=-CDZ*AREA*(MD-XA*ZD)
      A3=-(XG*WEIGHT-XB*BUO)*ZD+(WEIGHT-BUO)*MD
      A4= (ZG*WEIGHT-ZB*BUO)*ZD
      CALL EXNUMS(NUM,A1,A2,A3,A4,U)
      IF (J NE 1) GO TO 381
      UO=U
      NUMO=NUM
      GO TO 5
381   UN=U
      NUMN=NUM
      NDIF=IABS(NUMO-NUMN)
      IF (NDIF EQ 2) GO TO 382
      UO=UN
      NUMO=NUMN
      GO TO 5
382   U1=UO
      U2=UN
      DO 61 JJ=1,JU
       U=U1+(U2-U1)*(JJ-1)/(JU-1)
       A1= ZW*MD-MW*ZD
       A2=-CDZ*AREA*(MD-XA*ZD)
       A3=-(XG*WEIGHT-XB*BUO)*ZD+(WEIGHT-BUO)*MD
```

```
      A4= (ZG*WEIGHT-ZB*BUO)*ZD
      CALL EXNUMS(NUM,A1,A2,A3,A4,U)
      IF (JJ.NE.1) GO TO 383
      UO=U
      NUMO=NUM
      GO TO 61
383   UN=U
      NUMN=NUM
      NDIF=IABS(NUMO-NUMN)
      IF (NDIF.EQ.2) GO TO 384
      UO=UN
      NUMO=NUMN
 61 CONTINUE
    GO TO 5
384 U1=UO
    U2=UN
    DO 62 JJ=1,JU
      U=U1+(U2-U1)*(JJ-1)/(JU-1)
      A1= ZW*MD-MW*ZD
      A2=-CDZ*AREA*(MD-XA*ZD)
      A3=-(XG*WEIGHT-XB*BUO)*ZD+(WEIGHT-BUO)*MD
      A4= (ZG*WEIGHT-ZB*BUO)*ZD
      CALL EXNUMS(NUM,A1,A2,A3,A4,U)
      IF (JJ.NE.1) GO TO 386
      UO=U
      NUMO=NUM
      GO TO 62
386   UN=U
      NUMN=NUM
      NDIF=IABS(NUMO-NUMN)
      IF (NDIF.EQ.2) GO TO 385
      UO=UN
      NUMO=NUMN
 62 CONTINUE
    GO TO 5
385 UP=(UO+UN)/2.0
    IHS=IHS+1
    UPL=SQRT(UP/(32.2*LENGTH))
    XGL=XG/LENGTH
    IPF=10+IHS
    WRITE (IPF,100) XGL,UP
    UO=UN
    NUMO=NUMN
```

```
  5  CONTINUE
  4 CONTINUE
   GO TO 5000
C
C    PITCHFORK BIFURCATION SET
C
 390 DO 6 I=1,JXG
       WRITE (*,2000) I,JXG
       XG=XGMIN+(XGMAX-XGMIN)*(I-1)/(JXG-1)
       IHS=0
       DO 7 J=1,JU
        U=UMIN+(UMAX-UMIN)*(J-1)/(JU-1)
        A1= ZD*(ZG-ZB)*WEIGHT
        A2= 2.0*U*U*U*CDZ*AREA*(MD-XA*ZD)
        A3=-2*U*U*(U*U*(ZW*MD-MW*ZD)+ZD*(ZG-ZB)*WEIGHT)
        A4= 2.0*U*U*ZD*(XG-XB)*WEIGHT
        A5=-ZD*(XG-XB)*WEIGHT
        CALL PINUMS(NUM,A1,A2,A3,A4,A5,U)
        IF (J.NE.1) GO TO 391
        UO=U
        NUMO=NUM
        GO TO 7
 391    UN=U
        NUMN=NUM
        NDIF=IABS(NUMO-NUMN)
        IF (NDIF.EQ.2) GO TO 392
        UO=UN
        NUMO=NUMN
        GO TO 7
 392    U1=UO
        U2=UN
        DO 71 JJ=1,JU
         U=U1+(U2-U1)*(JJ-1)/(JU-1)
         A1= ZD*(ZG-ZB)*WEIGHT
         A2= 2.0*U*U*U*CDZ*AREA*(MD-XA*ZD)
         A3=-2*U*U*(U*U*(ZW*MD-MW*ZD)+ZD*(ZG-ZB)*WEIGHT)
         A4= 2.0*U*U*ZD*(XG-XB)*WEIGHT
         A5=-ZD*(XG-XB)*WEIGHT
         CALL PINUMS(NUM,A1,A2,A3,A4,A5,U)
         IF (JJ.NE.1) GO TO 393
         UO=U
         NUMO=NUM
         GO TO 71
```

```
393     UN=U
        NUMN=NUM
        NDIF=IABS(NUMO-NUMN)
        IF (NDIF.EQ.2) GO TO 394
        UO=UN
        NUMO=NUMN
 71   CONTINUE
      STOP 1111
394   U1=UO
      U2=UN
      DO 72 JJ=1,JU
        U=U1+(U2-U1)*(JJ-1)/(JU-1)
        A1= ZD*(ZG-ZB)*WEIGHT
        A2= 2.0*U*U*U*CDZ*AREA*(MD-XA*ZD)
        A3=-2*U*U*(U*U*(ZW*MD-MW*ZD)+ZD*(ZG-ZB)*WEIGHT)
        A4= 2.0*U*U*ZD*(XG-XB)*WEIGHT
        A5=-ZD*(XG-XB)*WEIGHT
        CALL PINUMS(NUM,A1,A2,A3,A4,A5,U)
        IF (JJ.NE.1) GO TO 396
        UO=U
        NUMO=NUM
        GO TO 72
396     UN=U
        NUMN=NUM
        NDIF=IABS(NUMO-NUMN)
        IF (NDIF.EQ.2) GO TO 395
        UO=UN
        NUMO=NUMN
 72   CONTINUE
      STOP 1112
395   UP=(UO+UN)/2.0
      IHS=IHS+1
      UPL=SQRT(UP/(32.2*LENGTH))
      XGL=XG/LENGTH
      IPF=10+IHS
      WRITE (IPF,100) XGL,UP
      UO=UN
      NUMO=NUMN
  7 CONTINUE
  6 CONTINUE
    GO TO 5000
C
C   SIMPLE PITCHFORK BIFURCATION SET
```

```
C
 410 DO 411 I=1,JXG
       WRITE (*,2000) I,JXG
       XG=XGMIN+(XGMAX-XGMIN)*(I-1)/(JXG-1)
       IHS=0
       DO 412 J=1,JU
        U=UMIN+(UMAX-UMIN)*(J-1)/(JU-1)
        A1= ZD*(ZG-ZB)*WEIGHT
        A3=-2*U*U*(U*U*(ZW*MD-MW*ZD)+ZD*(ZG-ZB)*WEIGHT)
        A4= 2.0*U*U*ZD*(XG-XB)*WEIGHT
        CALL SINUMS(NUM,A1,A3,A4,U)
        IF (J.NE.1) GO TO 413
        UO=U
        NUMO=NUM
        GO TO 412
 413    UN=U
        NUMN=NUM
        NDIF=IABS(NUMO-NUMN)
        IF (NDIF.EQ.2) GO TO 414
        UO=UN
        NUMO=NUMN
        GO TO 412
 414    U1=UO
        U2=UN
        DO 415 JJ=1,JU
         U=U1+(U2-U1)*(JJ-1)/(JU-1)
         A1= ZD*(ZG-ZB)*WEIGHT
         A3=-2*U*U*(U*U*(ZW*MD-MW*ZD)+ZD*(ZG-ZB)*WEIGHT)
         A4= 2.0*U*U*ZD*(XG-XB)*WEIGHT
         CALL SINUMS(NUM,A1,A3,A4,U)
         IF (JJ.NE.1) GO TO 416
         UO=U
         NUMO=NUM
         GO TO 415
 416     UN=U
         NUMN=NUM
         NDIF=IABS(NUMO-NUMN)
         IF (NDIF.EQ.2) GO TO 417
         UO=UN
         NUMO=NUMN
 415  CONTINUE
        STOP 1111
 417    U1=UO
```

```
      U2=UN
      DO 418 JJ=1,JU
        U=U1+(U2-U1)*(JJ-1)/(JU-1)
        A1= ZD*(ZG-ZB)*WEIGHT
        A3=-2*U*U*(U*U*(ZW*MD-MW*ZD)+ZD*(ZG-ZB)*WEIGHT)
        A4= 2.0*U*U*ZD*(XG-XB)*WEIGHT
        CALL SINUMS(NUM,A1,A3,A4,U)
        IF (JJ.NE.1) GO TO 419
        UO=U
        NUMO=NUM
        GO TO 418
419     UN=U
        NUMN=NUM
        NDIF=IABS(NUMO-NUMN)
        IF (NDIF.EQ.2) GO TO 420
        UO=UN
        NUMO=NUMN
418   CONTINUE
      STOP 1112
420   UP=(UO+UN)/2.0
      IHS=IHS+1
      UPL=SQRT(UP/(32.2*LENGTH))
      XGL=XG/LENGTH
      IPF=10+IHS
      WRITE (IPF,100) XGL,UP
      UO=UN
      NUMO=NUMN
412  CONTINUE
411 CONTINUE
   GO TO 5000
C
C    ANALYTIC BIFURCATION SET
C
430 WRITE (*,1017)
   READ (*,*)   ICUSP
   GO TO (432,433), ICUSP
C
C      EXACT" CUSP
C
432 DO 431 I=1,JU
      WRITE (*,2000) I,JU
      U=UMIN+(UMAX-UMIN)*(I-1)/(JU-1)
      DELTA=32.2*(ZW*MD-MW*ZD)/(ZD*WEIGHT)
```

```
      LAMBDA=U*U/(32.2*(ZG-ZB))
      BETA2=(8.0*U*U*(1.0+DELTA*LAMBDA)**3)/(27.0*LAMBDA**2)
      IF (BETA2.LT.0.0) GO TO 431
      BETA=SQRT(BETA2)
      XGB=U*U*BETA/32.2
      WRITE (10,100) U,XGB/LENGTH
 431 CONTINUE
   GO TO 5000
C
C    "APPROXIMATE" CUSP
C
 433 DO 434 I=1,JU
      WRITE (*,2000) I,JU
      U=UMIN+(UMAX-UMIN)*(I-1)/(JU-1)
      DELTA=32.2*(ZW*MD-MW*ZD)/(ZD*WEIGHT)
      LAMBDA=U*U/(32.2*(ZG-ZB))
      BETA2=(8.0*U*U*(1.0+DELTA*LAMBDA)**3)/27.0
      IF (BETA2.LT.0.0) GO TO 434
      BETA=SQRT(BETA2)
      XGB=U*U*BETA/32.2
      WRITE (10,100) U,XGB/LENGTH
 434 CONTINUE
C
 5000 STOP
 1001 FORMAT (' ENTER 1 : SOLUTION SETS      ',/
   1      '      2 : BIFURCATION GRAPHS   ')
 1009 FORMAT (' ENTER 1 : U  VARIATION ',/
   1      '      2 : XG VARIATION ')
 1002 FORMAT (' ENTER MINIMUM VALUE OF U')
 1003 FORMAT (' ENTER MAXIMUM VALUE OF U')
 1004 FORMAT (' ENTER NUMBER OF INCREMENTS')
 1005 FORMAT (' ENTER MINIMUM VALUE OF XG/L')
 1006 FORMAT (' ENTER MAXIMUM VALUE OF XG/L')
 1010 FORMAT (' ENTER VALUE OF XG/L')
 1012 FORMAT (' ENTER VALUE OF U')
 1013 FORMAT (' ENTER 1 : EXACT COMPUTATION      ',/
   1      '      2 : PITCHFORK APPROXIMATION',/
   2      '      3 : SIMPLE PITCHFORK      ',/
   3      '      4 : ANALYTIC SET          ')
 1017 FORMAT (' ENTER 1 : EXACT CUSP  ',/
   1      '      2 : APPROXIMATE CUSP  ')
 2000 FORMAT (2I5)
  100 FORMAT (2E15.5)
```

```
      END
C-----------------------------------------------------------------
      SUBROUTINE TRAP(N,A,B,OUT)
C
C     NUMERICAL INTEGRATION ROUTINE USING THE TRAPEZOIDAL RULE
C
      DIMENSION A(1),B(1)
      N1=N-1
      OUT=0.0
      DO 1 I=1,N1
         OUT1=0.5*(A(I)+A(I+1))*(B(I+1)-B(I))
         OUT =OUT+OUT1
    1 CONTINUE
      RETURN
      END
C-----------------------------------------------------------------
      SUBROUTINE EXSOLS(IVAR,L,IFC,U,XG,A1,A2,A3,A4,CDZ,AREA,ZW,
     &ZD,ZG,MW,MD,BUO,XA)
C
C     IT COMPUTES AND PRINTS THE EXACT SOLUTION SET THETA
C     (DEG.) VERSUS U OR XG
C
      REAL MW,MD,PRNT,PI
      DIMENSION VF(5,2)
      PI=4.0*ATAN(1.0)
      IF (IVAR.EQ.1) PRNT=U
      IF (IVAR.EQ.2) PRNT=XG
C
C     FIND FIRST ESTIMATE OF SOLUTIONS
C
      L=0
      VA=-89.5
      VA=VA*PI/180.0
      VAO=VA
      VO=THETEQ(1,VA,A1,A2,A3,A4,U)
      VAMIN=-89.5
      VAMAX=+89.5
      IVA=5000
      DO 10 I=2,IVA
         AI=I
         VA=VAMIN+(VAMAX-VAMIN)*(I-1)/(IVA-1)
C        VA=AI-90.5
         VA=VA*PI/180.0
```

```
      VAN=VA
      VN=THETEQ(1,VA,A1,A2,A3,A4,U)
      VP=VO*VN
      IF (VP.GE.0.0) GO TO 11
      L=L+1
      VF(L,1)=VAO
      VF(L,2)=VAN
 11   VO=VN
      VAO=VAN
 10 CONTINUE
C
C    EXACT COMPUTATION OF SOLUTIONS VIA NEWTON'S METHOD
C
    E=1.E-8
    IEND=500
    DO 20 J=1,L
      X=(VF(J,1)+VF(J,2))/2.0
C
      X1=X
      IXX=0
      IF (IXX.EQ.0) GO TO 35
C
      F=THETEQ(1,X,A1,A2,A3,A4,U)
      FDER=THETEQ(2,X,A1,A2,A3,A4,U)
      DO 30 K=1,IEND
        IF (FDER.EQ.0.0) STOP 1001
        DX=F/FDER
        X1=X-DX
        F=THETEQ(1,X1,A1,A2,A3,A4,U)
        FDER=THETEQ(2,X1,A1,A2,A3,A4,U)
        IF (F.EQ.0.0) GO TO 35
        A=ABS(X1-X)
        IF (A-E) 35,35,40
 40     X=X1
 30   CONTINUE
      GO TO 20
 35   SOL=X1*180/PI
C     WRITE (*,*) X1
      JPR=10+J
      WD=U*TAN(X1)
      DLT=((CDZ*AREA*WD*ABS(WD))-(ZW*U*WD))/(ZD*U*U)
        IF ((ABS(DLT).GT.0.4).AND.(CDZ.NE.0.0)) THEN
```

```
          CALL
SATUR(U,XG,CDZ,AREA,ZW,ZD,ZG,MW,MD,BUO,XA,DLT,PRNT)
         ELSEIF ((ABS(DLT).GT.0.4).AND.(CDZ.EQ.0.0)) THEN
          CALL
SATUR1(U,XG,CDZ,AREA,ZW,ZD,ZG,MW,MD,BUO,XA,DLT,PRNT)
         ENDIF
          IF (L.EQ.1.AND.IFC.EQ.0) WRITE (10,100) PRNT,SOL,DLT*180/PI
          IF (L.EQ.1.AND.IFC.EQ.1) WRITE (16,100) PRNT,SOL,DLT*180/PI
          IF (L.GT.1)          WRITE (JPR,100) PRNT,SOL,DLT*180/PI
  20 CONTINUE
    RETURN
 100 FORMAT (3E15.5)
    END
C-----------------------------------------------------------------
    SUBROUTINE
SATUR(U,XG,CDZ,AREA,ZW,ZD,ZG,MW,MD,BUO,XA,DLT,PRNT)
    REAL MW,MD,PRNT
C
C    USED TO COMPUTE SATURATION CONDITIONS FOR THE DIVE PLANE
WITH DRAG
C    COEFFICENT INCLUDED
C
    CD=CDZ
         IF (DLT.GT.0.0) THEN
              W1=(-ZW*U+SQRT((ZW*U)*(ZW*U)-4*(-CD*AREA)*ZD*U*U*0.4))
   &         /(2*(-CD*AREA))
               IF (W1.GT.0.0) THEN
                A=MW*U*W1-CD*XA*AREA*W1*W1-XG*BUO+MD*U*U*0.4
                B=-2.0*ZG*BUO
                C=MW*U*W1-CD*XA*AREA*W1*W1+XG*BUO+MD*U*U*0.4
                X1=(-B+SQRT((B1*B1)-4*(A*C)))/(2.0*A)
                SOL1=2.0*ATAN(X1)
                X2=(-B-SQRT((B1*B1)-4*(A*C)))/(2.0*A)
                SOL2=2.0*ATAN(X2)
                WRITE (21,200) PRNT,SOL1,SOL2
               ENDIF
              W2=(-ZW*U-SQRT((ZW*U)*(ZW*U)-4*(-CD*AREA)*ZD*U*U*0.4))
   &         /(2*(-CD*AREA))
               IF (W2.GT.0.0) THEN
                A=MW*U*W2-CD*XA*AREA*W2*W2-XG*BUO+MD*U*U*0.4
                B=-2.0*ZG*BUO
                C=MW*U*W2-CD*XA*AREA*W2*W2+XG*BUO+MD*U*U*0.4
                X1=(-B+SQRT((B1*B1)-4*(A*C)))/(2.0*A)
```

```
            SOL1=2.0*ATAN(X1)
            X2=(-B-SQRT((B1*B1)-4*(A*C)))/(2.0*A)
            SOL2=2.0*ATAN(X2)
            WRITE (22,200) PRNT,SOL1,SOL2
          ENDIF
        W3=(-ZW*U+SQRT((ZW*U)*(ZW*U)-4*(CD*AREA)*ZD*U*U*0.4))
&       /(2*(CD*AREA))
          IF (W3.LT.0.0) THEN
            A=MW*U*W3+CD*XA*AREA*W3*W3-XG*BUO+MD*U*U*0.4
            B=-2.0*ZG*BUO
            C=MW*U*W3+CD*XA*AREA*W3*W3+XG*BUO+MD*U*U*0.4
            X1=(-B+SQRT((B1*B1)-4*(A*C)))/(2.0*A)
            SOL1=2.0*ATAN(X1)
            X2=(-B-SQRT((B1*B1)-4*(A*C)))/(2.0*A)
            SOL2=2.0*ATAN(X2)
            WRITE (23,200) PRNT,SOL1,SOL2
          ENDIF
        W4=(-ZW*U-SQRT((ZW*U)*(ZW*U)-4*(CD*AREA)*ZD*U*U*0.4))
&       /(2*(CD*AREA))
          IF (W4.LT.0.0) THEN
            A=MW*U*W4+CD*XA*AREA*W4*W4-XG*BUO+MD*U*U*0.4
            B=-2.0*ZG*BUO
            C=MW*U*W4+CD*XA*AREA*W4*W4+XG*BUO+MD*U*U*0.4
            X1=(-B+SQRT((B1*B1)-4*(A*C)))/(2.0*A)
            SOL1=2.0*ATAN(X1)
            X2=(-B-SQRT((B1*B1)-4*(A*C)))/(2.0*A)
            SOL2=2.0*ATAN(X2)
            WRITE (24,200) PRNT,SOL1,SOL2
          ENDIF
      ELSE
        W1=(-ZW*U+SQRT((ZW*U)*(ZW*U)-4*(-CD*AREA)*ZD*U*U*
&       (-0.4)))/(2*(-CD*AREA))
          IF (W1.GT.0.0) THEN
            A=MW*U*W1-CD*XA*AREA*W1*W1-XG*BUO+MD*U*U*(-0.4)
            B=-2.0*ZG*BUO
            C=MW*U*W1-CD*XA*AREA*W1*W1+XG*BUO+MD*U*U*(-0.4)
            X1=(-B+SQRT((B1*B1)-4*(A*C)))/(2.0*A)
            SOL1=2.0*ATAN(X1)
            X2=(-B-SQRT((B1*B1)-4*(A*C)))/(2.0*A)
            SOL2=2.0*ATAN(X2)
            WRITE (31,200) PRNT,SOL1,SOL2
          ENDIF
        W2=(-ZW*U-SQRT((ZW*U)*(ZW*U)-4*(-CD*AREA)*ZD*U*U*
```

```
&          (-0.4))) /(2*(-CD*AREA))
             IF (W2.LT.0.0) THEN
              A=MW*U*W2-CD*XA*AREA*W2*W2-XG*BUO+MD*U*U*(-0.4)
              B=-2.0*ZG*BUO
              C=MW*U*W2-CD*XA*AREA*W2*W2+XG*BUO+MD*U*U*(-0.4)
              X1=(-B+SQRT((B1*B1)-4*(A*C)))/(2.0*A)
              SOL1=2.0*ATAN(X1)
              X2=(-B-SQRT((B1*B1)-4*(A*C)))/(2.0*A)
              SOL2=2.0*ATAN(X2)
              WRITE (32,200) PRNT,SOL21,SOL22
             ENDIF
            W3=(-ZW*U+SQRT((ZW*U)*(ZW*U)-4*(CD*AREA)*ZD*U*U*
&          (-0.4)))/(2*(CD*AREA))
             IF (W3.LT.0.0) THEN
              A=MW*U*W3+CD*XA*AREA*W3*W3-XG*BUO+MD*U*U*(-0.4)
              B=-2.0*ZG*BUO
              C=MW*U*W3+CD*XA*AREA*W3*W3+XG*BUO+MD*U*U*(-
0.4)
              X1=(-B+SQRT((B1*B1)-4*(A*C)))/(2.0*A)
              SOL1=2.0*ATAN(X1)
              X2=(-B-SQRT((B1*B1)-4*(A*C)))/(2.0*A)
              SOL2=2.0*ATAN(X2)
              WRITE (33,200) PRNT,SOL1,SOL2
             ENDIF
            W4=(-ZW*U+SQRT((ZW*U)*(ZW*U)-4*(CD*AREA)*ZD*U*U*
&          (-0.4)))/(2*(CD*AREA))
             IF (W4.LT.0.0) THEN
              A=MW*U*W4+CD*XA*AREA*W4*W4-XG*BUO+MD*U*U*(-0.4)
              B=-2.0*ZG*BUO
              C=MW*U*W4+CD*XA*AREA*W4*W4+XG*BUO+MD*U*U*(-
0.4)
              X1=(-B+SQRT((B1*B1)-4*(A*C)))/(2.0*A)
              SOL1=2.0*ATAN(X1)
              X2=(-B-SQRT((B1*B1)-4*(A*C)))/(2.0*A)
              SOL2=2.0*ATAN(X2)
              WRITE (34,200) PRNT,SOL1,SOL2
             ENDIF
          ENDIF
 200  FORMAT (3E15.5)
      END
C-----------------------------------------------------------------
      SUBROUTINE
SATUR1(U,XG,CDZ,AREA,ZW,ZD,ZG,MW,MD,BUO,XA,DLT,PRNT)
```

```
      REAL MW,MD,PRNT
C
C     COMPUTES DIVE PLANE SATURATION NEGLECTING DRAG
C
      PI=4.0*ATAN(1.0)
      A1=MD*U*U*0.4-MW*U*U*ZD*0.4-XG*ZW*BUO
      A2=-MD*U*U*0.4+MW*U*U*ZD*0.4-XG*ZW*BUO
      B1=-2.0*ZG*ZW*BUO
      C1=-MW*U*U*ZD*0.4+XG*ZW*BUO+MD*U*U*ZW*0.4
      C2=MW*U*U*ZD*0.4+XG*ZW*BUO-MD*U*U*ZW*0.4
      XCD1=((-B1/A1)+SQRT(((B1/A1)**2)-4.0*(C1/A1)))/2.0
      XCD2=((-B1/A1)-SQRT(((B1/A1)**2)-4.0*(C1/A1)))/2.0
      XCD3=((-B1/A2)+SQRT(((B1/A2)**2)-4.0*(C2/A2)))/2.0
      XCD4=((-B1/A2)-SQRT(((B1/A2)**2)-4.0*(C2/A2)))/2.0
      XC1=2.0*ATAN(XCD1)*180/PI
      XC2=2.0*ATAN(XCD2)*180/PI
      XC3=2.0*ATAN(XCD3)*180/PI
      XC4=2.0*ATAN(XCD4)*180/PI
      WRITE (20,100) PRNT,XC1,DLT*180/PI
      WRITE (41,100) PRNT,XC2,DLT*180/PI
      WRITE (42,100) PRNT,XC3,DLT*180/PI
      WRITE (43,100) PRNT,XC4,DLT*180/PI
  100 FORMAT (3E15.5)
      END
C-----------------------------------------------------------------
      SUBROUTINE PITSLS(IVAR,LL,IFC,U,XG,A1,A2,A3,A4,A5)
C
C     IT COMPUTES AND PRINTS THE PITCHFORK SOLUTION SET THETA
C     (DEG ) VERSUS U OR XG
C
      DIMENSION VF(5,2)
      PI=4.0*ATAN(1.0)
      IF (IVAR.EQ.1) PRNT=U
      IF (IVAR.EQ.2) PRNT=XG
C
C     FIND FIRST ESTIMATE OF SOLUTIONS
C
      L=0
      VA=-89.5
      VA=VA*PI/180.0
      VAO=VA
      VO=PITCEQ(1,VA,A1,A2,A3,A4,A5,U)
      DO 10 I=2,180
```

```
      AI=I
      VA=AI-90.5
      VA=VA*PI/180.0
      VAN=VA
      VN=PITCEQ(1,VA,A1,A2,A3,A4,A5,U)
      VP=VO*VN
      IF (VP.GE.0.0) GO TO 11
      L=L+1
      VF(L,1)=VAO
      VF(L,2)=VAN
 11   VO=VN
      VAO=VAN
 10 CONTINUE
C
C   EXACT COMPUTATION OF SOLUTIONS VIA NEWTON'S METHOD
C
    E=1.E-5
    IEND=500
    DO 20 J=1,L
      X=(VF(J,1)+VF(J,2))/2.0
      F=PITCEQ(1,X,A1,A2,A3,A4,A5,U)
C
      X1=X
      IXX=0
      IF (IXX.EQ.0) GO TO 35
C
      FDER=PITCEQ(2,X,A1,A2,A3,A4,A5,U)
      DO 30 K=1,IEND
        IF (FDER.EQ.0.0) STOP 1001
        DX=F/FDER
        X1=X-DX
        F=PITCEQ(1,X1,A1,A2,A3,A4,A5,U)
        FDER=PITCEQ(2,X1,A1,A2,A3,A4,A5,U)
        IF (F.EQ.0.0) GO TO 35
        A=ABS(X1-X)
        IF (A-E) 35,35,40
 40     X=X1
 30   CONTINUE
      GO TO 20
 35   SOL=X1*180.0/PI
      JPR=10+J
      IF (L.EQ.1.AND.IFC.EQ.0) WRITE (10,100) PRNT,SOL
      IF (L.EQ.1.AND.IFC.EQ.1) WRITE (16,100) PRNT,SOL
```

```
      IF (L.GT.1)          WRITE (JPR,100) PRNT,SOL
 20 CONTINUE
   RETURN
100 FORMAT (2E15.5)
   END
C-----------------------------------------------------------------------
   SUBROUTINE SIMSLS(IVAR,L,IFC,U,XG,A1,A3,A4)
C
C   IT COMPUTES AND PRINTS THE SIMPLE PITCHFORK SOLUTION SET
THETA
C   (DEG.) VERSUS U OR XG
C
   DIMENSION VF(5,2)
   PI=4.0*ATAN(1.0)
   IF (IVAR.EQ.1) PRNT=U
   IF (IVAR.EQ.2) PRNT=XG
C
C   FIND FIRST ESTIMATE OF SOLUTIONS
C
   L=0
   VA=-89.5
   VA=VA*PI/180.0
   VAO=VA
   VO=SIMPEQ(1,VA,A1,A3,A4,U)
   DO 10 I=2,180
      AI=I
      VA=AI-90.5
      VA=VA*PI/180.0
      VAN=VA
      VN=SIMPEQ(1,VA,A1,A3,A4,U)
      VP=VO*VN
      IF (VP.GE.0.0) GO TO 11
      L=L+1
      VF(L,1)=VAO
      VF(L,2)=VAN
 11   VO=VN
      VAO=VAN
 10 CONTINUE
C
C   EXACT COMPUTATION OF SOLUTIONS VIA NEWTON'S METHOD
C
   E=1.E-5
   IEND=500
```

```
      DO 20 J=1,L
         X=(VF(J,1)+VF(J,2))/2.0
C
         X1=X
         IXX=0
         IF (IXX.EQ.0) GO TO 35
C
         F=SIMPEQ(1,X,A1,A3,A4,U)
         FDER=SIMPEQ(2,X,A1,A3,A4,U)
         DO 30 K=1,IEND
          IF (FDER.EQ.0.0) STOP 1001
          DX=F/FDER
          X1=X-DX
          F=SIMPEQ(1,X1,A1,A3,A4,U)
          FDER=SIMPEQ(2,X1,A1,A3,A4,U)
          IF (F.EQ.0.0) GO TO 35
          A=ABS(X1-X)
          IF (A-E) 35,35,40
 40       X=X1
 30    CONTINUE
         GO TO 20
 35    SOL=X1*180.0/PI
         JPR=10+J
         IF (L.EQ.1.AND.IFC.EQ.0) WRITE (10,100)  PRNT,SOL
         IF (L.EQ.1.AND.IFC.EQ.1) WRITE (16,100)  PRNT,SOL
         IF (L.GT.1)              WRITE (JPR,100) PRNT,SOL
 20 CONTINUE
      RETURN
100 FORMAT (2E15.5)
      END
C-----------------------------------------------------------------
      SUBROUTINE EXNUMS(NUM,A1,A2,A3,A4,U)
C
C     IT COMPUTES THE NUMBER OF SOLUTIONS OF THE EXACT SOLUTION
SET
C
      PI=4.0*ATAN(1.0)
      L=0
      VA=-89.5
      VA=VA*PI/180.0
      VO=THETEQ(1,VA,A1,A2,A3,A4,U)
      DO 10 I=2,180
         AI=I
```

```
      VA=AI-90.5
      VA=AI*PI/180.0
      VN=THETEQ(1,VA,A1,A2,A3,A4,U)
      VP=VO*VN
      IF (VP.GE.0.0) GO TO 11
      L=L+1
 11   VO=VN
 10 CONTINUE
   NUM=L
   RETURN
   END
C-----------------------------------------------------------------
   SUBROUTINE PINUMS(NUM,A1,A2,A3,A4,A5,U)
C
C    IT COMPUTES THE NUMBER OF SOLUTIONS OF THE PITCHFORK
SOLUTION SET
C
   PI=4.0*ATAN(1.0)
   L=0
   VA=-89.5
   VA=VA*PI/180.0
   VO=PITCEQ(1,VA,A1,A2,A3,A4,A5,U)
   DO 10 I=2,180
      AI=I
      VA=AI-90.5
      VA=VA*PI/180.0
      VN=PITCEQ(1,VA,A1,A2,A3,A4,A5,U)
      VP=VO*VN
      IF (VP.GE.0.0) GO TO 11
      L=L+1
 11   VO=VN
 10 CONTINUE
   NUM=L
   RETURN
   END
C-----------------------------------------------------------------
   SUBROUTINE SINUMS(NUM,A1,A3,A4,U)
C
C    IT COMPUTES THE NUMBER OF SOLUTIONS OF THE SIMPLE PITCHFORK
C    SOLUTION SET
C
   PI=4.0*ATAN(1.0)
   L=0
```

```
      VA=-89.5
      VA=VA*PI/180.0
      VO=SIMPEQ(1,VA,A1,A3,A4,U)
      DO 10 I=2,180
         AI=I
         VA=AI-90.5
         VA=VA*PI/180.0
         VN=SIMPEQ(1,VA,A1,A3,A4,U)
         VP=VO*VN
         IF (VP.GE.0.0) GO TO 11
         L=L+1
   11    VO=VN
   10 CONTINUE
      NUM=L
      RETURN
      END
C-----------------------------------------------------------------
      FUNCTION THETEQ(K,XA,A1,A2,A3,A4,U)
C
C     IT COMPUTES THE VALUE OF THE EXACT EQUATION FOR
C     THETABAR FOR A GIVEN VALUE OF THETA
C
C     K = 1 : COMPUTE THE VALUE OF THE FUNCTION
C     K = 2 : COMPUTE THE VALUE OF ITS DERIVATIVE
C
      SP=SIN(XA)
      CP=COS(XA)
      AP=ABS(SP)
      TP=TAN(XA)
      ATP=ABS(TP)
      GO TO (10,20), K
   10 THETEQ=A1*U*U*SP*CP+A2*U*U*SP*AP+A3*CP**3+A4*SP*CP**2
C  10 THETEQ=A1*U*TP+A2*U*U*TP*ATP+A3*CP+A4*SP
      GO TO 50
   20 THETEQ=A1*U*U*CP*CP-A1*U*U*SP*SP-3.0*A3*CP*CP*SP+A4*CP**3
     &     -2.0*A4*SP*SP*CP+2.0*A2*U*U*CP*AP
   50 RETURN
      END
C-----------------------------------------------------------------
      FUNCTION PITCEQ(K,XA,A1,A2,A3,A4,A5,U)
C
C     IT COMPUTES THE VALUE OF THE PITCHFORK EQUATION FOR
C     THETABAR FOR A GIVEN VALUE OF THETA
```

```
C
C    K = 1 : COMPUTE THE VALUE OF THE FUNCTION
C    K = 2 : COMPUTE THE VALUE OF ITS DERIVATIVE
C
      TP =TAN(XA)
      CP =COS(XA)
      CP2=CP*CP
      AP =ABS(TP)
      GO TO (10,20), K
   10 PITCEQ=A1*(U*TP)**3+A2*U*U*TP*AP+A3*U*TP+A4+A5*U*U*TP*TP
      GO TO 50
   20 PITCEQ=3.0*U*U*U*TP/CP2+2.0*A2*U*U*AP/CP2+A3*U/CP2
     &     +2.0*A5*U*U*TP/CP2
   50 RETURN
      END
C-----------------------------------------------------------------
      FUNCTION SIMPEQ(K,XA,A1,A3,A4,U)
C
C    IT COMPUTES THE VALUE OF THE SIMPLE PITCHFORK EQUATION FOR
C    THETABAR FOR A GIVEN VALUE OF THETA
C
C    K = 1 : COMPUTE THE VALUE OF THE FUNCTION
C    K = 2 : COMPUTE THE VALUE OF ITS DERIVATIVE
C
      TP =TAN(XA)
      CP =COS(XA)
      CP2=CP*CP
      AP =ABS(TP)
      GO TO (10,20), K
   10 SIMPEQ=A1*(U*TP)**3+A3*U*TP+A4
      GO TO 50
   20 SIMPEQ=3.0*U*U*U*TP/CP2+A3*U/CP2
   50 RETURN
      END
```

```
% THIS IS PROGRAM BIFSU.M. IT COMPUTES THE BIASED BIFURCATION
CUSP FOR
% DELTA SATURATED INCLUDING DRAG TERMS. IT USES THE FZERO
FUNCTION TO
% SOLVE THE EQUATIONS.

global W B1 U n Zw Zdlt A XA CD rho;

% ESTABLISH GEOMETRIC PARAMETERS
W=1556.2363;B1=1.0001*W;
A=19.8473;XA=0.20126;
CD=0.3;
Iy=561.32;
g=32.2;
m=W/g;
rho=1.94;
L=13.9792;
xb=0;

Alphas=1;
Alphab=0;
zg=0.1;
zb=0;
zgb=zg-zb;

% NON-DIMENSIONING FACTORS
nd1=.5*rho*L^2;
nd2=.5*rho*L^3;
nd3=.5*rho*L^4;
nd4=.5*rho*L^5;

% HYDRODYNAMIC COEFFICIENTS
Zqdnd=-6.33e-4;Zwdnd=-1.4529e-2;Zqnd=7.545e-3;Zwnd=-1.391e-2;
Zds=-5.603e-3;Zdb=0.5*(-5.603e-3);Zdltnd=(Alphas*Zds+Alphab*Zdb);
Mqdnd=-8.8e-4;Mwdnd=-5.61e-4;Mqnd=-3.702e-3;Mwnd=1.0324e-2;
Mds=-0.002409;Mdb=0.5*(0.002409);Mdltnd=(Alphas*Mds+Alphab*Mdb);

Zqd=nd3*Zqdnd;Zwd=nd2*Zwdnd;Zq=nd2*Zqnd;Zw=nd1*Zwnd;
Zdlt=nd1*Zdltnd;

Mqd=nd4*Mqdnd;Mwd=nd3*Mwdnd;Mq=nd3*Mqnd;Mw=nd2*Mwnd;
Mdlt=nd2*Mdltnd;
```

```
% ESTABLISH SPEED RANGE
U=.9:0.01:2.6;
for n=1:length(U);

% SOLVES FORCE EQUATION USING FZERO FUNCTION
th(n)=fzero('satur',(-Zdlt/Zw),0.00001);

% COMPUTES RELATIONSHIP BETWEEN U AND Xgb WITH RESULTS FROM
ABOVE EQUATION
xg(n)=(Mw*U(n)^2*tan(th(n))-zg*W*sin(th(n))-(0.5)*rho*CD*A*XA*U(n)^2*...
tan(th(n))*abs(tan(th(n)))+Mdlt*U(n)^2*(0.4))/(W*cos(th(n)));
end;
XgbL=xg/13.9792;
Lp=sqrt(U.^2/(3.22));
for n=1:length(U);
th1(n)=fzero('satur1',(-Zdlt/Zw),0.00001);
xg1(n)=(Mw*U(n)^2*tan(th1(n))-zg*W*sin(th1(n))-(0.5)*rho*CD*A*...
XA*U(n)^2*tan(th1(n))*abs(tan(th1(n)))+Mdlt*U(n)^2*(-0.4))/(W*cos(th1(n)));
end;
XgbL1=xg1/13.9792;


% THIS IS PROGRAM SATUR.M. IT ESTABLISHES THE FUNCTION TO BE
SOLVED IN
% THE BIFSU.M PROGRAM.

function y=satur(th);
y=Zw*U(n)^2*tan(th)+(W-B1)*cos(th)+Zdlt*U(n)^2*(0.4)...
-(0.5)*rho*CD*A*U(n)^2*tan(th)*abs(tan(th));

% THIS IS PROGRAM SATUR1.M. IT ESTABLISHES THE FUNCTION TO BE
SOLVED IN
% THE BIFSU.M PROGRAM.

function y1=satur1(th1);
y1=Zw*U(n)^2*tan(th1)+(W-B1)*cos(th1)+Zdlt*U(n)^2*(-0.4)...
-(0.5)*rho*CD*A*U(n)^2*tan(th1)*abs(tan(th1));
```

APPENDIX B

DTRC SUBOFF MODEL CHARACTERISTICS

DESIGN PARAMETERS - HULL

Length Between Perpediculars	(LCP)	(ft)	13.9792
Length Overall	(LOA)	(ft)	14.2917
Length to the Center of Buoyancy	(LCB)	(ft)	6.6042
Length of Foreobody	(L_F)	(ft)	3.3333
Length of Parallel Middlebody	(L_P)	(ft)	7.3125
Length of Run	(L_R)	(ft)	3.6458
Diameter		(ft)	1.6667
Fineness Ratio			8.575

Item	Bare Hull	B.H. + Sail	B.H. + 4 Planes	B.H. + Ring Wing 1	Fully Appended
VOL(ft^3)	24.692	24.83434	24.78279	24.75678	24.98991
LCB(ft)	6.59003	6.5726	6.612732	6.60889	6.613906
VCB(ft)	0.0	-0.006711	0.0	0.0	-0.006669
WS(ft^2)	63.717	65.854	65.514	63.717	67.651
Buoyancy(lb)	1537.6841	1546.5483	1543.3380	1541.7183	1556.2363
m'	0.018078	0.018182	0.018144	0.018123	0.018296
$x_G' m' * 10^4$	0.388697	0.410569	-0.111173	-0.061235	-0.127467
I_y'	0.001053	0.001059	0.001066	0.001066	0.001084

Item	Fully Appended
VOL(ft^3)	24.9899
LCB(ft)	6.6139
VCB(ft)	-0.006669
WS(ft^2)	67.651
Buoyancy(lb)	1556.2363
m'	0.018296
$Z_G' m' * 10^4$	-0.127467
I_z'	0.001084

DESIGN PARAMETERS - SAIL

Span	(ft)	0.729
Root Chord	(ft)	1.208
Tip Chord	(ft)	1.208
FP to Sail LE Distance	(ft)	3.033
Aspect Ratio		0.603

CALCULATED PARAMETER - SAIL

Planform Area	(ft^2)	0.855

DESIGN PARAMETERS - CONTROL PLANE

Span	(ft)	0.438
Root Chord	(ft)	0.704
Tip Chord	(ft)	0.500
FP to Plane TE Distance	(ft)	13.146
Aspect Ratio		0.720
Section Profile (NACA)		0020

CALCULATED PARAMETER - CONTROL PLANE

Planform Area	(ft^2)	0.267

Nondimensional offsets and cross sectional areas for the hull.

STATION	B/B_X	A/A_X
0.0	0.00000	0.00000
0.1	0.29058	0.08444
0.2	0.39396	0.15520
0.3	0.46600	0.21715
0.4	0.52147	0.27194
0.5	0.56627	0.32066
0.6	0.60352	0.36424
0.7	0.63514	0.40340
1.0	0.70744	0.50047
2.0	0.84713	0.71763
3.0	0.94066	0.88484
4.0	0.99282	0.98570
7.7143	1.00000	1.00000
10.0	1.00000	1.00000
15.1429	1.00000	1.00000
16.0	0.97598	0.95253
17.0	0.81910	0.67093
18.0	0.55025	0.30278
19.0	0.26835	0.07201
20.0	0.11724	0.01375
20.1	0.11243	0.01264
20.2	0.10074	0.01015
20.3	0.07920	0.00628
20.4	0.03178	0.00101
20.4167	0.00000	0.00000

Nondimensional stability and control derivatives.

Vertical Plane

Item	Fully Appended
Z_v'	-0.013910
M_v'	0.010324
Z_q'	-0.007545
M_q'	-0.003702
$Z_{\dot{v}}'$	-0.014529
$M_{\dot{v}}'$	-0.000561
$Z_{\dot{q}}'$	-0.000633
$M_{\dot{q}}'$	-0.000860
G	-1.162874
$Z_{\delta s}'$	-0.005603
$M_{\delta s}'$	-0.002409

Horizontal Plane

Item	Bare Hull	B.H. + Sail	B.H. + 4 Planes	B.H. + Ring Wing 1	Fully Appended
Y_v'	-0.005948	-0.023008	-0.010494	-0.005943	-0.027834
N_v'	-0.012795	-0.015534	-0.011254	-0.012939	-0.013648
K_v'	-0.000019	-0.000697	-0.000033	-0.000019	-0.000584
Y_r'	0.001811	-0.000023	0.006324	0.003811	0.005251
N_r'	-0.001597	-0.002378	-0.003064	-0.002325	-0.004444
$Y_{\dot{v}}'$	-0.013278	-0.015042	-0.014711	-0.014899	-0.016186
$N_{\dot{v}}'$	0.000202	0.000008	0.000415	0.000625	0.000396
$Y_{\dot{r}}'$	0.000060	-0.000196	0.000465	0.000347	0.000398
$N_{\dot{r}}'$	-0.000676	-0.000710	-0.000744	-0.000787	-0.000897
G	-20.38506	-4.081818	-3.152048	-12.43748	-0.443297
$Y_{\delta r}'$					0.005929
$N_{\delta r}'$					-0.002217
$K_{\delta r}'$					-0.000005

LIST OF REFERENCES

1 Lindgren, A. G., Cretella, D. B., and Bessacini, A. F., "Dynamics and Control of Submerged Vehicles," *Transactions*, Instument Society of America, Vol. 6, No. 4, 1967.

2 Gueler, G. F., "Modelling, Design and Analysis of an Autopilot for Submarine Vehicles," *International Shipbuilding Progress*, Vol. 36, No. 405, 1989.

3 Healey, A. J., "Model-Based Manuevering Controls for Autonomous Underwater Vehicles," *Journal of Dynamic Systems, Measurement, and Control, Transactions of the ASME*, Vol. 114, pp. 614-622, 1992.

4 Goheen, K. R., Jefferys, E. R., and Broome, D.R., "Robust Self-Designing Controllers for Underwater Vehicles," *Journal of Offshore Mechanics and Arctic Engineering, Transactions of the ASME*, Vol. 109, pp. 170-178, 1987.

5 Yoerger, D. R., and Slotine, J. E., "Robust Trajectory Control of Underwater Vehicles," *IEEE Journal of Oceanic Engineering*, Vol. 10, No. 4, 1985.

6 Cristi, R., Papoulias, F. A., and Healey, A. J., "Adaptive Sliding Mode Control of Autonomous Underwater Vehicles in the Dive Plane," *IEEE Journal of Oceanic Engineering*, Vol. 15, No. 3, 1991.

7 Freidland, B., *Control System Design: An Introduction to State-Space Methods*, McGraw-Hill, 1986.

8 Golubitsky, M., and Schaeffer, D., "A Theory for Imperfect Bifurcation Via Singularity Theory," *Communications on Pure and Applied Mathematics*, Vol. 32, pp. 21-98, 1979.

9 Golubitsky, M., and Schaeffer, D., *Singularities and Group Bifurcation Theory I; Applied Mathematical Sciences 51*, Springer-Verlag, New York, 1985.

10 Papoulias, F. A., "A Qualitative and Quantitative Study of Steady State Response of Towed Floating Bodies," *Dynamics and Stability of Systems*, Vol. 3, Nos. 3&4, 1988.

11 Papoulias, F. A., "Stability and Bifurcations of Towed Underwater Vehicles in the Dive Plane," *Journal of Ship Research*, Vol. 36, No. 3, 1992.

12 Papoulias, F. A., "Dynamics and Bifurcations of Pursuit Guidance for Vehicle Path Keeping in the Dive Plane," *Journal of Ship Research*, Vol. 37, No. 2, 1993.

13 Clayton, B. R., and Bishop, R. E., *Mechanics of Marine Vehicles*, Gulf Publishing Co., Houston, 1982

14 Department of the Navy Technical Manual 0911-003-6010, *Fundamentals of Submarine Hydrodynamics, Motion and Control*, 1971.

15 David Taylor Research Center Report 2510, *Standard Equations of Motion for Submarine Simulations*, by M. Gertler and G. R. Hagen, 1967.

16 David Taylor Research Center Report 1298-08, *Investigation of the Stability and Control Characteristics of Several Configurations of the DARPA SUBOFF Model (DTRC model 570) from Captive-Model Experiments*, by R. F. Roddy, 1990.

17 Guckenheimer, J., and Holmes, P., *Nonlinear Oscillations, Dynamical Systems, and Bifurcation Vector Fields; Applied Mathematical Sciences 42*, Springer-Verlag, New York, 1983

INITIAL DISTRIBUTION LIST

1.	Defense Technical Information Center Cameron Station Alexandria, VA 22304-6145	2
2.	Library, Code 52 Naval Postgraduate School Monterey, CA 93943-5002	2
3.	Chairman, Code ME Department of Mechanical Engineering Naval Postgraduate School Monterey, CA 93943-5000	1
4.	Professor F. A. Papoulias, Code ME/Pa Department of Mechanical Engineering Naval Postgraduate School Monterey, CA 93943-5000	4
5.	LT Jeffery S. Riedel, USN 25 Vernon Street Plymouth, MA 02360	5
6.	Naval Engineering Curricular Office, Code 34 Naval Postgraduate School Monterey, CA 93943-5000	1